# INDUSTRIALLY SCALABLE HUMAN LIVER ORGANOIDS

Bryant Tai Wu

A thesis submitted to the faculty of the University of North Carolina at Chapel Hill in partial fulfillment of the requirements for the degree of
Master of Philosophy in the Department of Biomedical Engineering

Chapel Hill
2015

Approved by:

David Gerber

Robert Dennis

Lola Reid

©2015
Bryant Tai Wu
ALL RIGHTS RESERVED

## ABSTRACT

Bryant Tai Wu; Industrially Scalable Liver Organoids
(Under the direction of Lola M. Reid)

Tissue engineering research is a multidisciplinary effort that incorporates the use of resources from various fields to address specific problems. Biomatrix scaffolds have recently been more widely used to improve the culture of cells by supporting their differentiated functions more than any known matrix extract or purified matrix component. However, they are not readily converted to industrial scale usage. Additionally, improved imaging techniques using ultrasound have been developed and are being used to characterize the biomatrix scaffolds in more detail to assess which preparation might be best for industrially scaled studies. The primary objective of this thesis was to identify methods that would most optimally use the biomatrix scaffold extracts while preserving the critical components of the matrix but in a way that was scalable for use in industry. We also demonstrate the use of novel ultrasound technologies that are non-invasive and non-destructive in the evaluation of biomatrix scaffolds.

## ACKNOWLEDGEMENTS

I would like to express my sincere gratitude to my advisor, Dr. Lola Reid, for her guidance both in research and in my career and her encouragement to achieve my goals and pursue my dreams. Her continuous support and understanding made this work possible. I would like to extend my gratitude to the lab manager, Eliane Wauthier, who was always willing to help, Her care and support these past few years have been invaluable to my graduate education. I would also like to acknowledge the fellow members in my lab for all the technical and scientific support I have received in these past years, specifically Tsunekazu Oikawa and Ariel Hanson. I would like to thank the rest of my committee members including Dr. David Gerber and Dr. Bob Dennis for their helpful insights and contributions to the pursuit of my career aspirations. Lastly, I would like to thank my family for their unconditional love and support.

## TABLE OF CONTENTS

## LIST OF TABLES

## LIST OF FIGURES

## LIST OF ABBREVIATIONS

Acronyms for cell populations or tissues are preceded by a small letter to indicate the species: r= rat; h=human.

**AFP**: α-fetoprotein

**ALB**: albumin

**CD**: common determinant

**CD44**: hyaluronan receptor

**CD133**: prominin

**CFTR**: cystic fibrosis transmembrane conductance regulator

**CK**: cytokeratin protein

**CS-PG**: chondroitin sulfate proteoglycan

**CXCR4**: C-X-C chemokine receptor type 4 (CXCR-4) also known as fusin or CD184

**DS-PG**: dermatan sulfate proteoglycan

**ECM**: extracellular matrix

**EGF**: epidermal growth factor

**EpCAM**: epithelial cell adhesion molecule

**FBS**: fetal bovine serum

**FGF**: fibroblast growth factor

**FN**: fibronectin

**GAGs**: glycosaminoglycans

**GC**: Glisson's capsule

**HA**: hyaluronans

**HBs**: hepatoblasts

**HDM:** hormonally defined media- serum-free medium with constituents optimizing differentiation for a specific cell type such as liver (HDM-L)

**HGF**: hepatocyte growth factor

**HP-PG**: heparin proteoglycan

**HpSCs**: hepatic stem cells

**HS-PG**: heparan sulfate proteoglycan

**HUVECs**:human umbilical vein endothelial cells

**Hyp**: hydroxyproline

**ICAM1**: intercellular adhesion molecule-1

**iPSCs**: induced pluripotent stem cells

**iPSC-LB**: induced pluripotent stem cell liver buds

**KM**: Kubota's Medium (a serum-free medium designed for endodermal stem/progenitors)

***KRT***: cytokeratin gene

**LA**: laminin

**LGR5**: Leucine-rich repeat-containing G-protein coupled receptor 5 that binds to R-spondin

**MSCs**: mesenchymal stem cells

**NCAM**: neural cell adhesion molecule

**PLA2**: phospholipase A2

**PEG**: polyethylene glycol

**pLBM-HA**: hydrogels containing pulverized liver biomatrix scaffolds and hyaluronans

**SDC**: sodium deoxycholate

**SDS**: sodium dodecyl sulfate

**SEM**: scanning electron microscopy

**SDC**: sodium deoxycholate

**VEGF**: vascular endothelial cell growth factor

**VEGF-r**: vascular endothelial growth factor receptor

# CHAPTER I

## Background

### Need for *Ex Vivo* Human Cell Cultures as Models for Experimental Studies

Various limitations exist in the use of human and animal models in research ranging from a lack in availability of test subjects to the practicality of experimental protocols to handle large amounts of samples and even to ethical issues concerning the test subjects during experimentation. Additionally, the correlation between animal models and humans is often not sufficient to accurately model the clinical efficacy of certain treatments. Human tissues are obviously the ideal candidates for studies relevant to clinical programs, but the paucity of human tissues and the added costs and complications involved in experiments with these tissues results in severe limitations in accommodating the necessary experiments. The need for human model systems is great especially since there are factors associated with individual donors, such as certain genetic disorders and diseases that might be influential to experimental results. All of these issues and more lead to the necessity for human model systems that are standardized, reliable and industrially scalable.

These needs have driven the development of *in vitro* human models for preclinical drug development, for disease mechanism research, as well as for studies on drug efficacy, metabolism, and toxicity. The *in vitro* models provide a more repetitive and quantitative way to investigate the physiology of cells and tissues in drug development and discovery and can be more rigorously controlled in experimentation. They are also typically more cost effective and

efficient as compared to models involving primary cultures of donor tissues and the less reliable animal models, while enabling the possibility of evaluating many different experimental conditions at the same time.

**Development of *Ex Vivo* Cultures**

Monolayer cultures have been the most commonly used models for the study of hepatic cells because of the ease of handling and of assaying the cultures along with the clarity of observing the growth and morphological changes of the cells. However, when hepatocytes are isolated from their natural environment in the liver and cultured *in vitro* on plastic, the hepatocytes lose their differentiated functions within less than a week (11, 12). A variety of media have been used in these systems, which began with media supplemented with serum. Serum supplemented media, used for decades, are being replaced increasingly by supplementation with mixtures of defined and purified hormones and growth factors that form a serum-free, hormonally defined medium (HDM) tailored to the cell type, the maturational lineage stage of interest or the biological goal(s) of the experiment. The HDM have greatly improved cell functions in cultures, since serum is present *in vivo* only when there is a wound and contains factors driving tissues towards scar tissue formation and, therefore, fibrotic reactions (13). The differentiated cells require serum-free conditions to express their tissue-specific functions (11).

The HDM can be optimized for cell growth, for selection of specific cell types or maturational lineage stages, and can be optimized for tissue-specific gene expression. The primary cultures of selected cell populations can be sustained in culture for up to a week in serum-free HDM (11).

Additionally, homotypic and heterotypic interactions between cells have been observed in the co-culture of hepatocytes with non-parenchymal cells to greatly improve their survival and function (14-17). Co-culturing of hepatocytes with mesenchymal cells, ideally those with which that are partnered *in vivo,* has been observed to increase functions (18). More recently,

biomedical engineers have set up lab chips or microfluidics devices with co-culture systems resulting in parenchymal cells that are far more differentiated and last in culture for weeks (19). These are useful in microscale experiments for toxicological or pharmacological studies, but the cell numbers are too small to accommodate most biochemical studies.

In addition to co-cultures with non-parenchymal cells, *in vitro* culture systems of liver have been developed that utilize specific, purified components from the extracellular matrix, such as collagens or fibronectin, or attempt to mimic the native microenvironment through the use of other biomaterials (e.g. synthesized polymers). The use of purified extracellular matrix components in combination with serum-free HDM can enable the cells to be functionally stable for 1-2 weeks (11, 20-23). Other methods include the use of substrata consisting of extracellular matrix proteins to coat culture surfaces or fabrication of “sandwich cultures” in which the parenchymal cells are placed in between two layers of matrix components (24-28). All of these variations of the use of matrix components are helpful to achieve greater levels of differentiation. The phenotypic traits of the mature cells are dependent, in part, on certain matrix components found in the native microenvironment of these cells (24, 29-34). The extracellular matrix components, and factors bound to them, regulate the gene expression of these cells as well as their growth and morphology.

The methods that have seen the most success in the culturing of differentiated cells have been systems with 3D configurations that attempt to mimic the native microenvironment of the tissue *in vivo* as much as possible (35-37). Hepatocytes have been entrapped within a variety of biomaterials (38, 39). Some examples include embedding the cells within matrix components such as Matrigel or collagen-based hydrogels (40-42). Also, primary hepatocytes have been embedded in alginate and gelatin as well as in a PEG-based hydrogel (43-45).

**Organoid Cultures**

In recent years there has been a return to organoid cultures, aggregates of epithelia and their mesenchymal partners that form units of ~1000 cells/unit. These cultures survive for weeks and remain functional, albeit at muted functional levels (~5%) relative to *in vivo* functions. First utilized decades ago particularly with respect to cultures of embryonic tissues, the organoid culture systems were abandoned for decades because of the desire to have cultures derived entirely from a cloned cell population and to have the advantages of visualizing the cells in monolayers. Many investigators are now returning to organoid culture systems due to the increasing recognition of the importance of the epithelial-mesenchymal interactions and their paracrine signals that serve to stabilize the cells and their functions (46). Studies have shown that these types of cultures facilitate the formation of cell configurations and polarities that are closer to those found in the native tissue (47).

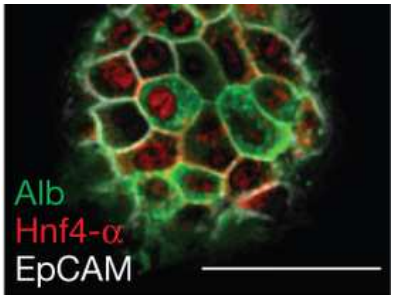


**Figure 1:** Clonal LGR5-derived Organoids (6)

Formation of organoids comprised of aggregates of parenchymal cells, endothelial and stellate cells, have been observed also to improve hepatocyte survival and functions (48-53). These categories of cells have been shown to co-exist *in vivo* and to participate in important cell-cell signaling necessary for proper liver functions that include homeostasis and regeneration (54-59). Interactions between endothelial cells and hepatocytes have been found to be important in the formation of vascular structures that lead to the morphogenesis of the liver (56, 60-62). Hepatic stellate cells have also been shown to participate in extracellular matrix synthesis and to direct signaling with

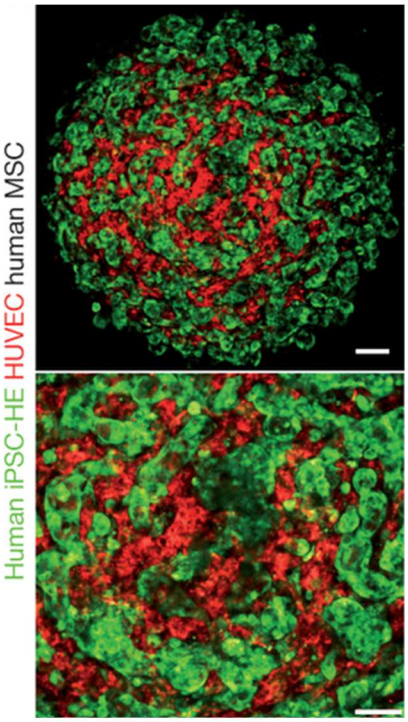


**Figure 2:** iPSCs-derived Liver Buds Co-cultured with HUVECs and MSCs (5)

cholangiocytes and with secondary effects on hepatocytes resulting in the promotion of the formation of various hepatic ultrastructures including desmosomes, bile canaliculi, and tight junctions (49-51). These cellular interactions are essential in regulating cell behavior and in maintaining the proper parenchymal phenotype.

Various investigators have utilized these cellular interactions to form organoids with improved hepatic functions. Huch et al. cultured LGR5-positive hepatic stem cells isolated from fetal livers and biliary ducts of mice in a 3D system consisting of Matrigel with a culture medium that included the Wnt agonist RSPO1, the ligand of LGR5 that promotes hepatocyte and bile duct generation *in vivo* (6). They were able to culture these organoids for up to 8 months. After 1-2 months, these organoids were found to express multiple hepatic-lineage and bile duct markers. These organoids, embedded in Matrigel, were able to attain expression of mature hepatocytic markers after induction with a differentiation medium that included FGF, EGF, and HGF. After these organoids were cultured in this medium for 13 days, the organoids achieved levels of functions that were about 5% of those in mature hepatocytes (e.g. albumin secretion). Thus, the organoids offered 3D cultures that are stable long-term and do preserve some degree of the functions albeit highly muted relative to that *in vivo.*

Takebe et al. were able to create “liver organ buds” *in vitro* from human induced pluripotent stem cells (iPSCs) (5). The endodermal cells that self-assembled into organoids were committed to a hepatic fate after being embedded in Matrigel for 5-6 days. They were able to attain hepatic differentiation of these iPSCs by further culturing the cells in differentiation medium for 3-4 days. These cells were then co-cultured with human umbilical vein endothelial cells (HUVECs) and human mesenchymal stem cells (MSCs) and were observed to self-organize for up to 48 hours after being seeded together. Gene expression showed that the iPSCs that were co-cultured expressed significantly higher levels of early hepatic markers compared to the iPSCs that had been differentiated to a hepatic lineage but cultured alone. The liver buds were transplanted into mice and were observed to connect with the host vasculature

within 48 hours. The hepatic cells within the liver buds proliferated at a high rate *in vivo* and were observed to form hepatic cord-like structures after 2 months. Significant levels of albumin secretion were observed 10 days after transplantation with albumin being secreted at an extremely high rate after 45 days. Gene expression analyses verified these results on the explanted liver bud after 60 days. The functional levels of the iPSC-derived liver buds were high relative to the starting points of the experiments and secreted almost double the albumin secreted by hepatocytes cultured *in vitro* but remained less than those functions of liver buds derived from fetal livers of 22-40 weeks old.

Soto-Gutierrez et al. co-cultured primary mouse hepatocytes with human non-parenchymal cells in Matrigel (62). The non-parenchymal cells included endothelial and stellate cell populations acquired from a variety of sources. They were found to form tube-like structures. The co-cultured hepatocytes were found to migrate to the tubes and remain attached while the hepatocytes that were cultured without these additional cell types formed independent organoids without any connection between them suggesting that these hepatocytes have tendencies to form structures similar to the sinusoids found in the native liver. When comparing hepatic functions, the organoids that were formed from the co-culture of the various cell types were found to have significantly increased albumin secretion after 4 days as compared to the cultures of primary hepatocytes alone. This significant increase was maintained even after 7 days with the spheroids of hepatocytes significantly decreasing in albumin secretion after 5 days. After a week of culture, the organoids were seen to maintain their high level of function.

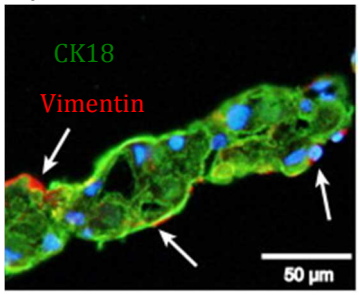


**Figure 3:** Hydrogel Fibers of Rat Hepatocytes Co-Cultured with Swiss 3T3 Cells (4)

Yamada et al. co-cultured primary rat hepatocytes sandwiched with 3T3 feeder cells in Ba-alginate hydrogel microfibers that allowed the formation of heterotypic micro-organoids in order to mimic the structure of the hepatic cords found in the native liver (4). The organoids remained viable after a

month of culture and hepatic functions were found to be significantly increased as compared to traditional cultures. When compared to hepatocytes cultured on a layer of type I collagen and microfiber cultures with only hepatocytes, albumin secretion was significantly improved with the 3T3-hepatocyte co-culture organoids gradually increasing in secretion levels out to 20 days and maintain this level for at least 50 days. The organoids were found to still be secreting albumin after 90 days. These results were consistent in the gene expression analysis of the organoids.

Lu et al. utilized a hollow fiber reactor with a polysulphone-g-poly (ethylene glycol) (PSf-g-PEG) membrane to culture primary rat hepatocytes that self-assembled into organoids along the hollow fibers (63). When compared to monolayer and sandwich culture, these organoids were found to have significantly increased albumin secretion and remained functional for at least 2 weeks. These findings were also verified by gene expression analysis.

Au et al. was able to fabricate arrays of hepatic organoids from the co-culturing of a cell line, HepG2, transformed hepatocytic committed progenitors,  and with NIH-3T3 cells embedded in 3D hydrogel matrices consisting of type I collagen (64). These organoids were cultured for up to 4 days at which point the majority of the cells remained viable. No difference in albumin secretion was found in the first 3 days of culture, but a significant difference was found on day 4 with the cultures containing both cell types secreting much more albumin than the cultures of HepG2 cells alone. This confirmed the importance of the interactions between the epithelial and mesenchymal cells for hepatic functions.

However, organoids are constrained to be miniscale models since large numbers cannot be sustained given the absence of vascular support. Novel forms of organoids that incorporate extracellular matrix chemistry may yield improved and a more stable differentiation of hepatocytes that can be scalable.

**Table 1. Comparison between Current Organoid Culture Methods**

| Species of Parenchymal Cells | Species of Non-Parenchymal cells | Hydrogel Material: Culture Method | Length of Time Cultures Viable | Functionality via Albumin Secretion | Level of Functions Relative to Cultured Isolated Hepatocytes | Reference |
|---|---|---|---|---|---|---|
| LGR5+ Liver Stem Cells (Mouse) | N/A | Matrigel: Embedded | 8 months | d13: Differentiation Medium 7x> Expansion RSPO Medium (Biliary Types)<br><br>d13: Hepatocytes 21x> Differentiation Medium | Albumin Secretion:<br><br>24h Hep 21x> LGR+ SCs D13 in DM | (6) |
| Hepatic-specific iPSCs (human) | HUVECs MSCs (human) | Matrigel: Embedded | >10 days<br><br>>2 months *in vivo* | d10: Co-culture buds>Hep alone<br><br>d45: Co-culture buds>>>Hep alone | Albumin Secretion:<br><br>Transplanted iPSC-LB d45 2x>d15 Hep | (5) |
| Primary Hepatocytes (Mouse) | Stellate TWNT-1 Endothelial TMNK-1 Cholangiocytic MMNK-1 (human) | Matrigel: Embedded | >1 week | d1-7: Co-cultures>Hep alone Increased until Day 5 then decreased | Ammonia & Lidocaine Metabolism:<br><br>Co-cultures>Hep alone | (62) |
| Primary Hepatocytes (Rat) | Swiss 3T3 (mouse) | Alginate: Microfluidic Hydrogel Fibers | 3 months | d1-90: Increased until day 20 then decreased<br><br>d7: Co-cultures>Hep alone<br>High O2>Normal O2 | Albumin Expression:<br><br>Co-cultures>Hep alone<br>Fiber = Plate | (4) |
| Primary Hepatocytes (Rat) | N/A | Collagen I: PSf-g-PEG Hollow Fiber Membrane | >2 weeks | d14: Organoid>Sandwich>>2D | Glucose Metabolism:<br><br>Organoid>Sandwich>>2D | (63) |
| HepG2 (human) | NIH-3T3 (mouse) | Collagen I Digital Microfluidics | >4 days | d4: Co-cultures>HepG2 alone | CYP3A Activity:<br><br>3D>2D | (64) |

In summary, 3D liver organoid cultures are now the dominant culture system under consideration for industry. The long-term viability and maintenance of diverse differentiated functions of these cells show the importance of paracrine signaling between parenchymal cells, endothelia and stellate cells. Some limitations include that they can only be used, due to the lack of vascularization, at a micro- to miniscale basis, and that the differentiated functions are a fraction of those *in vivo.* Although all of them make use of a matrix component(s) or a crude matrix extract such as Matrigel, there has been no systematic exploration of the effects of tissue-specific matrix components or extracts**.**

**The Liver and its Maturational Lineages of Parenchymal and Mesenchymal Cells**

The liver is organized into acini, with each acinus being hexagonal and demarcated by 6 sets of portal triads at the vertices; plates of liver cells extend from the portal triads to a central vein. The phenotypic traits of the cells are distinct in different regions of the liver acinus. The pattern of these traits constitute a maturational lineage of cells extending from the portal triads (zone 1), through the mid-acinar region (zone 2), and ending at the central vein (zone 3). The zonation of functions correlates with the maturational lineages of the cells, beginning with hepatic stem cells, located in special small channels termed “canals of Hering”, next to each of the portal triads in zone 1 (65-68). These

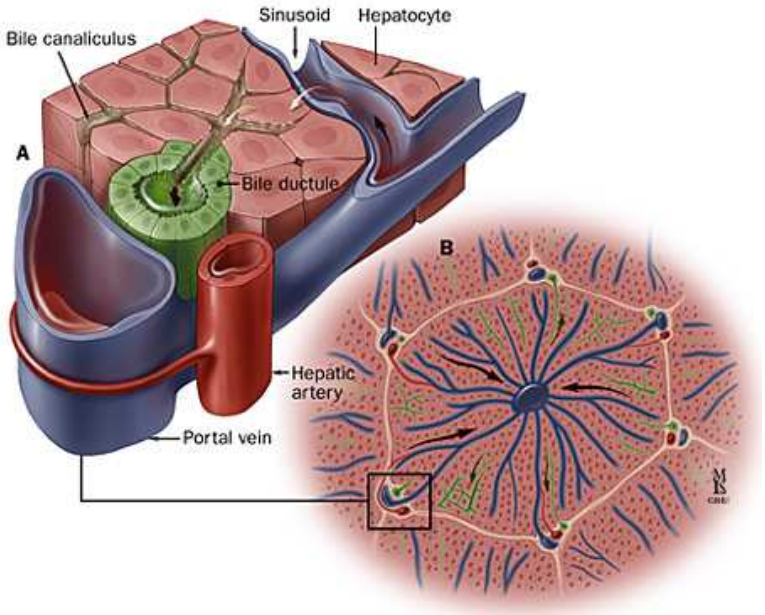


**Figure 4:** Structural Organization of the Liver (1)

differentiate into diploid adult hepatocytes in zone 1, into mature hepatocytes in the mid-acinar zone (zone 2), and into terminally differentiated and apoptotic cells in zone 3. Zone 3 is also the site that is replete with macrophages, found to facilitate aspects of the apoptotic process.

The maturational lineage stages have been defined in more detail in recent years resulting in recognition of at least 10 intrahepatic lineage stages (69, 70). Hepatic stem cells (HpSCs), which are multipotent cells, are known as intrahepatic lineage stage 1 in this classification system and are located within canals of Hering. They give rise to bipotent hepatoblasts (HBs, stage 2) that in turn produce committed hepatocytic and biliary progenitors (stage 3). The diploid subpopulations of the cholangiocytic and hepatocytic lineages (stage 4) are also in zone 1, the primary site for gluconeogenesis. The mid-acinus (zone 2) contains lineage stages 5-7 that can be diploid in humans (but are polyploid in old age) and are always tetraploid in 4-5 week old rats and tetraploid or octaploid in 3-4 week old mice; the mid-acinar hepatocytes are fully mature and able to regulate most tissue-specific genes (e.g. albumin, transferrin, tyrosine aminotransferase) both transcriptionally and posttranscriptionally. The pericentral zone (zone 3) contains terminally differentiated cells that are in lineage stages 8 and 9, and apoptotic cells (lineage stage 10). Humans have terminally differentiated cells that are tetraploid; rats have hepatocytes that are a mix of tetraploid and octaploid; and mice have zone 3 hepatocytes that are 16N to 32N. Zone 3 is the peak site for lipid metabolism and for detoxification enzymes (e.g. P450s). In summary, the plates of liver cells are comprised of different maturational lineage stages each one being defined by a unique set of phenotypic traits that include morphology, cell size, types of mitrochondria, gene expression, and ability to regulate a given gene transcriptionally or post-transcriptionally.

The lineages of parenchymal cells are paralleled by lineages of partner mesenchymal cells. Angioblasts are associated with hepatic stem cells and give rise to endothelial cell lineages associated with the hepatocytes and to stellate/fibroblasts/smooth muscle cell lineages

associated with the biliary cells (71, 72). The paracrine signaling between the epithelia and the mesenchymal cells forms a gradient of factors that are lineage-stage specific.

**Key Phenotypic Traits of the Distinct Lineage Stages of Cells**

The different lineage stages are recognizable by specific biochemical or antigenic biomarkers (67, 73). The hepatic stem cells (HpSCs) express epithelial cell adhesion molecule (EpCAM) throughout the cells and neural cell adhesion molecule (NCAM), enabling their isolation by immunoselection for cells expressing both markers. They also express cytokeratins 8, 18 and 19, a number of endodermal transcription factors (SOX9, SOX17, HES1) and low levels of pluripotency genes (OCT4, NANOG, KLF4). The angioblasts in association with the HpSCs express c-kit, CD133 (prominin), the vascular endothelial growth factor receptor (VEGF-r) and Von Willebrand factor (8, 65-67, 74). The HpSCs account for ~0.5-2% of the parenchymal cells in livers of all donor ages (65).

The HpSCs give rise to hepatoblasts and in parallel, the angioblasts give rise to the precursors of endothelia and stellate cells. The biomarkers for the hepatoblasts include AFP, albumin, EpCAM (localized now to the plasma membrane), intercellular adhesion molecule-1 (ICAM-1), P450 A7, and a loss of the pluripotency genes and of SOX17; their mesenchymal partners include the stellate cell precursors that express CD146 (Mel-CAM), alpha smooth muscle actin (α-SMA), and desmin; the endothelial cell precursors express CD31, CD133, VEGF-r and Von Willebrand factor (8, 65, 66, 69). The majority (>80%) of the parenchymal cells in the fetal liver are hepatoblasts but they rapidly decrease in numbers postnatally. Within a few months of birth, their percentage is <0.01% of all the parenchymal cells (20, 65, 68, 70, 73, 75, 76). Additionally, hepatoblasts express higher levels of albumin localized in discrete packets within the cytoplasm, increased levels of liver-specific genes such as the early P450s and CK7, ICAM-1 instead of NCAM, and have much higher levels of AFP expression (65, 77).

Hepatoblasts can be isolated via dual immunoselection for cells that are positive for EpCAM and ICAM-1 (8).

Lineage stage 3 consists of the committed progenitors, cells that are unipotent for either the hepatocytic or biliary lineage. They no longer express the endodermal transcription factors or the pluripotency genes but instead have hepatocytic or biliary marker expression intermediate between that found in hepatoblasts versus adult parenchymal cells. Although present in significant numbers in fetal livers, they are uncommon in normal adult livers although they can achieve significant numbers in livers of donors with chronic liver diseases (78-80).

The biliary committed progenitors give rise to small cholangiocytes (lineage stage 4) that express muscarinic acetylcholine receptor M3, histamine H1 receptor, and cystic fibrosis transmembrane conductance regulator (CFTR). They do not express anion exchanger 1 (Band 3), receptors for secretin or somatostatin, nor any hepatocytic genes. Large cholangiocytes have more rough endoplasmic reticulum as compared to small cholangiocytes (80). These cells line the interlobular ducts in the portal triads and the larger intrahepatic ducts. Like small cholangiocytes, they express CFTR but they also express anion exchanger 1 (Band 3) and receptors for secretin and somatostatin. (80, 81).

Lineage stage 4 hepatocytes, called small hepatocytes (17-21 μm) are all diploid and are bound together on their lateral borders enabling them to form plates or cords of cells (82-84) recognizable by the glucogenesis dominant in this region and for particular connexins (connexin 28). By zone 2 (lineage stages 5-7 cells), the plates of liver cells are distinctive in their relationship with the endothelia that are increasingly fenestrated (that is, have gaps) allowing plasma to contact the hepatocytes directly. The mid-acinar cells have production of specific elongation factors needed to translate transferrin mRNA among other factors to produce detectable levels of the protein even though the mRNA is already expressed in all earlier lineage stages (69, 85-87). Additionally, hepatocytes at these stage produce especially high levels of albumin and tyrosine aminotransferase due to their peak expression of transcription

factors associated with the regulation of the protein (88, 89). These hepatocytes have the highest activities in gluconeogenesis, urea synthesis, glutathione peroxidase, and the metabolism of amino acids and ammonia (90).

Hepatocytes in lineage stages 8-9 are located pericentrally (zone 3) and are in association entirely and only with fenestrated endothelial cells. They can synthesize DNA but do not undergo cytokinesis and so become polyploid, of which a subset are undergoing apoptosis (91, 92). The pericentral hepatocytes express albumin, transferrin, tyrosine aminotransferase, glutathione transferases, heparin proteoglycans and the late P450s (93). Kupffer cells are found in high abundance pericentrally and are in association with the apoptotic cells (92).

**Extracellular Matrix Composition**

The extracellular matrix (ECM) is an insoluble complex of components secreted by all cells and is located outside of the cells; the ECM forms the chemical scaffolding for the cells in a tissue or organ. These components are important for intracellular communication via cell-cell connections, induce the polarization of cells (94) and provide signals dictating gene expression and differentiation (95).

The major components of all ECMs are collagens, which are the insoluble proteins that form the framework of the ECM. There are over 25 types of collagens identified. The ECM of the liver is typical of organs in which the majority of the collagens consist of type I, III, IV, V, VI and XVIII (96). Bound to these collagens are numerous other insoluble components that include attachment proteins (multiple forms of laminins and fibronectins) and proteoglycans. These proteoglycans have a core protein to which are attached glycosaminoglycan (GAG) chains, which are sulfated polymers of uronic acid-amino sugar dimers (97). There are some proteoglycans, such as perlecan, that are present in the ECM but are not bound to cell membranes. There are also forms of proteoglycans that are associated with the membranes such as syndecans and glypicans. All of the GAGs are chemical scaffolds for signaling

molecules such as growth factors and cytokines that dictate which receptor(s) these signals bind and/or influence facets of the signal transduction process. Also present are specialty molecules such as fibrillin. They are components of microfibrils to which are bound elastin, a key component in a tissue's elasticity, and nidogen (also called entactin), a sulfated glycoprotein bound tightly to laminin (98-100).

The collagens are molecules consisting of 3 amino acid chains woven together in a braid-like structure in the regions comprised of *glycine-proline-X*. These form a triple-helical region that is very stable with globular domains at the ends of the collagen molecules and with amino acid sequences that are distinct for each collagen type. The molecules are synthesized and subsequently modified by posttranslational processing mechanisms to have one or both globular domains eliminated, and with various other modifications that guide fibrollogenesis into collagen fibers. The different types of collagen fibers are the result of multiple collagen molecules organized in fibrillar structures. The collagens, especially the fibrillar collagens, provide mechanical stability and tensile strength to the ECM particularly in the direction and orientation of the fibers (99, 101).

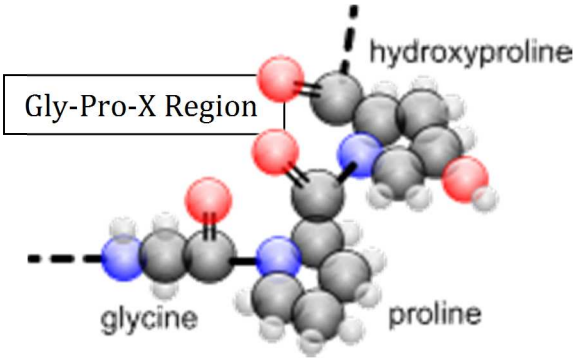


**Figure 5: Fibrillar Collagens.** The 3 amino chains can be identical (homotrimers) or distinct (heterotrimers). Each of the more than 20 fibrillar collagen types has a unique amino acid sequence. The fibrillar collagens offer greater mechanical support than network network collagens and primarily in the orientation of the fiber (2).

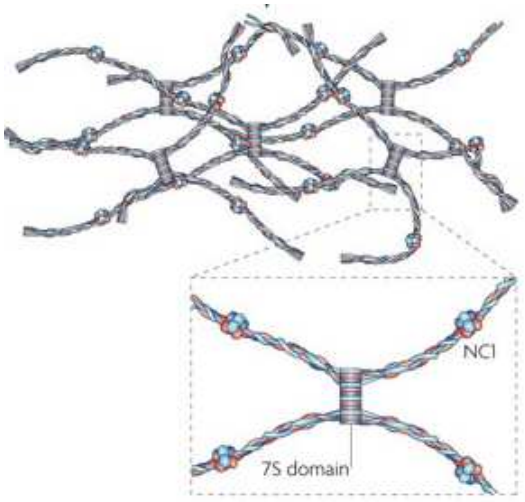


**Figure 6: Network collagens.** 7S domain is the site to which laminin is bound. These collagens form a single collagen molecular layer adjacent to cells and offer flexible in all directions (3).

Exceptions occur for the network collagens (e.g. collagen types IV and VI) that keep both

globular domains and then form a single molecular layer of a net-like structure that connects to cells via specific attachment proteins such as one of the 15 known forms of laminin. Type I collagen has 5 molecules per fibril and confers the greatest tensile strength; it is found in sites requiring stability and mechanical strength. Type III collagen is chemically very similar to type I collagen but has fewer molecules per fibril and forms delicate fibers (also known as reticulin) that provide a "nesting" framework for cells. This molecule is present throughout the liver plates. Type V collagen is found in sites of active growth and is often in complexes with type I. Type IV and VI collagen form single molecular layers that are present in the basal lamina. Type XVIII combines properties of collagens and proteoglycans and has bound heparan sulfate chains; it is associated with basement membranes of endothelia.

The attachment proteins include multiple classes, but two of the most common are laminin, for which there are at least 15 known isoforms, and fibronectins, which are also found in multiple isoforms. Two of the major ones are tissue fibronectin, which have cell binding domains, and plasma fibronectin, devoid of cell binding domains and found in blood and lymph.

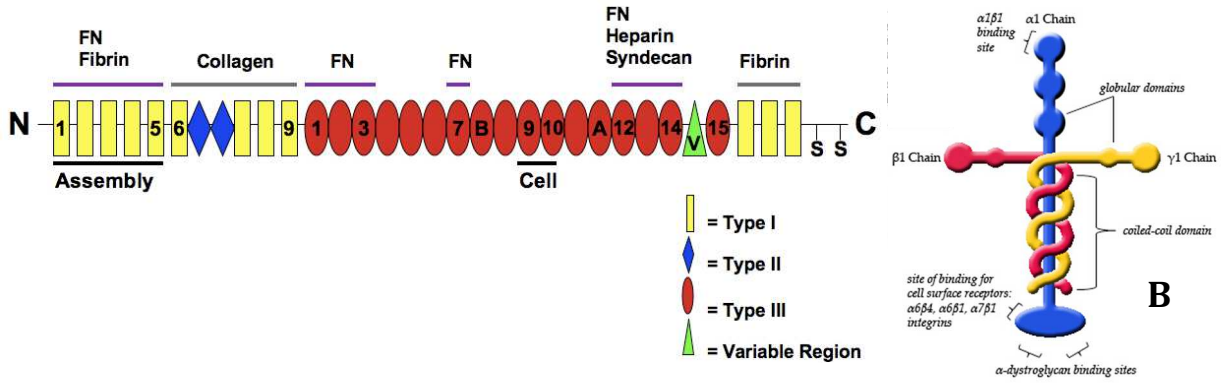


**Figure 7: Families of attachment proteins:** fibronectins (a) and laminins (b). Both have cell binding domains and sites at which other matrix molecules can attach. The attachment proteins have various signals (e.g. EGF) hardwired" into their aminoacid sequence. Therefore, dissolution of these proteins releases the signals into the local microenvironment (9, 10)

These various components of the ECM bind cells to specific cell receptors (e.g. integrins). Elastin and fibrillin are part of the microfibrils that are also responsible for many of the mechanical properties of tissues and bind to other ECM molecules, including some collagens and proteoglycans. Fibronectin is secreted by cells and is central to the stability of the ECM.

This adhesion molecule is also important in the cell growth and contractility that is dependent on cellular adhesion (102-104). The fibrils of fibronectin are formed by the polymerization and deposition of this molecule, which control the deposition of collagen I and III (102-104).

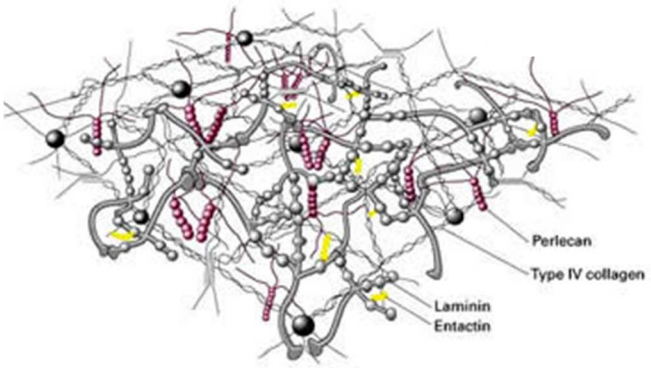


**Figure 8:** The various matrix molecules aggregate to form an insoluble complex adjacent to cells (1)

**Organization of the Liver ECM in Chemical Gradients Correlated with Liver Histology**

The Glisson's capsule around the liver and periportal regions have a basement membrane that consists of collagens IV and VI, laminin, nidogen, and perlecan. The portal space interstitium contains types I, III, IV, V collagen, and fibronectin (97). These molecules have specifically been seen to localize around areas that include the basement membranes beneath the endothelial lines of hepatic arteries, portal veins, around bile ducts, lymphatic vessels and nerve axons (105). Collagen IV has also been found to be around the central vein and in the Space of Disse (105). Fibronectin is absent around the lymphatic vessels and bile ducts but is found throughout the liver plates (106). Elastin can be found in the vasculature and the Glisson's capsule (106). Collagen IV and fibronectin are the only matrix molecules found across all the acini between the liver cell plates and the endothelial lining but also around the central vein in the sinusoidal lining (105).

Fibrillar structures with type I, III, and V collagen have specifically been seen to localize around the portal triads, ductal plates, hepatic cords, framework of the sinusoids, Glisson's capsule, and the canals of Hering (106). Collagen IV, laminin, and nidogen have been seen in the basement membrane and around the portal triads (106). The space of Disse located between the sinusoidal endothelial cells and the hepatocytes lacks the continuous laminin, perlecan, and entactin/nidogen found in the majority of basement membranes whereas type III

and IV collagen along with fibronectin are abundant (105, 107). A continuous network of collagen I fibers connect the lobular areas to the adjacent portal tracts (97). Collagen VI fibers are found primarily in the portal spaces and form continuous layers in the sinusoids while collagen XVIII is also found in the basement membranes (97, 107).

The liver ECM in the canals of Hering is comprised of hyaluronans (HA), non-sulfated or minimally sulfated glycosaminoglycans (GAGs), primarily chondroitin sulfates, along with minimally sulfated forms of proteoglycans (PGs). Outside of these niches, the proteoglycans have sulfated GAGs that include heparan sulfates (HS) and heparins (HPs), which are polymers of glucuronic acid and glucosamine, as well as chondroitin sulfates (CS) and dermatan sulfates (DS), which are polymers of glucuronic acid and galactosamine (108, 109). Although these are all found throughout the liver, the HS-PGs and HP-PGs are dominant with respect to the hepatocytes and with the extent of sulfation increasing with proximity to the central vein. The CS-PGs and DS-PGs become more dominant with respect to the biliary lineages. CS-PGs and DS-PGs are secreted by lipocytes, while HS-PGs and HP-PGs are secreted by both hepatocytes and lipocytes. These PGs are localized predominantly in the Space of Disse between the hepatocytes and the endothelia, and are important for inducing cell polarity, facilitating communication via gap junctions, and in regulating tissue-specific gene expression (83, 110). The HS-PGs/HP-PGs specific to the liver include perlecan, syndecans, glypicans, and fibroglycan. Perlecan is not in contact with the plasma membrane of the cells but is known to be a reservoir of various signals that are bound to its GAGs; localized secretion of particular enzymes result in the release of signals to the microenvironment. This molecule is known to affect cell migration, proliferation, and differentiation by facilitating cell signaling that is mediated with the activation of various growth factors (101). Syndecans are proteoglycans that have core proteins that are transmembrane; glypicans are bound to the plasma membrane via phosphotidyl inositol linkages. These proteoglycans are the most active in regulating signal transduction processes by influencing which receptors are available for particular signals and for

influencing facets of the signal transduction processes that regulate cell growth and differentiation (101). Fibroglycan is also localized in the basement membrane and has also been seen to have a role in the development of the liver (110).

**Extracellular Matrix Gradients in Fetal versus Adult Livers**

The liver is an incredibly dynamic organ that changes throughout fetal development and there are variations in the proportions of matrix molecules in the fetal liver as compared to a mature liver. The fetal liver can be characterized as labile and is predominantly comprised of type III, IV, and V collagens as well as laminins, hyaluronans and minimally sulfated proteoglycans. Mature livers are much more stable and have a distinct matrix molecule composition that consist of type I, III, IV, V, VI and XVIII collagens as well as fibronectins, laminins, and the proteoglycans. The matrix chemistry in the stem cell niche is only partially defined but include hyaluronans, type III collagen, fetal forms of laminins (e.g. laminin 5) and minimally sulfated CS-PGs. The cells that are immediately outside of the stem cell niche (e.g. hepatoblasts) are associated with hyaluronans, type IV and V collagens, fetal laminins and minimally sulfated forms of HS-PGs. With progression across the acinar plates, there is an increase in more sulfated HS-PGs that qualify as HP-PGs at sites near the central vein. Such gradients in the matrix appear in the second and third months of gestation in humans (106, 111, 112).

Zone 1 has a matrix composition similar to that in fetal livers and primarily consist of type III and IV collagen, laminin, HA, and minimally sulfated proteoglycans including HS-PGs and CS-PGs (113-115). The midacinar region (zone 2) can be characterized by a decrease in type IV collagen, laminin, and the minimally sulfated HS-PGs with an increase in type III collagen and heparin PGs (115). Zone 3 is the region surrounding the central vein and contains the most mature hepatocytes. This zone is comprised of fenestrated endothelia with a matrix chemistry primarily comprised of heparin PGs (113, 115).

**Tissue-specific Extracellular Matrix Extracts Generated by Decellularization Methods**

Organs and tissues can be decellularized to provide a matrix extract that reproduces the tissue-specific *ex vivo* environments used in directing and maintaining the differentiation of both mature and stem/progenitor hepatic phenotypes *in vitro* (8, 116-118). Isolated extracellular matrices, prepared by the decellularization of organs, provide important sets of these regulatory signals to the cells and act as a more native substratum than tissue culture plastic, purified individual matrix components (e.g. collagen or fibronectin), and even mixtures of matrix components (119-121). The importance of the interactions between the complexity of the extracellular matrix and cells has been confirmed and further investigated in a variety of tissues and organs (122-126). However, further studies need to be performed to determine how this decellularized matrix can be best utilized to support the *ex vivo* maintenance of these cells. Liver scaffolds generated by a variety of decellularization procedures have been recellularized with hepatocytes in hopes of culturing the cells in an environment that mimics the native liver as close as possible (127-130).

The use of decellularized tissue in the culture of cells allows for a more natural representation of the various biological, chemical, and mechanical properties found in the native liver. The process of decellularization maintains the structural integrity of the organ while preserving the necessary molecular components important in maintaining cell viability and function in an acellular scaffold (7, 131-134). Success of these decellularization procedures has implications in the use of these scaffolds not only in the culture of cells but also in the future for organ transplantation of liver lobes prepared by using a human liver scaffolds recellularized with human cells and perhaps even autologous cells (135).

The various decellularization procedures that have been developed can be classified as physical, enzymatic, or chemical. Some mechanical procedures include agitation, sonication, and freezing. Enzymatic procedures include the use of trypsin, endonucleases, and

exonucleases. Chemical procedures used have included acidic or alkaline solutions as well as ionic, non-ionic, and zwitterionic detergents among others. These procedures each result in a scaffold with distinct sets of matrix molecules at varying concentrations (134). Procedures that utilize alkaline and acidic solutions typically remove the majority of the cellular components while preserving the structural integrity and the collagens but eliminate important molecules such as the GAGs (136-138). The use of non-ionic solutions such as Triton X-100 has been shown to remove all the GAGs in certain tissue types (139). Decellularization with this solution has also led to the loss of laminin and fibronectin, cellular material remaining after treatment, and the alteration of certain mechanical properties (139). Ionic detergents such as SDS also often lead to mechanical deformation and the removal of the GAGs while preserving the collagens (140) but the SDS binds tightly to the matrix extract and can be toxic. Another ionic detergent utilized is sodium deoxycholate (SDC), a bile salt that at low concentrations is reasonably gentle (141, 142). CHAPS, a zwitterionic solution, changes the mechanical integrity of the scaffold (143).

The procedures that have seen the most success in the decellularization of organs generally utilize a combination of these solutions. Uygun et al. and Ott et al. have utilized a combination of SDS, Triton X-100, and water to fully decellularize the heart and liver tissue respectively (127, 144). The decellularized heart retained most of the cross-linked type I and III collagens, laminin, fibronectin, and GAGs but the non-crosslinked collagens and nascent (newly synthesized) collagens and factors bound to them are lost. Additionally, some (but not all) of the structural properties were preserved.

Decellularization of the liver with these solutions resulted in a scaffold that retained most of the cross-linked type I and IV collagens and fibronectin (127). However, only 50% of the GAGs remained and the majority of the laminin was lost. Baptista et al. utilized a combination of Triton X-100 with ammonium hydroxide and long washes with distilled water to fully decellularize the liver (7). The scaffolds retained essentially none of the non-crosslinked

collagen and some of the cross-linked type I, III, and IV collagen, laminin, and fibronectin. In summary, all of these procedures retain subsets of the matrix components, primarily those that can survive low ionic strength buffers or distilled water.

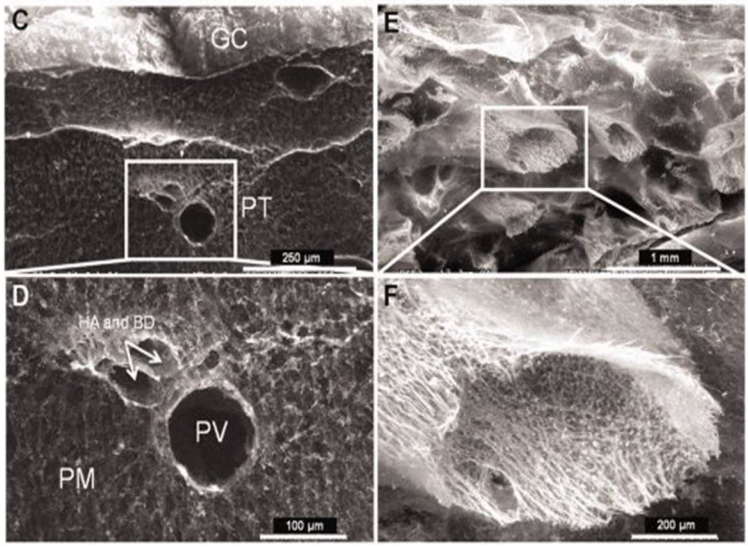


**Figure 9:** Matrix scaffolds prepared by delipidation followed by distilled water rinses. The procedure isolates the cross-linked collagens and factors bound to them. Most of the attachment proteins and the proteoglycans are missing making it difficult to get cells to attach during the recellularization process and requiring weeks to achieve differentiation of the cells. However, the vascular channels are patent (7).

The most successful procedures have been a protocol derivative of the methods of Ted Miller (145, 146), a collagen chemist at the University of Alabama and who made use of buffers with specific salt concentrations to keep collagens insoluble. He prepared extracts with high salt buffers keeping all the collagens insoluble and then used a stepwise dilution of the buffers to isolate specific collagen types in solution. This strategy was used with great success to isolate specific collagen types. Rojkind et al. utilized a protocol derived from these methods to isolate matrix extracts that could be used for cell culture (147). This sequential solubilization of the tissue resulted in a scaffold that retained >85% of the native collagens including the cross-linked and uncross-linked collagens plus some of the nascent collagens. Frozen sections of the matrix extracts, called “biomatrices”, were used as substrata for the culture of liver cells and were able to keep the cells viable and functional for more than a year in culture. The cells did not grow unless the biomatrices were prepared from regenerating liver (148).

This protocol was further improved by modifications reported by Wang et al. who used a very gentle delipidation step that combined dilute sodium deoxycholate (a bile salt) in combination with phospholipase A2. Delipidation was achieved in 10-20 minutes, which was then followed by a sodium chloride buffer with a concentration ranging from 3.4-3.5M needed to keep all of the collagens in the liver insoluble (8). The resulting enriched matrix extract, termed biomatrix scaffolds, retained >98% of the collagens (of all known collagen types in the liver and including the cross-linked, non-crosslinked, and nascent forms) as well as all of the known adhesion molecules (fibronectin, laminin, nidogen). Also retained was elastin and all of the known proteoglycans. Although GAGs not bound to PGS were lost, those associated with the PGS were retained resulting in the ability to preserve physiological levels of all known cytokines and growth factors (including more than 60). Moreover, the location of the various factors correlated with the histology of the tissue.

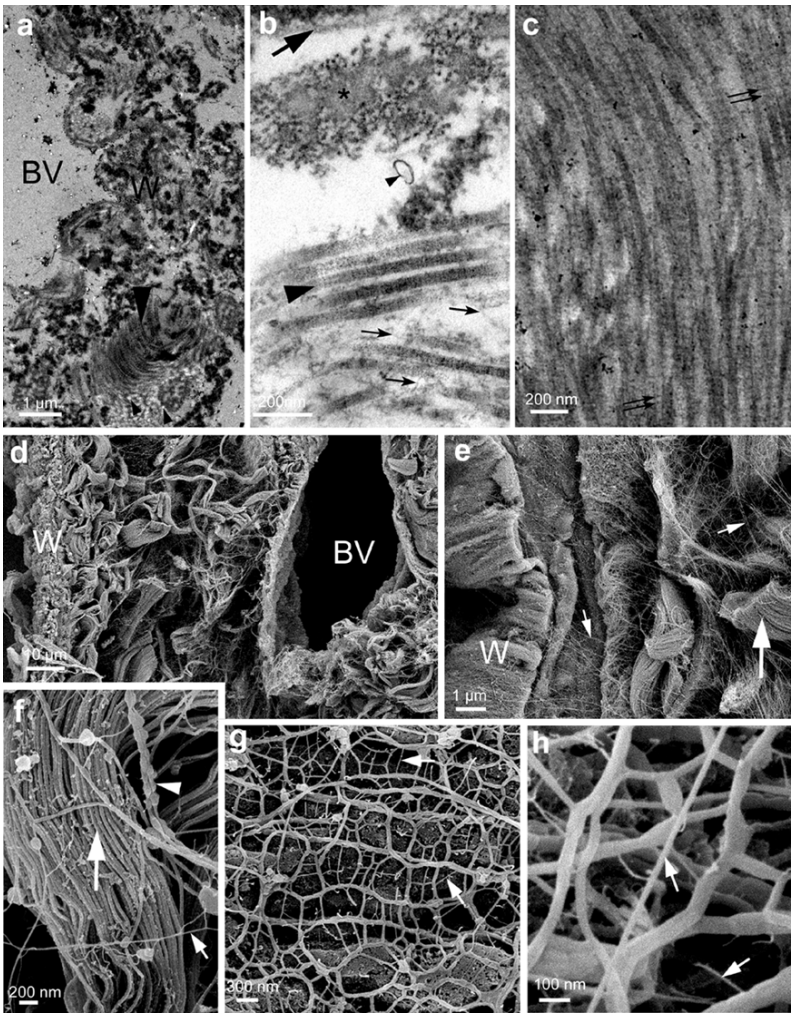


**Figure 10:** Biomatrix scaffolds prepared by gentle delipidation and high salt buffer washes. The matrix extract contains essentially all of the collagens (>98% of cross-linked and non-cross-linked as well as nascent collagens) and all factors bound to them (fibronectins, laminins, nidogen, proteoglycans, etc.). Notice the complexity of the matrix and the diverse types of matrix components present. The vascular channels are patent. Cells attach within minutes and differentiate within a few days (8).

# CHAPTER II

## Motivation for Studies on Imaging Techniques

Tissue engineering research is a multidisciplinary effort that incorporates the use of resources from various fields to address specific problems more efficiently and effectively. This approach has enabled the research in this field to become more rigorous and has accelerated the progression of these technologies from *in vitro* and animal studies to quickly becoming realized in clinical applications. As these technologies are developed and improved, the fabrication or isolation of the biomaterials used in these studies becomes increasingly complicated and requires more sophisticated tools of evaluation. To properly develop advanced tissue engineering constructs, versatile imaging methods are needed that allow the evaluation and monitoring of morphological changes in the construct while acquiring functional and molecular information. Many current studies still utilize the traditional tools of imaging that include the typical histological techniques. However, these methods are limited in the information they can provide particularly when utilized in preclinical studies. The visualization of these matrix extracts with the traditional methods is done typically with an endpoint assay (e.g. histology, immunohistochemistry, electron microscopy) and necessitates the destruction of the sample. This severely limits the ability for researchers to gather information during experimentation. Improved imaging techniques have been developed using ultrasound and are being used in the evaluation of tissue engineering constructs. We demonstrate here the use of

such novel ultrasound technologies – ones that are non-invasive and non-destructive in the evaluation of biomatrix scaffolds.

The biomatrix scaffolds that were produced by the protocols from Wang et al, 2011 were subjected to imaging using novel ultrasound imaging technologies developed in Dr. Paul Dayton's laboratory at UNC. Biomatrix scaffolds preserve the most matrix components of any known scaffold preparation and are unique in preserving the components in accurate histological locations. In this publication, we analyzed the biomatrix scaffolds to assess facets of their complexity both macroscopically and at levels close to capillary beds.

## CHAPTER III

## Functional Ultrasound Imaging for Assessment of Biomatrix Scaffolds Used for Liver Organoid Formation[1]

### Synopsis

A novel form of 3D functional ultrasound imaging has been developed to enable non-destructive assessment of extracellular matrix scaffolds that have been prepared by decellularization protocols and are intended for recellularization to create organoids. A major challenge in organ decellularization is retaining patent microvascular structures crucial for nutrient access and functionality of organoids. The imaging method described here provides statistical distributions of flow rates throughout the tissue volumes; 3D vessel network architecture visualization; characterization of microvessel volumes and sizes; and delineation of cells from portal circuits. The imaging protocol was tested on biomatrix scaffolds that are tissue-specific, but not species-specific, matrix extracts, prepared by a process that preserved >98% of the collagens, collagen-associated matrix components, and matrix-bound growth factors and cytokines. Image-derived data are discussed with respect to assessment of scaffolds followed

---

[1]This chapter previous appeared as an article in *Biomaterials*. The original citation is as follows: Ryan C. Gessner, Ariel Hanson, Steve Feingold, Avery Cashion, Ana Corcimaru, Bryant Wu, Christopher Mullins, Stephen R. Aylward, Lola Reid*, Paul A. Dayton*. (*co-equal senior authors). New Ultrasound Perfusion Imaging Techniques Enable Functional Assessment of Matrix Scaffolds for Human Organoid Formation**. *Biomaterials*** 2013; 34(37):9341-9351.

by proof-of-concept studies in organoid establishment using Hep3B, human hepatoblast-like cells. Histology showed that the cells attached to scaffolds with patent vasculature within minutes; achieved engraftment at near 100%; expressed liver-specific functions within 24 hours; and yielded evidence of proliferation and increasing differentiation of cells throughout the two weeks of culture studies. This imaging method should prove valuable in analyses of such matrix scaffolds.

**Introduction**

Liver transplantation is the primary treatment for end-stage liver disease (149). Currently, more than 16,000 adults and children are on the national list for liver transplants. Unfortunately, the number of livers available for transplantation are approximately 5-6,000/year (150). An alternative to organ transplantation is to support patients using an extracorporeal liver assist device (LAD). A LAD is a bioreactor comprised of liver cells isolated from donor livers and incorporated into a network of hollow dialysis fibers that mimic blood vessels, which is able to connect to the patient and thus able to serve as a bioartificial liver (151, 152). Such bioartificial liver devices provide temporary relief for one to two weeks or until an organ is available for transplantation. They cannot be used longer, since liver cells seeded into all extant forms of bioreactors attach and deposit extracellular matrix and other cellular components onto the hollow fibers, causing “fouling” or clogging of the fibers’ pores, limiting the life span of the device (153).

A more robust alternative is to develop human liver organoids that can be incorporated into a LAD to enable hemodialysis; this provides a more stable and fully functional bioartificial liver in which vascular channels are provided by the native extracellular matrix components lined by endothelia. The organoids can be formed by preparing matrix scaffolds from decellularized livers and then recellularizing the scaffolds with human cells. Biomatrix scaffolds, a particularly rich form of extracellular matrix extract [15], can be recellularized in two stages:

first, the vascular channels are recellularized with endothelia through which medium and then blood can be perfused; and second, the rest of the matrix is recellularized with a combination of hepatic and mesenchymal stem cell populations that will mature into fully functional liver parenchymal cells along with their mesenchymal cell partners. Current efforts are making use of human hepatic cell lines for human liver organoid formation to establish optimal recellularization protocols. Successful protocols will then be used with freshly isolated human hepatic and mesenchymal stem cell populations and endothelia.

For recellularized scaffolds to yield a human liver organoid able to support patients as a bioartificial liver, cell functions must be comparable to those of normal human livers. Since cell seeding and organoid functionality are directly related to the patency and structure of microvascular matrix remnants in the scaffold, there is a crucial need for non-destructive assessment of the structural characteristics of the scaffold, particularly its vascular matrix. Without adequate perfusion, the process of reseeding biomatrix scaffolds with new cells cannot be accomplished, since this process relies on fluid transport through the matrix remnants of the vascular bed for the delivery of the cells. Also, after cells have been engrafted throughout the scaffolds, their continued functions depend on a long-term delivery of nutrients and oxygen. For this reason, a method to image both the anatomy and flow within the sample in a non-destructive manner is highly desirable.

There are many methods currently employed to image tissue scaffolds, including scanning and transmission electron microscopy (SEM and TEM), optical microscopy (154), magnetic resonance (MR) imaging and microscopy (155), computed tomography (CT) (156), optical coherence tomography (OCT) (157), and Doppler ultrasound (158). The selection of any one modality will always yield inherent tradeoffs such as cost, invasiveness to the sample, field of view, resolution, acquisition time, and type of information gleaned. From this list, the imaging modalities that can non-invasively image a 3D scaffold with a significant thickness are MR, CT, and ultrasound. MR and CT are widely available in both clinical and research contexts. These

modalities have the best field of view, although they require expensive hardware (particularly MR imaging). MR can also require long image acquisition times. On the other hand, CT suffers from poor soft tissue contrast and can cause radiation damage to cells. Ultrasound has many benefits over MR and CT in that it is real-time, relatively inexpensive, non-invasive, does not use ionizing radiation, and has excellent soft-tissue contrast. In addition, ultrasound is able to assess multiple different qualities of a tissue volume (applicable to both *in vivo* volumes and *in vitro* biomatrix scaffolds), including tissue structure with standard b-mode (159), mechanical stiffness (160), microvascular perfusion architecture (161), and parametric perfusion rate (162). One possible challenge hindering ultrasound's utility for scaffold perfusion assessment to date has likely been the modality's limited field of view, allowing for freehand visualization of different 2D slices, or small 3D sub-volumes, but traditionally not visualization or quantitation of a large field of view. Our objective in this study was to explore the application of ultrasound to perform 3D visualization and quantification of perfusion throughout a biomatrix scaffold.

In these studies, we have developed a protocol to enable detailed assessment of vascular structural and functional characteristics within scaffolds in a non-destructive manner. We have had two objectives: the first has been to explore the application of ultrasound to perform 3D visualization and quantification of perfusion throughout an extracellular matrix scaffold, here being biomatrix scaffolds; the second has been to demonstrate using of an hepatic cell line, Hep3B, that the imaging assessments can identify scaffolds that will be successful for cell seeding and nutrient delivery to create human liver organoids.

## Materials and Methods

### Decellularization of Rat Livers

Wistar rats (weights 250-300 g) were obtained from Charles River Laboratories, Wilmington, MA, and housed in animal facilities handled by the University of North Carolina (UNC) Division of Laboratory Animal Management. They were fed ad libitum until used for

experiments. All experimental work was approved by and performed in accordance with the UNC Institutional Animal Use and Care Committee guidelines.

The protocol for decellularizing livers to produce biomatrix scaffolds has been described previously (8). Images of tissue in the process of decellularization are given in the online supplement **Figure S1,** and results using this protocol are compared to results using other decellularization protocols (**Table S1)**. Male rats were anesthetized with Ketamine-Xylazine, and their abdominal cavity opened. The portal vein was cannulated with a 20-gauge catheter to provide a perfusion inlet to the vasculature of the liver, and the vena cava was transected to provide an outlet for perfusion. The liver was removed from the abdominal cavity and placed in a perfusion bioreactor. The blood was removed by flushing the liver with 300 ml of serum-free DMEM/F12 (Gibco, Grand Island, NY). A delipidation buffer, comprised of 36 U/L of phospholipase A2 in 1% sodium deoxycholate (Fisher, Pittsburgh, PA) was used to remove plasma and nuclear membranes, and was perfused through the liver for ~30 minutes (up to an hour) or until the tissue became transparent.

This was followed by perfusion for 90 minutes with a high salt buffer (NaCL). Solubility constants for known collagen types in liver are such that 3.4 M NaCL is adequate to keep them all in an insoluble state, along with any matrix components and cytokine/growth factors bound to the collagens or the collagen-bound matrix components. The liver was rinsed for 15 minutes with serum-free DMEM/F12 to eliminate the delipidation buffer and then followed by perfusion with 100 ml of DNase (1 mg per 100 ml; Fisher, Pittsburgh, PA) and RNase (5 mg per 100 ml; Sigma Aldrich, St. Louis, MO) to remove any residual contaminants of nucleic acids from the scaffold. The final step was to rinse the scaffolds with serum-free DMEM/F12 for 1 hour to eliminate any residual salt or nucleases. Images are provided in **Figure S1**. The decellularized liver scaffolds were stored overnight at $4^0$C and perfused with serum-free DME/F12 basal media at 3 ml/min via a peristaltic pump (Masterflex, Cole-Parmer, Vernon Hills, IL) before the imaging study was performed. Prior to an imaging study, the scaffold was transferred from the perfusion

bioreactor into the sample imaging chamber (**Figure 1**). When in the sample imaging chamber, perfusion was maintained at 4 ml/min through the matrix scaffold remnant of the portal vein via the same peristaltic pump.

**Contrast Imaging**

An overview of the image data processing workflow is provided (**Figure 2**). Flash replenishment imaging was performed using an Acuson Sequoia 512 equipped with a 15L8 transducer (Siemens Medical Solutions USA Inc, Mountain View, CA). The "CPS Capture" software algorithm was used to measure perfusion time. The 3D images of the liver biomatrix scaffold were acquired by scanning the transducer in the elevational direction using a linear stage and motion controller (UTS150PP and ESP300, Newport, Irvine, CA) interfaced through LabVIEW (National Instruments, Austin, TX) as described by Feingold et al (162). Perfusion images were parametrically mapped to contrast arrival times between 1 and 10 seconds. These images were stored in DICOM format with JPEG compression and analyzed offline in MATLAB (Mathworks, Natick, MA). Perfusion times within the regions of interest were assessed.

Acoustic angiography was performed on a prototype dual frequency probe (163) with imaging parameters previously described (161). The imaging system was a VisualSonics Vevo770 (Toronto, ON, Canada), with pulses emitted at 4 MHz at 1.23 MPa, and echoes received on a 30 MHz transducer with 100% bandwidth after being passed through a 15 MHz high pass filter to remove non-contrast signal. Three-dimensional images were acquired with the VisualSonics 1D linear motion stage with inter-frame distance of 100 μm to yield nearly isotropic voxels. Images were acquired with a frame rate of 2 Hz, with 5 frames averaged at each location. High resolution b-mode images were also acquired with the Vevo770 system using the same imaging parameters, except the transmit frequency changed to 30 MHz. After imaging, data was exported from the ultrasound system as 8 bit uncompressed AVIs. The microvessels were then segmented from these images using an algorithm originally designed for human

magnetic resonance angiography images, as previously demonstrated by our group (161). These segmentations yielded XYZ points with subvoxel spacing along vessel centerlines, with estimates of vessel radii at each location. These segmentations were used to assess vessel network architecture.

All three scaffold samples imaged required the registration of multiple sub-volumes for holistic visualization. Perfusion rate information required two sub-volumes for all samples, while the anatomical information and acoustic angiography data required three sub-volumes for sample #1, and two for samples #2 and #3. Once completed, the acoustic angiography data was displayed via maximum intensity projections (MIPs) (**Figure 3)**. Anatomical b-mode data cannot be displayed in this fashion, so XZ slices through the merged volumes were displayed.

**Imaging the Biomatrix Scaffolds**

Image acquisition for each sample (**Figure 4, Panels 1 and 2**) required approximately 50 minutes total, due to the small step sizes used in each case to obtain high resolution images (800 μm steps for the anatomical and perfusion images, and 100 μm steps for the acoustic angiography). Standard grayscale ultrasound images provided reference for the scaffold "anatomy" but provided no functional information. Acoustic angiography provided high-resolution images of the branching microvasculature structure, with no tissue background. Perfusion imaging provided spatial distributions of local flow rates (images not shown). All image sets were co-registered using major anatomical landmarks. Total field of view for the regions of interest acquired was approximately 4 x 4 x 3 cm (axial x lateral x elevation) for the anatomical and perfusion images, and approximately 4 x 3 x 1.4 cm for the acoustic angiography.

**Scanning Electron Microscopy (SEM)**

Samples of normal rat liver versus rat liver biomatrix scaffolds were fixed with 4% buffered formaldehyde and examined by SEM at high vacuum (Quanta 200 Field Emission Gun, FEI™, Hillsborough, OR) at the Chapel Hill Analytical and Nanofabrication Laboratory on the UNC campus.

**Recellularization of Biomatrix Scaffolds**

Biomatrix scaffolds with intact vasculature were seeded with human hepatoblast-like cells, Hep3B cells **(ATCC® HB-8064™)**. These cells were introduced by perfusion through the matrix remnants of the portal vein via a peristaltic pump (Masterflex, Cole-Parmer, Vernon Hills, IL) (see **Figure S3**) and cultured in Hep3B medium (DMEM + 10% Fetal Bovine Serum). Approximately 130 $x10^6$ cells were perfused into a scaffold in steps with 20 minutes intervals. During each interval, 30 $x10^6$ cells were perfused at 15 ml/min for 10 minutes, followed by 10 minutes of rest (0 ml/min). This was repeated 4 times. Once all of the cells were introduced into a biomatrix scaffold, the flow rate was lowered to 1.3 ml/min and the scaffolds were perfused with the culture medium. The medium was changed after 24 hours and again every 3 days.

The reseeded biomatrix scaffolds were cultured in the bioreactors (**Figure S3**) for up to 14 days. After 14 days, lobes of the reseeded biomatrix scaffold were either frozen for histology and immunohistochemistry, or fixed for scanning electron microscopy (SEM) imaging (using the method noted above). Sections of the reseeded biomatrix scaffolds were assessed also by immunohistochemistry and immunofluorescence for cell distribution (Hematoxylin and Eosin), cell proliferation (Ki67) and apoptosis, as well as for albumin and urea protein expression. SEM images were also taken to view cell location with respect to vasculature. Antibody information and dilutions are provided in the supplemental materials.

## Results

### Sample Imaging Chamber

In order to image the delicate tissue scaffold, a chamber (**Figures 1 and 2**) was designed to allow a tissue sample to be imaged while submerged in media, since ultrasound imaging at the frequencies utilized requires coupling of the imaging transducer to the sample with liquid. The fluid bath allows for non-contact image acquisition, as opposed to gel-based coupling that is typical for ultrasound imaging exams, while preserving the hydration of the scaffold. Because there was no contact pressure between the tissue and the imaging transducer, tissue was not deformed during imaging; this resulted in better registrations of multiple sub-volumes of image data.

The imaging chamber designed for this purpose was composed of two concentric 0.25 inch thick acrylic cylinders, each 3 inches tall. The outer diameters of the outer and inner cylinders were 6 and 5 inches, respectively. The outer cylinder was mounted to the 6 X 6 X 0.3 inch acrylic base of the imaging chamber using acrylic glue. The inner cylinder was fit to the imaging chamber's base over a Vaseline-lubricated silicone O-ring to allow for quick coupling with a tight seal. Though not implemented in this study, this O-ring design also enables bi-directional imaging orientations (*i.e.* it is possible to rotate the inner chamber and image the contralateral side of the tissue sample). The interior cylinder served several purposes. It provided a frame for the tissue sample support webbing, made from 5.0 silk sutures (Ethicon, Somerville, NJ). This support webbing held the sample suspended in the interior of chamber. Additional suture was loosely tethered over the top of the tissue to prevent flotation or shifting during the imaging study. The interior cylinder of the sample imaging chamber also allowed for efficient buffer circulation but limited turbulence near the sample.

Preliminary studies showed that the peristaltic pump, which powered flow circuit #1, caused a slight periodicity in the flow rate through the scaffold samples as a result of the pump's rotary wheel design; this affected perfusion measurements. To prevent this artifact, a pulse

dampener (Model 07596-20, Cole-Parmer, Vernon Hills, IL) was placed between the output from the peristaltic pump and the input to the sample. Preliminary studies also showed that contrast agent exiting the sample into the surrounding fluid after perfusing through the portal circuit resulted in a decrease in image quality over time as contrast agent floated between the imaging transducer and the sample. To prevent this, a clearance fluid circuit was implemented (**Figure 1**). This circulated the fluid surrounding the scaffold sample though a microbubble sequestration and destruction chamber (MSDC) before reinjection into the imaging chamber. The MSDC was a 2 L Erlenmeyer flask in which a 1 MHz unfocused piston transducer was suspended (Valpey-Fisher, Hopkinton, MA) to facilitate contrast destruction. The 1 MHz piston transducer was pulsed at 10 Hz with a pressure of 460 kPa via a pulser (Model 801A, Ritec, Warwick RI). Under these conditions, free contrast agent in the solution flowing through the chamber was destroyed and thus removed from the circulating media. Media surrounding the scaffold was continually pumped through this chamber at 1 ml/min using a centrifugal pump (Model PQ-12, Greylor, Cape Coral, FL) powered by an external DC power supply (Model DIGI360, Electro Industries, Westbury, NY). Four nylon luer fittings were attached to the outer cylinder for coupling the sample imaging chamber to the two flow circuits. All fluid circuits used 0.125 inch inner diameter Tygon tubing, except between the catheter entering the scaffold sample and the outer cylinder of the imaging chamber (0.062 inch in diameter).

The microbubbles used in this study were prepared as previously described (164). Microbubbles were introduced to the perfusion fluid circuit through a T-valve injection port located between the pulse dampener and the biomatrix scaffold. A 24-gauge needle was used to pierce the septum, and microbubbles could then be injected into the fluid circuit via a computer-controlled syringe pump (Harvard Apparatus, Holliston, MA). Microbubbles were administered into the fluid circuit at a concentration of $1.5 \times 10^9$ per mL in a 1 cc syringe and at a rate of 20 μL/min.

Three liver biomatrix scaffolds were imaged (**Figure 3**), hereafter referred to as samples 1 through 3. The left lateral lobe (LLL) of each scaffold was selected as the lobe of interest, because it is easily accessed for imaging. Another advantage is its narrow morphology; the Vevo770 has a fixed acoustic focus, and thus has a narrow depth of field (< 1 cm). Our goal was to provide a holistic assessment of perfusion throughout a volume of tissue, and the left lateral lobe was most amenable to this objective. It should be noted that the techniques presented here could be extended to the entire volume of tissue using a transducer with a larger axial field of view. Each liver biomatrix scaffold was imaged with two imaging modes: flash replenishment and acoustic angiography.

**Registration of Sub-volumes**

Because the lateral field of view of the ultrasound transducers used for these imaging studies was insufficient to capture the entirety of the liver lobe of interest, multiple sub-volumes were acquired on each system and later registered together offline. The term “sub-volume” is used to describe a 3D volumetric image that does not holistically capture a tissue of interest. Registration of these sub-volumes was performed within the open source 3D Slicer environment (ver 4.2.1, National Alliance for Medical Image Computing) using the Merge module, part of the TubeTK extension. This module is designed to register together two images that have a small degree of overlap along one of the axes. When the sub-volumes were registered together using the Merge module, they formed a single cohesive volume for the liver lobe of interest for each image type (b-mode, flash replenishment, and acoustic angiography). The transform module was then used to register the three types of ultrasound image data to each other, creating a single composite 3D image for each of the livers imaged.

**Grayscale Anatomical Imaging**

Grayscale imaging (*i.e.* the standard non-contrast enhanced imaging) enabled tissue visualization for 3-dimensional region of interest (ROI) segmentations. These data were utilized to calculate tissue volumes of the left lateral lobe (LLL), which were 7.24, 5.93, and 7.79 mL for samples #1-3, respectively.

**Acoustic Angiography**

Vessel network architecture was assessed using more than 1,700 vessel segmentations extracted from the acoustic angiography image data. These data were rendered in 3D and color coded based on whether vessels are inside or outside the manually defined tissue boundary (**Figure 4, Panels 1 and 2**). Different numbers of vessels were extracted from each sample: for sample #1 (N = 415 vessel segmentations), sample #2 (N = 702 vessel segmentations), and sample #3 (N = 671 vessel segmentations). The volumes of these vessel network segmentations were computed to be 142.6, 226.6, and 241.3 µl and the total lengths were computed to be 1.0245, 1.6177, and 1.4646 meters for samples #1, #2, and #3, respectively.

The vascularity ratios were 1.97%, 3.82%, and 3.10% for samples #1, #2, and #3, respectively **(Figure 4, Panel 1d)**. Although these metrics revealed sample #1 to contain fewer perfused vessels (both in total volume of the vessel network, and as a proportion of total volume of the biomatrix scaffold) the distribution of vessel sizes were similar between all three samples **(Figure 4, Panel 2 - top)**.

**Perfusion Imaging**

Using regions of interest as defined based on anatomical data, the perfusion values within each volume were assessed. Histograms of the perfused pixels within the scaffold volumes were computed and plotted as a function of perfusion time (**Figure 4, Panel 2 - bottom**). Samples #2

and #3 had similarly shaped histograms with similar mean perfusion times of 3.128 ± 1.923 sec, and 3.017 ± 1.677 sec (mean μ ± σ), respectively. Sample #1, on the other hand, had a negatively skewed monotonically decreasing histogram with a mean perfusion of 1.381 ± 1.328 sec. This result was in alignment with the differences in the perfusion images, which could be qualitatively observed; sample #1 had a larger proportion of faster perfusing regions than samples #2 and #3 (Figure 4).

**Scanning Electron Microscopy of Intact Liver versus Biomatrix Scaffolds**

Scanning electron microscopy (SEM) of liver versus biomatrix scaffolds (**Figure 5, Panel 1, 5a and 5b**) indicated that the decellularization protocol preserves the liver's histological infrastructure, and that the macro- and micro-vascular channels are clearly intact in the liver biomatrix scaffolds (see arrows). These SEM images are complemented by our prior studies showing that all known extracellular matrix components, including all known collagen types, are present and preserved at >98% of the levels found in normal liver, and that the scaffolds are negligible for nucleic acids and for cytoplasmic components (8). All known matrix components in liver versus scaffolds were assessed by immunohistochemistry and found to be in their correct histological sites, meaning that the liver acinar zonation (zones 1-3) is preserved in terms of gradients of matrix components (8, 115).

**Engraftment Efficiency of Scaffold Recellularization**

As a proof-of-concept towards human liver organoid formation, biomatrix scaffolds with patent vasculature were reseeded with approximately 130 x $10^6$ Hep3b cells, human hepatoblast-like cells of an hepatic cell line (ATCC® HB-8064™). This cell line was established by Barbara Knowles and associates from a tumor from an 8-year old patient.(165) and has been extensively characterized with respect to liver-specific gene expression by Darlington and

associates (166). The Hep3B cells were introduced into the biomatrix scaffold by perfusion through the matrix remnants of the portal vein using a peristaltic pump. The cells attached within minutes, and engraftment efficiency was near 100% by the end of the seeding process.

Over the course of 14 days, the medium from bioreactors with reseeded scaffolds was collected at varying time points and assayed by ELISA for secreted products (**Figure 6)**. At the end of the 14 day culture period, scaffolds were evaluated by SEM, histology and immunohistochemistry. SEM images (**Figure 5, Panel 1**) show cells that have engrafted onto or into the biomatrix scaffold. Hematoxylin and eosin stained sections revealed a wide cell distribution throughout the scaffolds (**Figure 5, Panel 2, 5a**). The seeded cells actively proliferated throughout the 14 days of culture, as demonstrated by Ki67 staining (**Figure 5, Panel 2, 5b**), but they did not show any evidence of apoptosis (data not shown). In addition, the reseeded cells expressed liver-specific proteins in patterns correlated with their known locations in the normal liver acinus *in vivo*. Albumin (**Figure 5, Panel 2, 5c**) was found in all of the cells but at higher levels in regions of the scaffolds correlated with acinar zones 2 and 3, whereas epithelial cell adhesion molecule, EpCAM (**Figure 5, Panel 2, 5d**), was expressed only by cells clustered near the matrix remnants of portal triads, acinar zone 1. EpCAM is a marker of hepatic stem/progenitors (8). Hep3B cells have phenotypic traits indicating that they are hepatoblast-like (166); normal hepatoblasts are found only in zone 1 of the pediatric and adult liver acinus, and are at a lineage stage in which EpCAM is a key phenotypic trait.

**Discussion**

We describe a method of imaging for the evaluation of matrix extracts prepared by decellularization of tissues. Our techniques may provide important information regarding vascular patency, which is particularly important if such scaffolds are to be used as substrata for cell populations as part of organoid formation. The ultrasound images described here provide insights into the complexity of the matrix remnants of the liver architecture and of the vascular

channels. The dimensions of the channels can be quantified precisely using these ultrasound technologies and corresponding segmentation algorithms, enabling the identification of categories of blood vessels for which such dimensions are known (up to 100 μm). Furthermore, these techniques provide a non-destructive method to assess vascular functionality.

When using ultrasound, contrast agents are utilized to image and quantify flow in microvessels that is due to the poor acoustic contrast from blood. Microbubble contrast agents are the predominantly used vascular contrast agent for ultrasound. They are micron-sized lipid encapsulated gaseous spheres which, when immersed in a fluid, provide a strongly reflective interface and thus a high degree of contrast in an ultrasound image. Microbubble contrast agents (diameters typically between 1-5 μm) are much larger than vascular fenestrations, which allow them to remain within the luminal space. At the same time, they are small enough to pass through capillary beds. Since their rheology is similar to red blood cells (167), they are a suitable contrast agent for spatial mapping of vascular channel networks within biomatrix scaffold networks, thereby serving as surrogate markers for mapping cell movement within the scaffold.

In addition to traditional “grayscale” ultrasound to provide reference images of the scaffold physical structure, two different contrast enhanced ultrasound techniques were utilized in this work to provide functional information about biomatrix scaffold microvasculature. The first technique, referred to as “flash replenishment”, or “dynamic contrast-enhanced perfusion imaging” (DCE-PI), allows relative blood perfusion to be spatially mapped by assessing the speed at which contrast agents refill a sample volume after clearance (168). While this technique is not new, it has not previously been performed in this type of scaffold imaging application.

The other contrast imaging approach implemented in this study is a technique we refer to as “acoustic angiography”. This newly developed imaging method differs from traditional ultrasound imaging in that it is designed to visualize vascular and microvascular structure at high resolution rather than tissue anatomy (163, 169). Unlike flash replenishment, acoustic

angiography does not yet have the ability to parametrically map perfusion rates. However, it can provide detailed visualization of vessel architecture and provide a high resolution dataset from which vessels can be segmented and quantitatively mapped (vessel network volume, length, etc.). High resolution acoustic angiography requires a new type of transducer developed by our lab with collaborators in F. Stuart Foster's group at the University of Toronto, Sunnybrook (163) that is not yet available on commercial ultrasound systems. The protocol utilized for this work involves three imaging scans: the first defines the scaffold's physical structure (anatomy) with standard "b-mode" or grayscale ultrasound as is commonly used clinically; the second maps vessel architecture with high resolution acoustic angiography for vascular network visualization and quantitation; the third maps perfusion rates with flash replenishment. All three studies could be performed sequentially with appropriate system hardware.

The analyses of these scaffolds by imaging modalities provide evidence for the complexity of the matrix remnants of the liver architecture and of the vascular channels, as well as evidence of the scaffolds' biological efficacy. These analyses also provide assistance with recellularization protocols. The dimensions of the channels can be quantified precisely using these ultrasound technologies and corresponding segmentation algorithms; this enables identification of categories of blood vessels for which such dimensions are known.

From a quantitative standpoint, sample #1 was noticeably different from samples #2 and #3 in both the acoustic angiography and perfusion images. Sample #1 illustrated a similar vessel size distribution to the other two samples, but showed a grossly reduced perfusion rate. This was due to a defect in sample #1 – the scaffold was damaged, resulting in several low resistance outlets for flow exiting the system. Although we were not able to perceive this damage prior to imaging, it was clearly reflected in the functional data. One perforated outlet was clearly visible within the acoustic angiography image set (**Figures 3 and 4**, **Sample 1, yellow arrow**).

Furthermore, during contrast infusion, it was possible to delineate vessels as part of either the hepatic or portal circulatory networks within the tissue volume (**Figure 3, white vs. black arrows, respectively**). Because contrast was infused though the portal vein, the hepatic circuit did not contain contrast and thus was not visualized under acoustic angiography. When the b-mode volumes were registered to the acoustic angiography volumes, flow voids in the b-mode, which were not perfused within the acoustic angiography dataset, could be classified as components of the hepatic circuit. Alternatively, we could have perfused the hepatic and portal circuits separately, although this was not done in our experiments for simplicity.

The ultrasound approaches we describe offer a non-destructive, high-resolution, and potentially inexpensive technique for visualization of scaffold perfusion. Additionally, these approaches offer a better depth of penetration into the scaffold than optical imaging approaches, allowing for the visualization of the entirety of the LLL (at the expense of both axial and lateral resolution, which is worse than systems imaging at optical wavelengths).

While the advantages of this protocol are numerous, there are also several drawbacks to this approach. Currently, the imaging technology presented for the Acoustic Angiography vessel mapping is not commercially available. Also, while several groups have made strides toward calibrating flash replenishment imaging against gold standards for perfusion rate (168, 170), the technique currently provides only relative quantitative measures for perfusion. This is adequate for assessing differences in regions within a given sample, such as would be necessary for identifying pockets of occlusion. It does not yet allow determination of absolute flow rates ($mL \cdot s^{-1} \cdot cm^{-3}$) within the scaffold without prior calibration based on the tissue volume. Finally, our technique was relatively slow, due to the 1-D form factor of our transducers, which were able to image only a single 2-D image slice at a time and required us to mechanically scan the transducers across the tissue volume. The 2-D matrix ultrasound transducers now in development are able to acquire entire image volumes at a much higher frame rate, although

transducers required to perform real time 3D contrast imaging at the resolution described here are not yet commercially available.

The rapid and successful recellularization of the scaffolds with the Hep3b cells demonstrated the patency and functionality of the matrix remnants of the vascular network. It is interesting that, although the vascular walls remain sufficiently patent to constrain 1-5 micron microbubble contrast agents, the cells were still able to cross the matrix remnants of the vascular channels and engraft into all parts of the matrix, including that associated with parenchymal cells (**Figure 5, Panel 1, 5c)**. It is unclear how the cells were able to engraft after seeding by perfusion into a decellularized liver, since the matrix remnants of the vascular channels were intact. Many researchers who have successfully seeded cells into decellularized organs used decellularization protocols that destroyed facets of the vascular matrix (128). Of those using protocols resulting in patent vascular channels ((7), it has never been explained how the cells are able to breach patent vascular matrix walls and engraft. Baptista et al. (7) hypothesized that their method of decellularization by harsh detergents followed by distilled water perfusion may have caused structural damage to the vascular architecture such as thinning of the matrix or creating small holes; this might, in turn, have allowed cells to migrate across the permeabilized walls.

We have confirmed that our decellularization method results in intact scaffolds without evidence of a defect: there were no breaches of the vascular matrix greater than 5 microns prior to seeding. An alternative explanation for the cells' ability to breach matrix walls and engraft derives from hepatocyte transplantation studies (171, 172). In these studies it was shown that sinusoidal endothelial cells can shift to allow the hepatocytes access to larger fenestrae through which they achieve access and integrate into the parenchymal cell plates. SEM imaging of our reseeded scaffolds suggest that cells are attaching to and engaging the matrix and perhaps are able to squeeze through residual fenestrae left behind after decellularization (**Figure 5, Panel 1, 5d, arrows)**.

Non-destructive 3D perfusion imaging of decellularized organs and tissues could have significant value in tissue engineering investigations and also in tracking recellularization. Contrast ultrasound techniques have been shown to have utility in measuring microvasculature structural information and relative flow rate correlated with anatomical orientation in tissue scaffolds. The recellularization studies presented here indicate that cells are successfully being delivered and engrafting into the matrix remnants of the liver parenchyma by perfusion seeding (**Figure 5, Panel 2**). This perfusion seeding method is only possible in a patent vascular network, which is confirmed through the use of this high resolution acoustic angiography technology. Ongoing current studies include the correlation of structural information, such as vessel diameters, perfusion rates, local fluid shear rates, and patency with the gold standard of histological data after recellularization procedures are complete. Also, ligand-bearing microbubbles could be implemented to perform 3D ultrasonic molecular imaging, which can be used to spatially map specific regions of cell attachment and cell differentiation using biomarkers (161) and thus could be used to detect spatial distributions of different types of cells or varying biological states of cells in the scaffold.

The imaging method is essential for evaluation of scaffolds to be used for organoid formation. Extracellular matrix scaffolds prepared by decellularization protocols are central to the strategies for organoid formation, since individual and purified matrix components give only partial effects in induction and maintenance of differentiated cells. Efforts to isolate successful matrix scaffolds have dominated recent investigations (7, 127, 128, 173-176). All of the protocols have proven successful in isolating matrix extracts dominated by cross-linked collagens. However, most do not generate scaffolds with patent vasculature (128, 173), or they yield scaffolds in which uncross-linked, nascent collagens and associated matrix components are lost (7). The protocol we present here preserves both the cross-linked and the uncross-linked nascent collagens and preserves more of the adhesion molecules, proteoglycans and growth factors/cytokines that are bound to these matrix components (8). The proof-of-principle

studies with Hep3B cells indicate that the richer matrix extracts such as the biomatrix scaffolds confer very rapid attachment (within minutes), near 100% engraftment, and significant induction of tissue-specific functions (to the extent possible with a transformed hepatic cell line).

Human liver organoids are being established for use as bioartificial livers through which a patient's blood can be perfused for detoxification and synthesis of critical liver-specific products. We have previously shown that normal liver cells bound to frozen sections of biomatrix scaffolds and maintained in a serum-free, hormonally defined media designed for mature cells are fully functional and stable *ex vivo* for months (8). If this proves true for the scaffolds used intact (*i.e.* not as frozen sections) for organoid formation, when these scaffolds are recellularized with freshly isolated human cells they will offer opportunities for liver-assist devices for patients. They also will offer the potential to generate grafts for transplantation into patients.

**Conclusions**

Non-destructive 3D perfusion imaging of decellularized organs and tissues has significant value in tissue engineering investigations and also in tracking recellularization processes of matrix scaffolds in organoid formation. Contrast ultrasound techniques have been shown to have utility in measuring microvasculature structural information and relative flow rate correlated with anatomical orientation in tissue scaffolds. The recellularization studies presented here indicate that cells are successfully being delivered and engrafting into intact scaffolds by perfusion seeding. This perfusion seeding method is only possible in a patent vascular network, a finding that is confirmed through the use of this high resolution acoustic angiography technology.

**Figures and Tables**

**Figure 11**. Schematics for the sample imaging chamber. a) Assembled sample imaging chamber and b) exploded view of the sample imaging chamber. c) A top-down cartoon schematic illustrating the two flow circuits in the setup. Flow Circuit 1 provided perfusion and microbubbles to the liver scaffold, while Flow Circuit 2 provided continuous circulation through the microbubble sequestration and destruction chamber (MSDC) to remove contrast excreted from the sample.

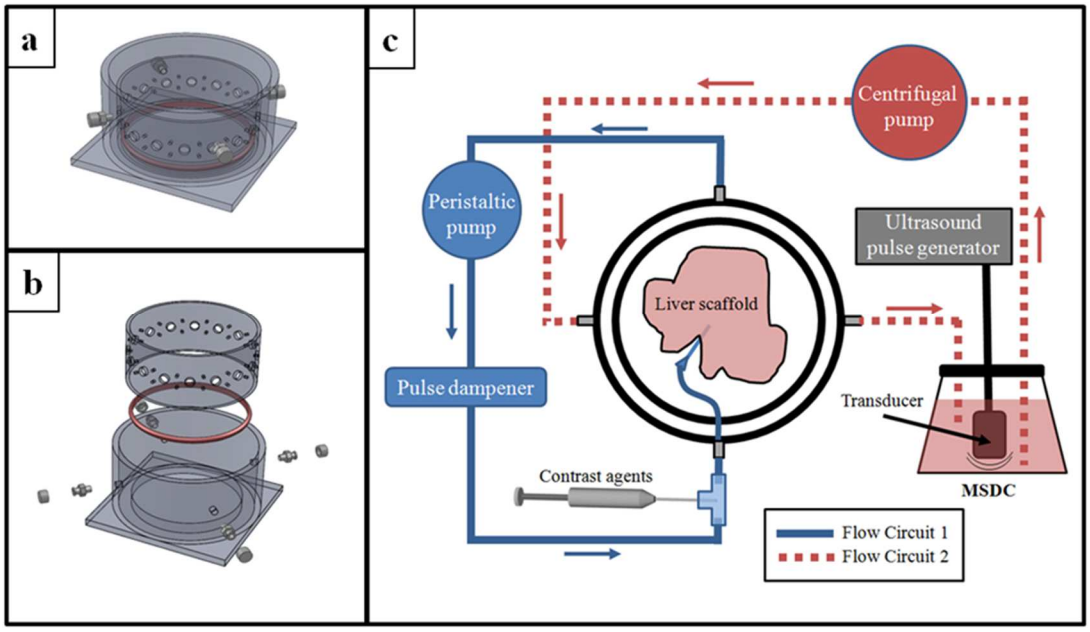

**Figure 12.** The orientation of the biomatrix scaffold sample as viewed from above with the following visible lobes labeled: a) left lateral lobe (LLL), inferior right lobe (IRL), anterior caudate lobe (ACL), posterior caudate lobe (PCL), superior right lobe (SRL), and median lobe (ML). The LLL was the lobe imaged in this study. Lobes were identified in this figure via an available surgical guide. b) Orientation of the imaging sub-volumes relative to the tissue sample. XY dimensions were lateral and axial axes within the ultrasound coordinate space, with the Z-axis being the elevational scan direction. c) Schematic explaining the registration of multiple 3D volumes from three distinct ultrasound imaging approaches into the final composite volume.

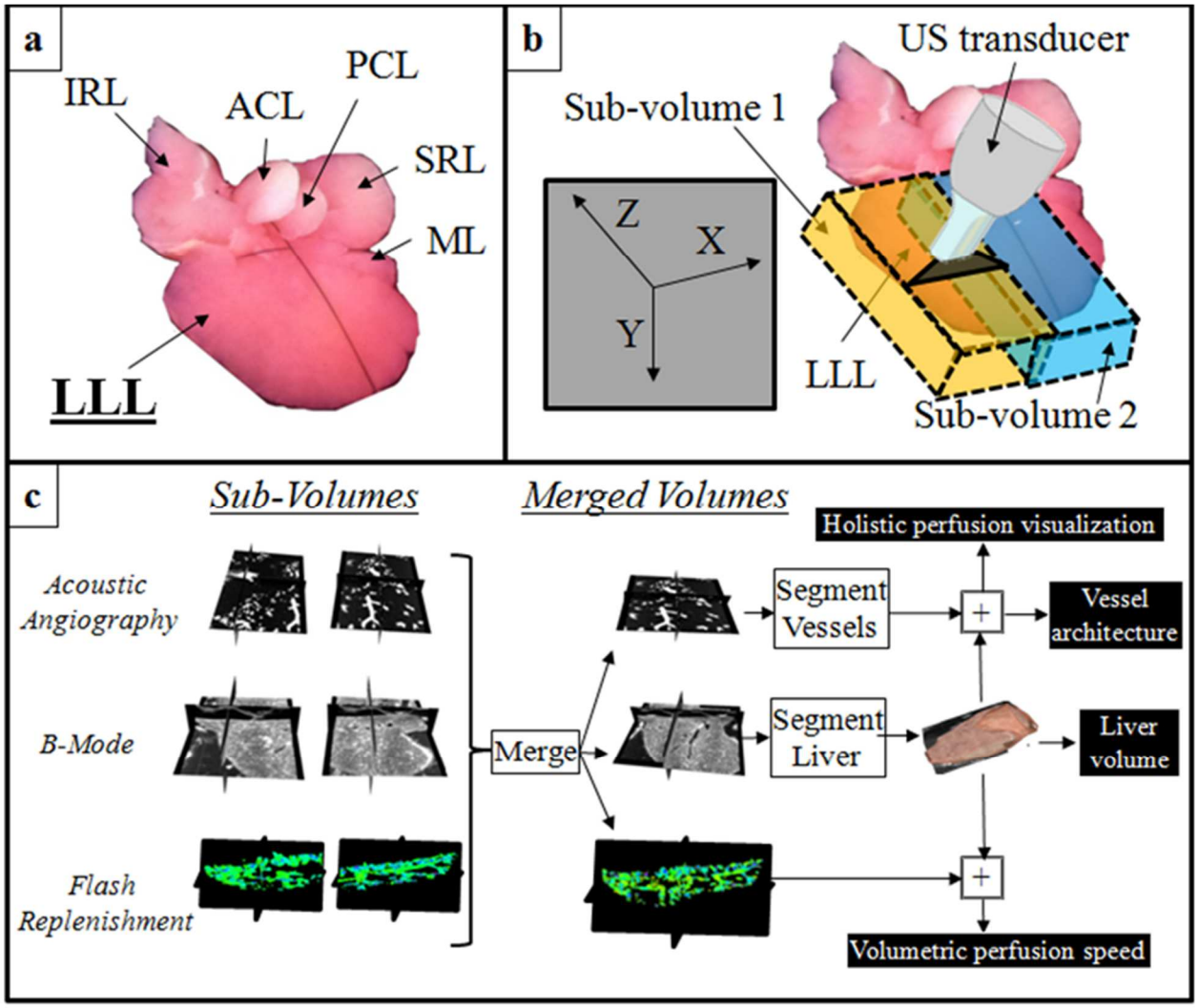

**Figure 13**. A compilation of image data acquired of the three biomatrix scaffold samples. Yellow arrow indicates location of sample #1, which was perforated and thus leaking microbubbles. Each row was acquired with the following imaging modes (from top to bottom): Acoustic angiography, semi-automated segmentations from acoustic angiography data, and b-mode. White and black arrows on the b-mode images indicate vessels identified as part of either the portal or hepatic circuits, respectively.

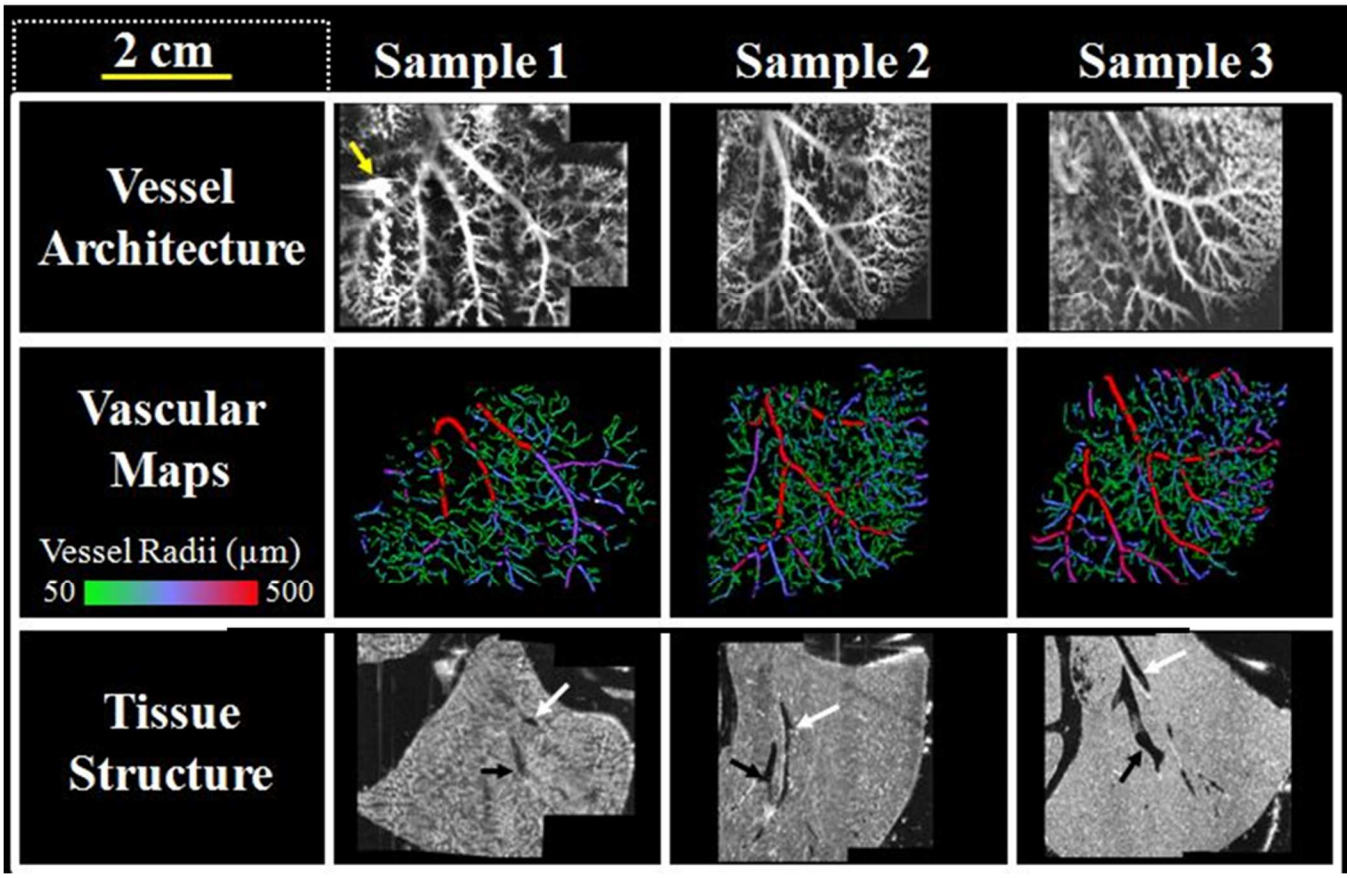

**Figure 14, Panel 1.** a-c) 3D renderings of the biomatrix acoustic angiography data. Color is defined as either inside (green) or outside (purple) of the manually defined tissue border. d) Quantitative assessments of vascular network volume, length, and vascularity ratio. Data are normalized to sample #1.

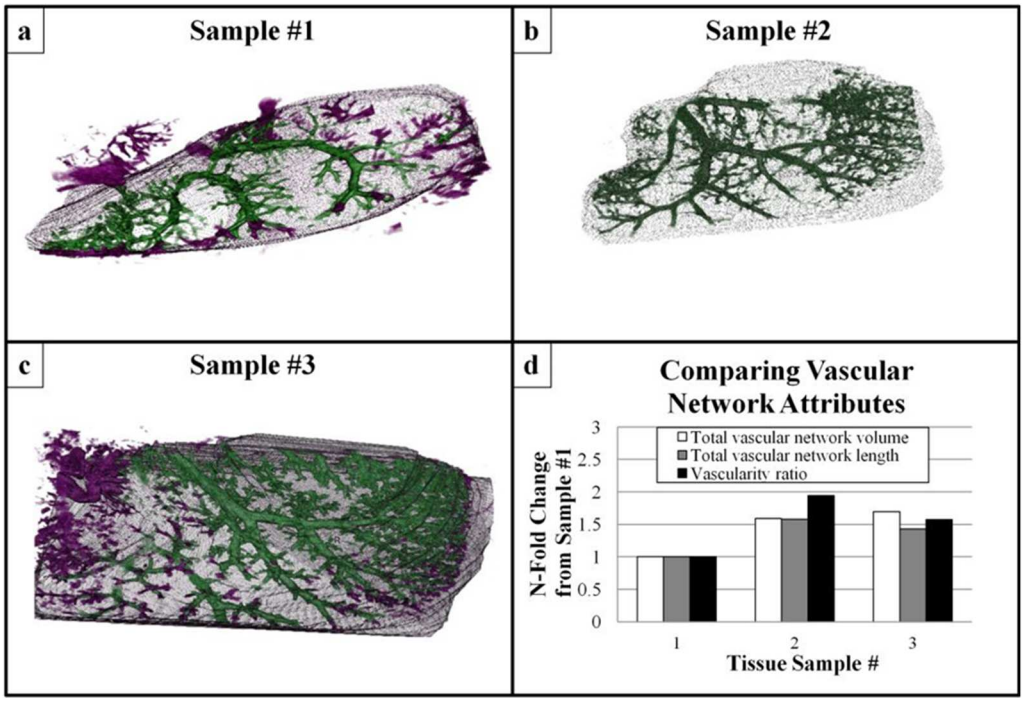

**Figure 14, Panel 2.** Perfusion comparisons between the three liver scaffolds evaluated from the flash-replenishment imaging. (Top) Area normalized vessel size histograms computed from the vessel segmentations. (Bottom) Area normalized perfusion rate histograms.

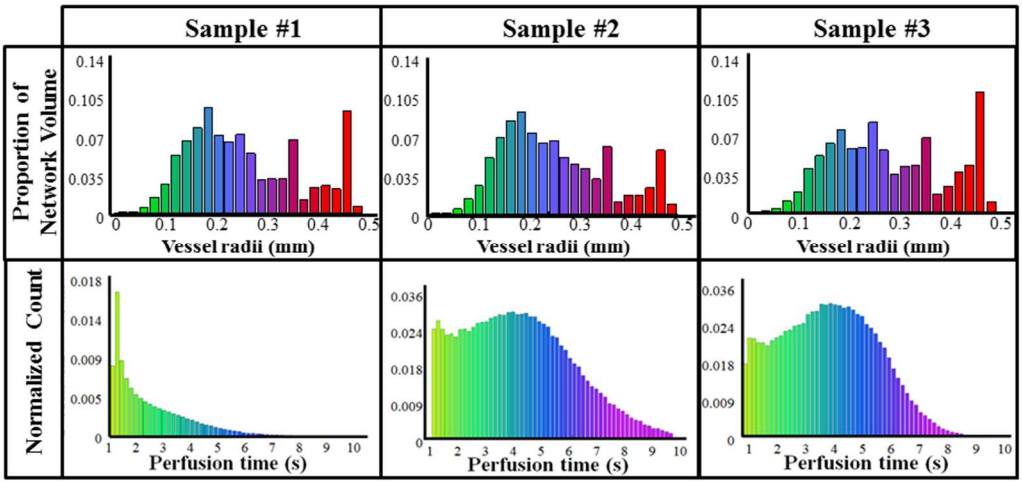

**Figure 15, Panel 1. Scanning Electron Microscopy (SEM)**

**a)** Normal adult rat liver fixed with 4% paraformaldehyde and subjected to SEM.

**b)** Normal rat liver biomatrix scaffold. The major and minor vascular channels are evident in both the liver and in the scaffold. Empty spaces are visible where parenchymal cells previously resided (thin arrow). Major vascular channels are also visible (thick arrow).

**c)** Low magnification image of rat liver biomatrix scaffold reseeded with Hep3b cells. Large numbers of cells are found bound to the matrix throughout the scaffolds. This attachment occurs within minutes of seeding the cells and results in near 100% engraftment by the end of the seeding process.

**d)** Higher magnification image of rat liver biomatrix scaffold showing Hep3b cells that have attached, spread and are forming classic cellular extensions and connections with each other. They engage (thick white arrow) the lumen of the vessel wall and perhaps pass through the fenestrae (thin white arrow) that remain following decellularization.

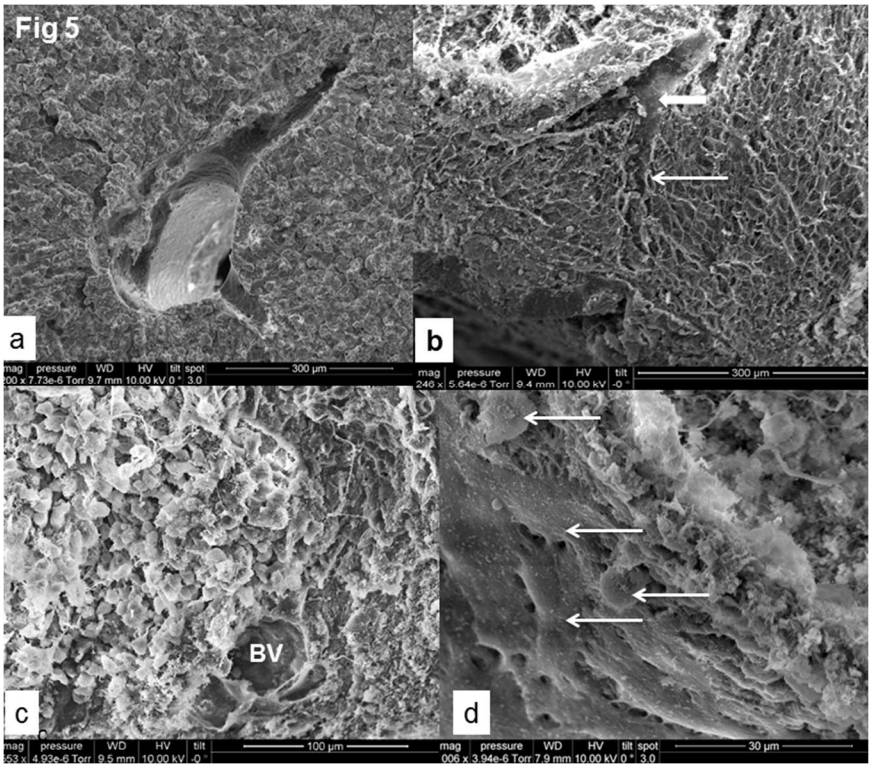

**Figure 15, Panel 2.** a) Hematoxylin and eosin stained sections revealed a cell distribution throughout the biomatrix scaffolds. b) The seeded cells actively proliferated through day 14, demonstrated by Ki67 staining (seen in magnified version in b'). c) The Hep3b cells expressed peak albumin levels (albumin=green, DAPI=blue) in regions of the matrix scaffolds correlated with zones 2 and 3 of the liver acinus. d) Cells bound to matrix remnants of the portal triads (zone 1) expressed albumin more weakly than elsewhere on the matrix. By contrast, EpCAM expression was quite strong in the cells bound in these regions but weak or negligible if in matrix regions associated with zones 2 and 3 (EpCAM=green, DAPI=blue). This is surprising, given that the test cells are a cell line and yet they apparently still have the capacity to show some degree of zonation of functions if bound to specific regions of the biomatrix scaffolds.

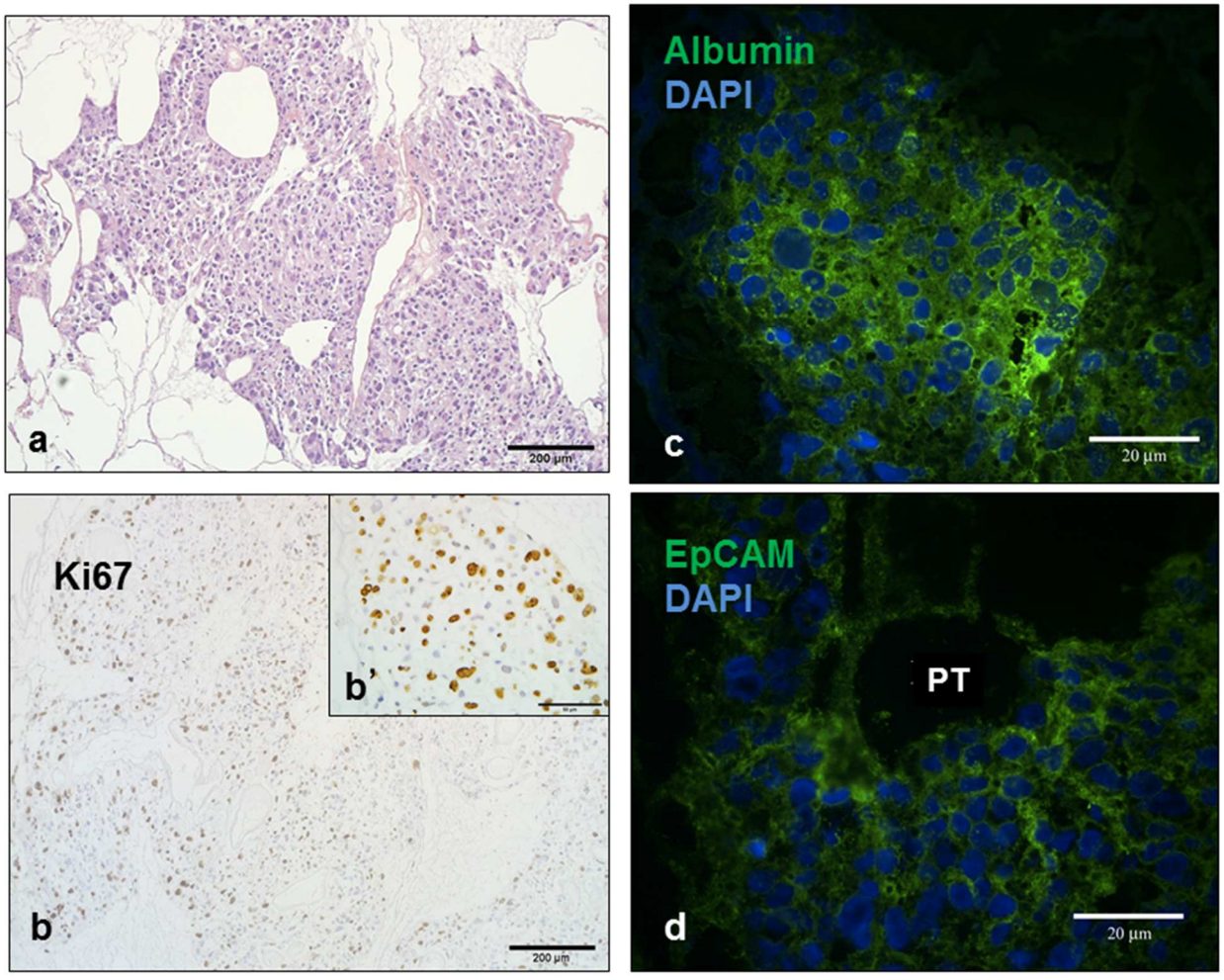

**Figure 16.** Measurements of albumin and urea secretion by Hep3B cells seeded in biomatrix scaffolds (n=3) and cultured over a 14-day period. Levels are normalized to the number of initial number of cells seeded into the scaffold. Symbols indicate media collection over 24 hours ($), 48 hours (x), 72 hours (*), and 96 hours (+). Statistical analyses were unable to be performed, and, therefore, raw data are presented.

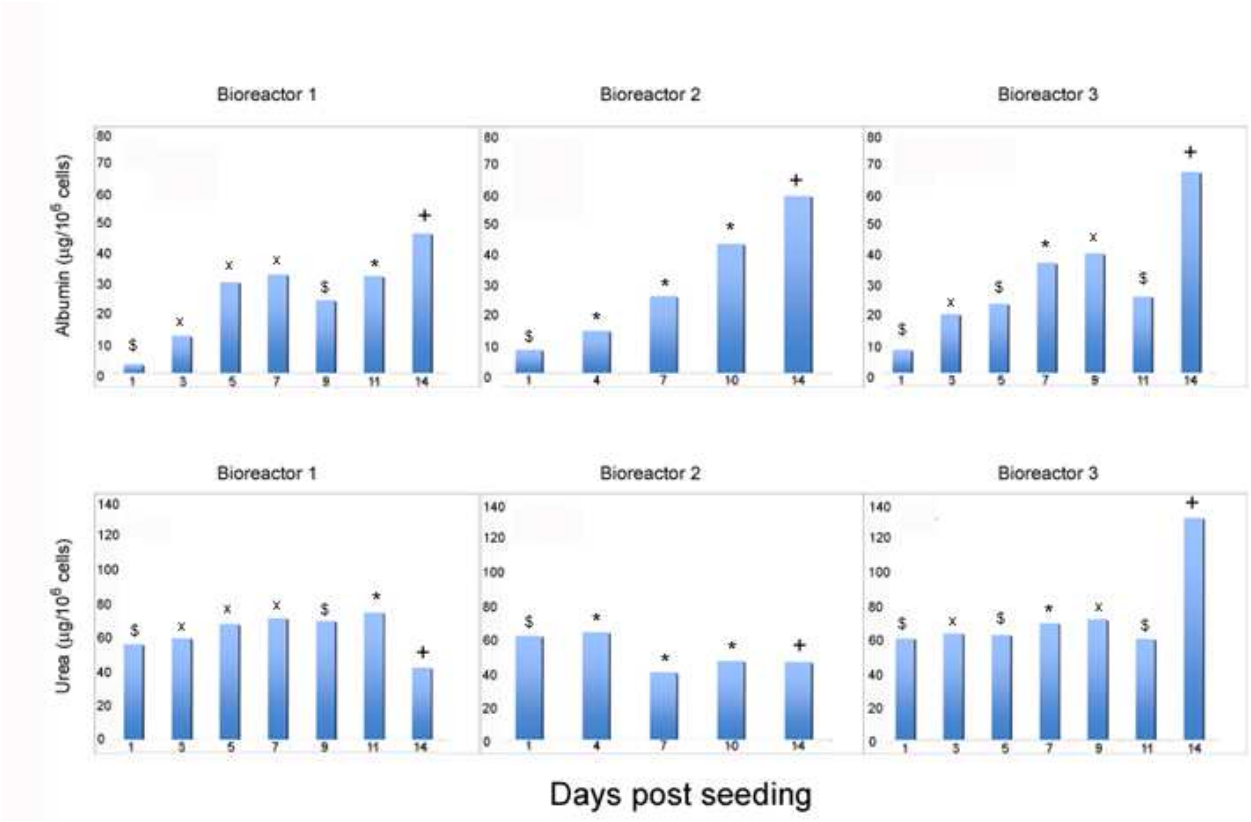

**Online Supplement**

**1. Media and Solutions**

All media were sterile-filtered (0.22-μm filter) and kept in the dark at 4°C before use. To keep collagens stable, the pH of the perfusion media for matrix scaffold preparation was kept at 7.5-8.0. DME/F12 (Gibco/Invitrogen, Carlsbad, CA) was used as the basal medium. All reagents except those noted were obtained from Sigma (St. Louis, MO).

1.1 Kubota's medium (KM):

KM was designed originally for hepatoblasts (177) and now has been found effective for human hepatic stem cells and progenitors (8, 65, 74, 76), and for biliary tree stem cells and progenitors(178, 179), including pancreatic committed progenitors(180). It consists of any basal medium (here being RPMI 1640) with no copper, low calcium (0.3 mM), $10^{-9}$ M Selenium, 0.1% BSA, 4.5 mM Nicotinamide, 0.1 nM Zinc Sulfate heptahydrate nd), $10^{-8}$ M hydrocortisone, 5 μg/ml transferrin/Fe, 5 μg/ml insulin, 10 μg/ml high density lipoprotein, and a mixture of free fatty acids that are added bound to purified human serum albumin. Details of its preparations are given also in a recent methods review(11).

1.2 Hormonally defined media for differentiation (11):

Supplementation of KM further with calcium to achieve 0.6 mM concentration, 1nM tri-iodothyronine (T3), 7 ng/ml glucagon, $10^{-12}$ M copper. The cells were seeded in this medium, supplemented also with 5% FBS (HyClone, Waltham, MA), and switched to serum-free conditions thereafter. In parallel experiments, cultures were kept in the medium with 5% FBS throughout, but the

presence of serum was found to cause the cells to lose differentiated functions over time. The highly functional cultures lasting 8 weeks or longer were achieved using a serum-free differentiation medium with William's Medium as a base, together with the supplements for Kubota's Medium and those above. The soluble factors requirements are less than normal for cultures on other substrata, given that so many of the factors are bound to the matrix scaffolds; thus, for example, EGF, FGF, and HGF, are classic factors needed for mature hepatocytes.

1.3 Matrix scaffolds:

Protocols to decellularize organs differ among labs resulting in scaffolds with differing subsets of the tissue's matrix molecules. Those utilizing matrix-degrading enzymes (128, 174), low ionic strength buffers (127) or distilled water (7) result in scaffolds with significant losses of matrix components. The losses limit recellularization, nutrient delivery, cell growth and differentiation (99, 181). Various methods (*e.g*. perfusing scaffolds with purified matrix components) can facilitate cellular engraftment. However, the extent of differentiation of the recellularized scaffolds (*e.g*. albumin and urea secretion) is very low relative to that for normal livers. See Table S1 for comparisons.

| Table 2: Comparison of Protocols used in Decellularization of Livers | | | |
|---|---|---|---|
| **Decellularization method** | **Analysis of Scaffold Matrix Chemistry** | **Effects of the Scaffold on Cell Functions** | **References** |
| Perfusion initially with distilled water followed by Triton X-100 or SDS | Patent vasculature evaluated by dextran beads or corrosion casting but possible thinning of the walls and small holes in the lumen. Histological confirmation of retention of cross-linked collagens. However significantly decreased content of fibronectins, laminins elastin, decorin and sulfated glycosaminoglycans (GAGs), and proteoglycans | To achieve significant cell attachment, investigators used either Matrigel, adding attachment proteins into the recellularization buffers, and/or long periods of time for cell seeding. Human fetal liver cells achieved partial hepatic differentiation. Human fetal hepatocyte function was not significantly different from static 2D cultures. | (7, 176, 182, 183) |
| Perfusion initially with Triton X-100 and/or SDS followed by saline solutions. | Vascular patency was determined by corrosion casting or not at all. Cross-linked collagens were retained but much less than in native tissue. Decreased amounts of fibronectin and elastin were found by Western blots or histology. Almost all GAG content was diminished by decellularization. SDS causes much more significant loss of matrix molecules as compared to Triton X-100. It also binds very tightly to collagens and can make the scaffolds toxic to cells. | Approximately 90% of cells adhered within 24 hours. Cells showed damage, as evaluated by lactate dehydrogenase release, for several days following reseeding. Cumulative albumin and urea levels were somewhat greater then static 2D cultures. | (128, 174, 184-186) |
| Freezing/thawing of tissue and then perfusion with either trypsin/EDTA or SDS. This was followed by perfusion with Triton X-100 | Histology confirms presence of collagen I and IV, laminin and fibronectin. Only partial retention of growth factors. Corrosion casts were used to confirm patent vasculature. | Cell attachment was achieved in 40 minutes but it took several days for cells to leave the vasculature and distribute throughout the matrix associated with the parenchyma. UDP-glucuronosyl transferase and Glucose-6-phosphatase expression, and LDH release were found at day 2. Transplanted for 8 hours *in vivo* as an auxiliary liver. | (127, 132) |

| | | | |
|---|---|---|---|
| Matrix scaffolds.<br>Any basal medium is perfused in order to remove blood. Then the tissue is perfused with low concentrations of sodium deoxycholate used in combination with phospholipase A2; results in very rapid delipidation (~30 minutes). This is followed by perfusion with high salt buffers (with NaCL at a concentration chosen to ensure insolubility of those collagen types identified in the tissue). This is followed by nuclease treatment, prepared in basal media, to eliminate residual nucleic acids | Scaffolds contain (qualitatively) all known matrix components (collagens, fibronectins, laminins, nidogen, elastin, proteoglycans) found in the tissue *in vivo*. The scaffolds have >98% of the collagens and all of the collagen types found in the tissue. Glycosaminoglycan/ proteoglycan types and amounts are near normal. Growth factor array analyses indicate that all of the known growth factors and cytokines are present at physiological levels and bound to the matrix. All matrix and growth factors/cytokines are in accurate histological locations. | Cells attach to scaffolds within seconds to minutes. Engraftment in intact scaffolds is near 100% within 24 hours of perfusion and with distribution to all parts of the scaffolds. Tissue-specific functions occur within a few hours. Optimized extent of differentiation occurs within a few days.<br>Studies on normal hepatocytes bound to frozen sections of scaffold indicated that tissue-specific functions are similar to those of freshly isolated liver cells and stably remain so for more than 8 weeks. Studies on normal hepatic stem cells indicated that they bind to frozen sections of scaffold within minutes, proliferated for 2-3 days, then differentiated to fully mature liver cells by ~day 6-7 and finally remained stably differentiated for months. | (8) |

**2. Decellularization of livers**

2.1 Animals:

Wistar rats (weights 250-300 g) were obtained from Charles River Laboratories, Wilmington, MA, and housed in animal facilities handled by the UNC Division of Laboratory Animal Management. They were fed ad libitum until used for experiments. All experimental work was approved by and performed in accordance with the UNC Institutional Animal Use and Care Committee guidelines.

2.2 Decellularization protocol:

The protocol for decellularizing livers to produce matrix scaffolds has been described in prior publications(8). Male rats were anesthetized with Ketamine-Xylazine, and their abdominal cavity opened. The portal vein was cannulated with a 20-gauge catheter to provide a perfusion inlet to the vasculature of the liver, and the vena cava transected to provide an outlet for perfusion. The liver was removed from the abdominal cavity and placed in a perfusion bioreactor. The blood was removed by flushing the liver with 300 ml of DMEM/F12 (Gibco, Grand Island, NY). Delipidation (36 U/L of phospholipase A2 in 1% sodium deoxycholate; Fisher, Pittsburgh, PA) was used to remove plasma and nuclear membranes. This delipidation buffer was perfused through the liver for 1 hour or until the tissue became transparent. This was followed by perfusion for 90 minutes with a high salt buffer. Solubility constants for known collagen types in liver are such that 3.4 M NaCL is adequate to keep them in an insoluble state. The liver was rinsed for 15 minutes with serum-free DMEM/F12 to eliminate the delipidation buffer; this was followed by perfusion with 100 ml of DNase (1 mg per 100 mL; Fisher, Pittsburgh, PA) and RNase (5 mg per 100 mL; Sigma Aldrich, St. Louis, MO) to remove any

residual contaminants of nucleic acids from the scaffold. The final step was to rinse the scaffolds with DMEM/F12 for 1 hour to eliminate any residual salt. Images are provided in **Figure S1**. The decellularized liver was stored overnight at $4^0$C and perfused with media at 3 ml $min^{-1}$ via a peristaltic pump (Masterflex, Cole-Parmer, Vernon Hills, IL) before the imaging study was performed. Prior to an imaging study, the scaffold was transferred from the perfusion bioreactor into the sample imaging chamber (**Figure 1**). When in the sample imaging chamber, perfusion was maintained at 4 ml $min^{-1}$ through the portal vein via the same peristaltic pump.

**3. Further details on imaging technologies**

3.1 Validating imaging consistency:

Microbubble buoyancy and floatation within syringes is known to cause a variation in contrast concentration over time (187) in long-term infusion studies. To mitigate this effect, the syringe was gently agitated throughout the imaging procedure as described previously (187). To characterize the degree to which this affected the consistency in the reported perfusion data extracted from the image data, a study was performed in which the transducer was fixed at a single location and flash replenishment images were acquired approximately every minute for 30 minutes. The data were exported to MATLAB for analysis. A region of interest (ROI) was defined around the perimeter of the lobe being imaged. Two quantities were assessed at each time point within the ROI: the total number of perfused pixels; and the average perfusion value. Two scaffolds were used for this study. The first was imaged with the non-agitating protocol susceptible to microbubble floatation. After data were analyzed offline, a second liver scaffold was imaged to observe the effects of syringe agitation on perfusion assessment consistency. Results illustrated a substantial improvement in repeatability of measurements with the syringe mixing strategy (**Figure S2**).

3.2 Assessing liver matrix scaffold perfusion:

Because the two perfusion imaging modes implemented in this study (acoustic angiography and flash replenishment) were acquired on different ultrasound systems, an initial registration step was necessary prior to merging the volumetric datasets in the same coordinate system. This registration step was performed via a rigid transform within the Slicer Transforms module. The lobe of interest could then be manually segmented, and the same ROI could be used for all three datasets. The segmentation of the LLL was performed in Matlab as previously described (164). The volume of the liver lobe was measured in Slicer by creating a Model from the binary 3D ROI and using the Label Statistics module to sum the voxels occupied by the liver lobe. Because the segmentation and registration process was performed entirely offline, it was impossible to re-collect the ultrasound data of a scaffold if it became clear that small portions of the tissue were not imaged. In these cases, ROIs were defined to the edge of the available image data, or across regions of tissue if it was obvious to the viewer what path the tissue boundary was taking.



Each voxel within the flash replenishment images represented a spatially localized estimate of perfusion speed. To assess perfusion throughout the volume of tissue, all values were vectorized and histograms were created for each sample. These perfusion histograms were binned by perfusion time, and area was normalized by total perfused voxels (*i.e*. the integral of the histogram was set to unity). The segmentations extracted from the acoustic angiography images were used to compute total length and volume of the vessel network, vascularity ratio (volume of vessel network/volume of liver lobe). The volume of each discretized location in the segmented vessel network was computed and summed to yield total vessel network volume and length. The proportion of the vessel network occupied by vessel segments of a range of radii between 50 um (minimum voxel size) and 500 um was computed.

3.3 Limitations:

During the offline registration and segmentation processing steps, it was discovered that some portions of the LLL were excluded from analysis. This was due to the transducers' form factors being too large to image the portions of the scaffold tissue close to the sample imaging chamber's wall (as shown in **Figure S3** b-mode images for samples #1 and #2). We estimate this lack of image data to result in relatively minor errors in ROI definition, and thus relatively small errors in the estimates for perfusion since the periphery of the LLL would be most affected. Since the periphery of the liver's lobes are predominantly occupied by slowly perfusing vasculature (188), the mean perfusion values reported via these manual segmentations will not be affected by the exclusion or inclusion of a small proportion of this region of tissue. Nonetheless, these errors are preventable by adjusting the experimental system.

**Supplemental Figures and Tables**

**Table 3. Biological Assays Used to Evaluate the Reseeded Matrix Scaffolds with Hep3B cells**

| Reagent | Supplier | Dilution Factor |
|---|---|---|
| Ki67 | abcam (#ab16667) | 1:100 |
| Albumin | abcam (#ab2406) | 1:200 |
| EpCAM | Thermo Scientific (#MS-181-P1) | 1:250 |
| Human Albumin ELISA Quantification Set | Bethyl Laboratories, Inc. (#E80-129) | |
| QuantiChrom Urea Assay Kit | BioAssay Systems (#DIUR-500) | |

**Figure 17. Decellularization process**:

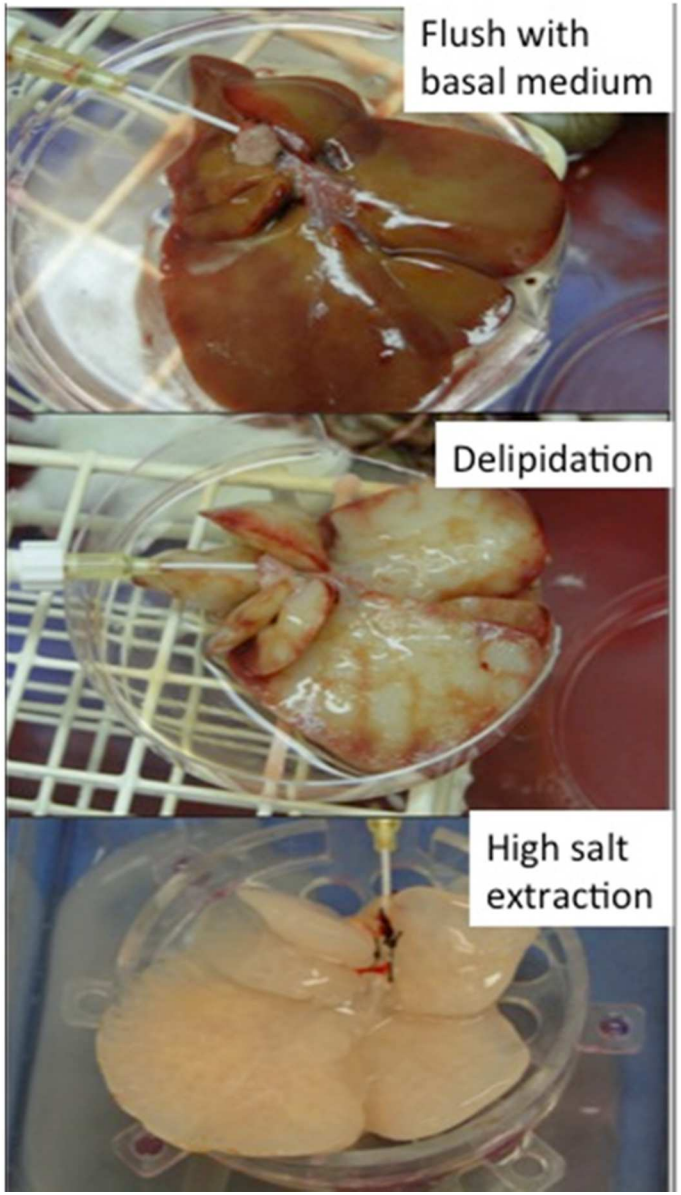


*Top*: Flushing liver with a serum-free basal medium (*e.g.* DME/F12) to remove blood.

*Middle*: Delipidating with phospholipase A2 (PLA2) and then with PLA2 combined with deoxycholate; rinsing with serum-free DME/F12; perfusing with 3.4 M high salt buffer (salt concentration dictated by collagen types in the tissue), with soybean trypsin inhibitor, with all kept at a pH of 7.5-8.0; rinsing to remove salt.

*Bottom*: Treating with nucleases to remove residual nucleic acids and then rinsing with serum-free basal medium and stored at 4° C. The liver's collagen types include types I, III, IV, V, VI, and XVIII.

**Figure 18.** Data illustrating the stability of the normalized perfusion area (NPA) and normalized perfusion speed (NPS) before and after modifying the contrast injection protocol. Images A and B represent data before syringe mixing, while C and D show after syringe mixing. Note the improvement in consistency (i.e. the reduction in percent standard deviation) for both parameters after implementing syringe mixing.

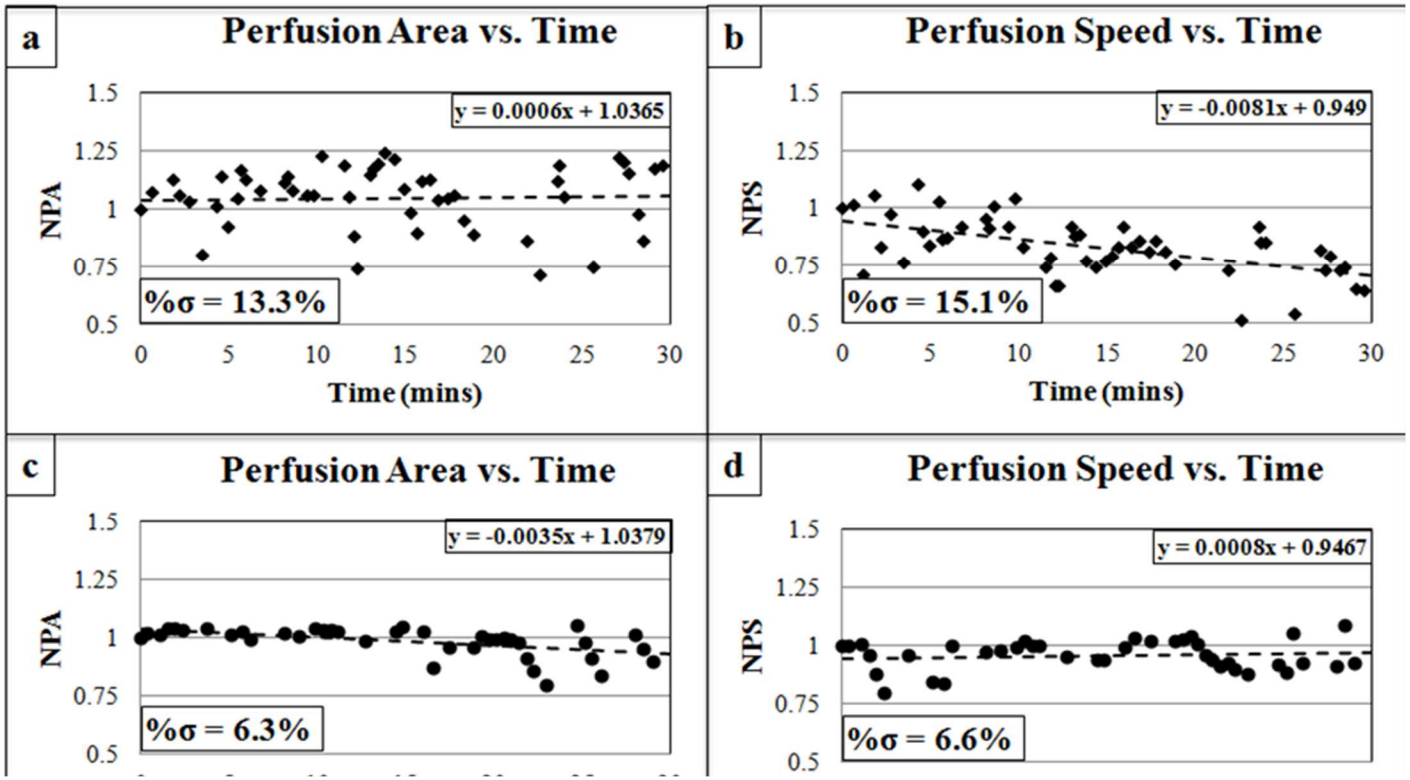

**Figure 19**. The matrix scaffold was housed in a bioreactor containing 200 ml of medium. A) The hepatoblast-like cells, Hep3bs, were introduced into the matrix scaffold by perfusion through the portal vein via a peristaltic pump. B) Photograph of a reseeded matrix scaffold housed in the bioreactor.

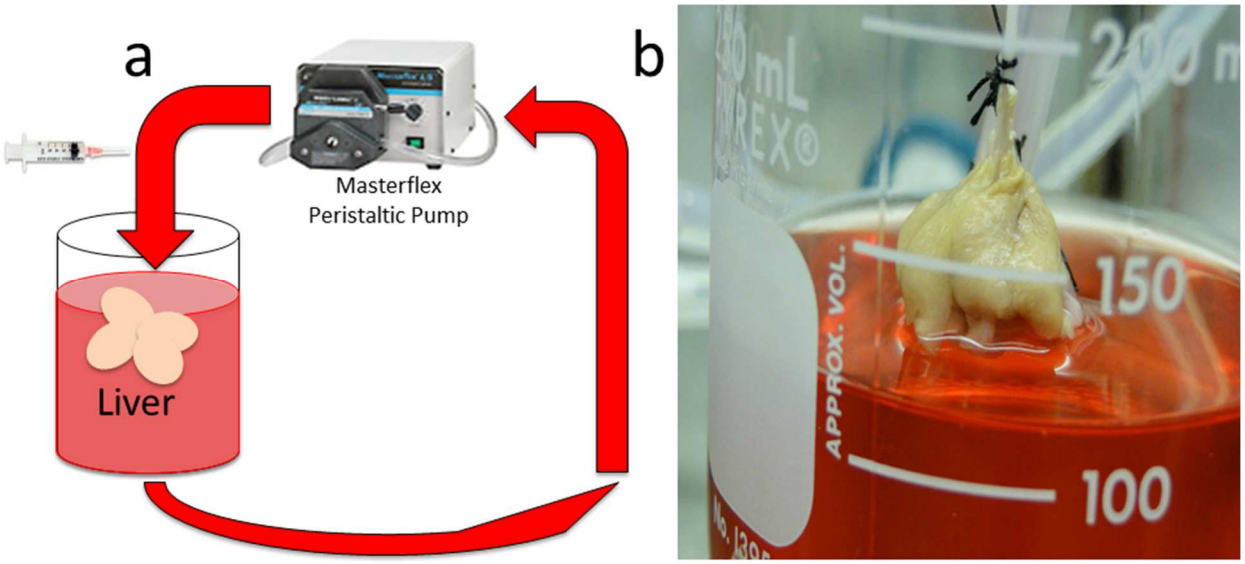

# CHAPTER IV

## Motivation for Organoid Studies

The biomatrix scaffolds are improving the culture of cells by supporting their differentiated functions of cells more than any known matrix extract. However, they are not readily converted to industrial scale usage. Wang et al. pulverized the biomatrix scaffolds and the powder was allowed to sediment onto culture dishes (8). The dishes coated with biomatrix scaffold powder did indeed support rapid attachment and differentiation, but the extent of differentiation was significantly lower than when frozen sections were used (8) or when the scaffolds were used intact (Arial Hanson et al, manuscript in preparation). We hypothesized that the pulverization process resulted in many of the matrix components, especially the proteoglycans, became vulnerable to solubilization in media. The primary objective of this thesis was to identify methods that would most optimally use the biomatrix scaffold extracts to preserve the critical components of the matrix but in a way that was scalable for use in industry.

The current status of drug testing in the industry is an area that has potential for substantial improvement. Many of the drugs in development fail and do not pass the stringent regulations set by the Food and Drug Administration (FDA). These drugs candidates have been selected from thousands of others and are required to be investigated by numerous preclinical studies. Success in these studies will allow the drug candidates to proceed to clinical trials. Unfortunately, more than half of these drug candidates fail. At this point, a significant amount of time and capital has already been invested into these drug candidates, and these failures in clinical trials are a source of major losses in finances and resources within the industry. A widely

recognized solution is the identification and elimination of drugs early on in the development process. There is a demand for a method(s) that not only accurately models the drug biology in humans but is also cost effective with scalability. Many recent studies have focused on mimicking the native biology as closely as possible but disregard the importance of scalability to the feasibility of successfully implementing these methods in the industry. Biomatrix scaffolds are constrained by the size of the native organ and limit culture availability. A method that can be scaled would enable a more cost effective high-throughput preclinical screening of drugs and allow a more thorough assessment of the potential for a drug to succeed in clinical trials. This would help in eliminating more candidates early on in the process and help minimize the loss of resources.

# CHAPTER V

## Stem-cell derived, Functional Human Hepatic Organoids in Hyaluronan Hydrogels containing Pulverized Liver Biomatrix Scaffolds[1]

### Synopsis

The success of *ex vivo* models for industrial applications is closely linked to their ability to mimic physiological/biological processes. We have established functional human hepatic organoids by culturing human hepatic stem cells (hHpSCs) in a serum-free, hormonally defined medium (HDM) and in hyaluronan hydrogels containing pulverized biomatrix scaffolds obtained from decellularization of liver tissue. The decellularization process results in extracts containing ~99% of the liver's collagens (cross-linked, non-cross-linked and nascent ones), essentially all known collagen-associated matrix components, and physiological levels of matrix-bound growth factors and cytokines. Within a few days in the hydrogel and decellularized matrix mixture, hHpSCs differentiated to have a gene expression profile similar to that of mature hepatocytes and with secreted proteins associated with hepatic metabolism. The effects proved concentration dependent for the biomatrix scaffold components. This method has the potential for industrial scalability and thus has implications for therapeutic and industrial applications.

---

[1]This chapter features a manuscript in preparation at the time this thesis was published: Bryant Wu, Eliane Wauthier, Ariel Hanson, Mitsuo Yamauchi, and Lola M. Reid. Stem-cell derived, Functional Human Hepatic Organoids in Hyaluronan Hydrogels containing Pulverized Liver Biomatrix Scaffolds. Manuscript in preparation.

**Introduction**

*Ex vivo* models of human livers are highly desired by investigators in academia and industry especially given the difficulties in obtaining high quality human livers for the purpose of research. Efforts to establish such models have been ongoing for more than 50 years with varying degrees of success (189, 190). Requirements for the most successful versions of such models include a need for 3-dimensionality (3D) and a mixture of the epithelial and mesenchymal cells such as that which occurs in organoids (6, 46, 64, 191). Also required are a) serum-free media with wholly defined hormonal and nutritional constituents (11), b) co-cultures with tissue-specific and lineage specific mesenchymal cell partners that confer essential paracrine signaling (76, 192), and c) complex mixtures of extracellular matrix components (7, 8, 128). In addition, the limitation in available, freshly isolated human liver cells coupled with their limits in proliferation have caused investigators to pursue various forms of stem cell populations that can self-replicate extensively and then can be lineage restricted to an adult hepatic fate.

Decellularization of organs to yield tissue-specific extracts enriched in the complex mixture of extracellular matrix components that can support differentiation has been known for over 30 years (147, 148). Renewed interest in these strategies has occurred in recent years and has resulted in the generation of scaffolds being tested for their efficacy in differentiating cells *ex vivo* and even *in vivo* (7, 8, 130). Although studies are ongoing that analyze matrix scaffolds of many tissue types, the most extensively characterized ones have focused on liver. In all those studied, the scaffolds have been prepared for use in monolayer cultures (8) or as intact scaffolds(7, 132) – forms that limit scalability for industrial use.

Hepatic organoids are aggregates of hepatic parenchymal cells that include hepatocytes and cholangiocytes, along with their partner mesenchymal cells that include endothelia and hepatic stellate cells. When the cells are kept in suspension under appropriate conditions, they aggregate into subunits mimicking their cellular relationships *in vivo*. They can last in culture for

weeks to months and yield the best functionality of parenchymal cells maintained *ex vivo* (19). Their ability to be industrially scaled is limited by the lack of vascularization.

Each organoid typically consists of around 10,000 hepatocytes and is limited in the numbers sustainable per culture volume and thus limited in scalability. Moreover, there is limited proliferation of adult cells when triggered to generate organoids, meaning that one has to prepare them with freshly isolated cells.

Here we show that one can achieve scalability of organoid cultures by taking advantage of the proliferative capacity of hepatic stem cells, maintained under self-replicative conditions, and then use the stem cells to generate large numbers of functional hepatic organoids by subjecting them to differentiation conditions. Identification and isolation of human hepatic stem cells (or biliary tree stem cells) from human livers of all donor ages were demonstrated previously (65, 69). The hepatic stem cells and subpopulations of biliary tree stem cells (178) are able to be expanded *ex vivo* on culture plastic or on hyaluronan substrata and in serum-free Kubota's Medium (KM) designed for culture selection and maintenance of endodermal stem/progenitor cells (76, 177).

The colonies of hepatic (or biliary tree) stem cells can be transferred to differentiation conditions that lineage restrict them to adult parenchymal cell fates by conditions comprised of a serum-free hormonally defined medium (HDM) and substrata of biomatrix scaffolds (8), designed to differentiate the cells to adult liver. Here we adapt this strategy to one that is scalable by using the HDM in combination with embedding the stem cells into hyaluronan hydrogels containing pulverized liver biomatrix scaffolds, a potent mixture of signals and factors that drive the stem cells to hepatic organoids within 5 days.

## Materials and Methods

### Companies

The companies from which tissues or reagents were obtained include: Advanced Biological Resources (Alameda, CA): ALPCO Diagnostics (Salem, NH); Applied Biosystems (Grand Island, NY); Becton Dickenson (Franklin Lakes, NJ); Bethyl Laboratories (Montgomery, TX); Biotime (Alameda, CA); Cedarlane Labs (Burlington, NC); Charles River Laboratories Int'l (Wilmington, MA); Clontech Laboratories (Mountain View, CA); Gibco (Grand Island, NY); Invitrogen (Grand Island, NY); Molecular Devices (Sunnyvale, CA); Olympus (Melville, NY); PhoenixSongs Biologicals (Branford, CT); RayBiotech, Inc (Norcross, Georgia); Sigma (St. Louis, MO); Spex SamplePrep (Metuchen, NJ); Thermo Fisher Scientific (Waltham, MA); Triangle Research Laboratories (RTP, NC).

### Animals

Sprague Dawley Rats were obtained through Charles River Laboratories International. The liver biomatrix scaffold isolation protocol was reviewed and approved by the Institutional Animal Care and Use Committee (IACUC) at the University of North Carolina at Chapel Hill.

### Media and solutions

All media were sterile-filtered (0.22-μm filter) and kept in the dark at 4°C before use. To keep collagens stable in the biomatrix scaffolds during decellurization, the pH of the perfusion media was kept at 7.5-8.0. DMEM/F:12 (Gibco) was used as the basal medium for preparation of biomatrix scaffolds. RPMI-1640 (Gibco) was used for cultures of hepatocytes or HpSCs.

### Kubota's medium

KM consists of any basal medium, here being RPMI 1640 (Gibco), supplemented with 0.1% BSA (fatty acid-free bovine serum albumin, Fraction V; Sigma) and niacinamide (Sigma),

with no copper, 0.3 mM calcium concentration, supplemented with trace elements – zinc ($10^{-12}$M), selenium ($10^{-9}$M), insulin and iron-saturated transferrin (both at 5 μg/ml; Sigma-Aldrich), hydrocortisone ($10^{-7}$M), a mixture of free fatty acids bound to bovine serum albumin, L-Glutamine (200 mM), and antibiotics (AAS; Invitrogen). Detailed methods for its preparation are given in a published review (11).

**Hormonally defined Medium for Differentiation of Cells to Adult Liver Cells (HDM-L)**

The HDM-L was prepared by supplementing KM with calcium to achieve 0.6 mM concentration, 1nM tri-iodothyronine (T3), 7 ng/ml glucagon, $10^{-12}$M copper, and 2 g/L galactose. Classic factors needed for mature hepatocyte differentiation were also added including epidermal growth factor (EGF, 20 ng/ml), basic fibroblast growth factor (bFGF, 10 ng/ml), hepatocyte growth factor (HGF, 10 ng/ml), and Oncostatin M (10 ng/ml) (76). Detailed methods for its preparation are again given in the published methods review (11).

**Human fetal liver processing**

Fetal liver tissues were provided by an accredited agency (Advanced Biological Resources) from fetuses between 16-20 weeks gestational age obtained by elective pregnancy terminations. The research protocol was reviewed and approved by the Institutional Review Board for Human Research Studies at the University of North Carolina at Chapel Hill. Suspensions of fetal human liver cells were prepared as described previously (65, 76). All processing and cell enrichment procedures were conducted in Kubota's Medium. Liver tissue was subdivided into 3-ml fragments (total volume ranged from 2-12 ml) for digestion in 25 ml of cell wash buffer containing type IV collagenase and deoxyribonuclease (both at 6 mg/ml; Sigma) at 32°C with frequent agitation for 15-20 min. This resulted in a homogeneous suspension of cell aggregates that were passed through a 40-gauge mesh and spun at 1,200 RPM for 5 min before resuspension in cell wash solution. Erythrocytes were eliminated usually

by slow-speed centrifugation (76). They were eliminated in a few studies by treating suspensions with anti-human red blood cell antibodies (1:5,000 dilution; Rockland) for 15 min, followed by LowTox Guinea Pig complement (1:3,000 dilution; Cedarlane Labs) for 10 min, both at 37 ° C; this was not done routinely, since there was some loss of the stem cell subpopulations. Estimated cell viability by Trypan blue exclusion was routinely >95%.

**Culture selection for Hepatoblasts (HBs) versus Hepatic Stem Cells (HpSCs)**

Freshly processed human fetal liver cell suspensions are comprised mostly of hepatoblasts (hHBs; 80-85%), a small percentage of hepatic stem cells (hHpSCs; ~0.5-2%), and the remainder are hematopoietic cells (~14%) and various mesenchymal cells (3-5%). Of the parenchymal cell fraction the hHBs are ~98% and the hHpSCs are ~1-2%. All were plated onto culture plastic and in serum-free Kubota's Medium (KM) and placed in an incubator at 5% CO2/air mix and 37°C. Immediately after plating, and for up to 5 days, the cultures were comprised primarily of the larger (12-15 μm) hHBs. After 5 days, the hHBs and all other cell types die under these conditions, except for the smaller (7-9 μm) hHpSCs. Bound to the hepatic stem cells are their mesenchymal partners, angioblasts. These hHpSCs and their angioblast partners survive indefinitely in these conditions and are culture selected within ~one week; that is all other cell types and lineage stages of cells die. Colonies of the hHpSCs reach a size of ~2000 cells/colony within 10-14 days.

The plating conditions consisted of the cell suspension seeded at ~300,000 cells per 100 $mm^2$ round culture dish (78.5 $cm^2$ surface area). Cells were plated with 5% fetal bovine serum (FBS) for 20-24 hrs (ideally for only ~6 hrs) to facilitate attachment. Afterwards cell media were changed every 4-6 days with serum-free KM. The low seeding numbers resulted in sparse plating that is optimized for culture selection of the hHpSCs, and that in combination with the absence of serum (except for the initial plating) minimized the conditions for any mature

hepatocytes or for the non-parenchymal cells (with any serum supplementation, the mesenchymal cells rapidly take over the cultures).

The typical plates had single cells and small cell clusters that adhered after the initial 24 hrs. Colonies formed within 5-7 days and were observed for up to 3 months by which time each colony contained approximately 2,000-5,000 cells per colony. Non-parenchymal cells, found to be a mix of precursors for hepatic stellate cells and endothelial cells, also continued to grow on the plates, typically around the perimeters of the colonies; the colonies grew forming a smooth supporting edge or sometimes formed large, confluent tightly bound cells.

The hHpSC colonies were isolated after 14-18 days by using a pipette tip to pick the colonies by hand using an inverted microscope (1X-FLAIII; Olympus). The colonies were attached primarily at their perimeters, whereas the centers of the colonies were not attached, making recovery by this manual method logical. The colonies were then suspended in serum-free KM. The average number of cells/colony was ~2500 cells. The hHpSC colonies were allowed to settle to the bottom of microcentrifuge tubes for collection (**Figure 4**).

**Human adult liver cell isolation and culture**

Fresh human hepatocyte cell suspensions were obtained from Triangle Research Laboratories (RTP, NC), and then either were processed immediately for RNA/DNA quantitative analysis or seeded into pulverized biomatrix-hyaluronan cultures with a serum-free, hormonally defined medium (HDM) tailored for maintenance of adult hepatocytes (*PhoenixSongs Biologicals*; Catalog # MM250) at cell densities recommended by TRL.

**Quantitative Analyses of DNA and RNA Content**

To assess total DNA remaining in the decellularized livers, fresh rat liver tissue and liver biomatrix scaffolds were weighed, cut and digested with Proteinase K and total cellular DNA was isolated following published protocols (193). To assess total RNA remaining in the liver

biomatrix scaffolds, both fresh rat liver tissue and rat liver biomatrix scaffolds were weighed and homogenized in TRIzol solution (Invitrogen), and total cellular RNA was isolated following manufacturer's instructions.

**Collagen and adhesion molecule chemistry analysis**

The amount of collagen in the biomatrix scaffolds was evaluated based on the hydroxyproline (hyp) content. Samples of whole livers (n=4) and of biomatrix scaffolds (n=6) were pulverized, washed and lyophilized. Aliquots were then hydrolyzed and subjected to amino acid analysis (194), and the collagen content per total protein was estimated based on the hyp value of 300 residues/collagen. Assays were measured individually with a cytofluor Spectramax 250 multi-well plate reader (Molecular Devices).

**Growth factor assays**

Samples of rat livers and rat liver biomatrix scaffolds were subjected to analyses for growth factors. The samples were flash-frozen in liquid nitrogen, pulverized into a powder, and sent in for analysis to RayBiotech, Inc. (Norcross, GA). These were then assayed with 1 mg/ml protein, yielding fluorescence, defined in fluorescent intensity units (FIUs). Semi-quantitative growth factor assays were done using the RayBio® Human Growth Factor Arrays, G Series 1. The FIUs were reduced by that for negative controls for non-specific binding and normalized to protein concentration. The data from the duplicates were averaged. Forty growth factors were assayed on fresh, rat liver tissue (n=3) and compared to assays from biomatrix liver scaffolds (n=3). Although the assays were developed for human growth factors, there is sufficient overlap in cross-reaction to rat growth factors to permit use for both the rat and human samples.

**Quantitative Real Time PCR (qRT-PCR) analyses**

Total RNA from monolayer cultures (positive control cells: hHpSC colonies) and freshly isolated hHBs were extracted with the RNeasy Mini Plus kit (QIAGEN) and by using TRI

Reagent (Invitrogen). Total RNA from the biomatrix/hyaluronan cultures was extracted using the TRI Reagent (Invitrogen). The cDNA was generated using the Takara Prime Script First Strand cDNA Synthesis Kit (Clontech Laboratories). Gene-specific primers (**Supplemental Table 1**) were validated using cDNA templates generated from relevant cell lines expressing each gene of interest. Gene expression baselines were defined using cDNA templates generated from hHBs and monolayer cultures (2D) of hHpSC colonies obtained from 3 different fetal livers. The hHBs were isolated from initial fetal liver preparations and constituted 98% of the parenchymal cell fraction (11, 65). The hHpSCs were derived from culture-selected colonies from plating of the fetal liver cell suspension in KM. Gene expression levels of hHpSCs in HA hydrogels were measured for 8 different biomatrix scaffold concentrations (2 samples per formulation, ~0.25 ml sample volume, seeding density: 50-100 colonies/sample) with hHpSC colonies obtained from the same fetal liver source; incubated in parallel with medium changes of KM every other day; collected after 5-7 days of culture; and fully repeated for 2 different fetal livers. Quantitative Real Time PCR (qRT-PCR) measurements were performed with an Applied Biosystems® 7500 Real-Time PCR System available in the Functional Genomics Core Facility at UNC Chapel Hill for the following genes: EpCAM, CXCR4, CK7, CK19, AFP, Albumin, Transferrin, TAT, and G6PC (**Supplemental Table 1**). All measurements of relative expression were normalized with respect to GAPDH by the absolute quantification method described elsewhere (195, 196).

**Analyses of secreted protein production**

Concentration levels of secreted AFP and albumin in culture media were measured to determine hepatic functions of hHpSCs in biomatrix/hyaluronan hydrogels with different biomatrix concentrations throughout 5-7 days of culture. Media supernatants were collected every other day from cultures of cells in 8 different biomatrix scaffold concentrations (2 samples per formulation, ~0.25 ml sample volume) starting 24 hours post-seeding and stored frozen at -20°C until analyzed. Secretion of AFP was measured by enzyme-linked immunosorbent assays

(ELISA) using human AFP ELISA kits (ALPCO Diagnostics). Albumin production was measured by ELISA using human albumin ELISA quantitation sets (Bethyl Laboratories). All assays were measured with a Cytofluor Spectramax 250 multi-well plate reader (Molecular Devices).

**Statistical analysis**

Experiments were repeated at least 2-3 times with duplicate or triplicate samples for each condition. Data from representative experiments are presented; similar trends were seen in multiple trials. Experimental quantitative data are displayed in a mean ± 1 standard deviation format in charts or displayed in a mean ± 1 standard error format in plots (as indicated). Significance of gene expression levels with respect to both hHpSCs (p-value: * < 0.05, ** < 0.01, *** < 0.001) was determined by two-tailed Student's t-test. All individual sample measurements were performed at least in duplicate.

**Results**

**Liver Biomatrix Scaffold Preparation**

Rat liver biomatrix scaffolds were prepared by decellurizating the livers from Sprague Dawley rats. Prior to surgery, the rats were anesthetized with 100 mg/kg of Ketamine and 10 mg/kg of Xylazine. After becoming unconscious from the anesthetic, the rat's abdomen was exposed by making an incision from the pelvis to the sternum. The sternum was cut and removed while avoiding the diaphragm and rib cage, prolonging the beating of the heart in order to maintain blood flow through the liver. A catheter was used to cannulate the portal vein, and blood in the liver was removed via perfusion with DMEM/F:12 for 30-40 minutes. After the blood was removed, the liver was perfused with a phosphate buffered saline (PBS) solution containing 1% (w/v) sodium deoxycholate (Sigma), 0.1mg/mL $CaCl^2$ (Fisher), and 36 units/L of Phopholipase A2 (Sigma) for 50 minutes until the tissue became transparent. These conditions rapidly degrade the enzymes produced by the disrupted cells during delipidation and so the

conditions preserve the native liver matrix components (e.g. adhesion molecules, proteoglycans, and glycosaminoglycans). Subsequently, the liver was perfused for 100 minutes with a buffer containing 3.4 M NaCl and supplemented with soybean trypsin inhibitor (Sigma); it was then rinsed by perfusion with DMEM/F:12 for 30 minutes. The buffer conditions are at salt concentrations that keep all of the collagens in the liver insoluble, whereas other cellular components that are not collagen-bound are solubilized and can be eliminated. The initial rinse was comprised of trypsin inhibitor (Sigma), DNase (Sigma) and RNase (Sigma) for 15 minutes; and finally rinsed by perfusion with DMEM/F:12 for another 30-60 minutes (**Figure 1**). The liver was then removed and cut into small pieces to be flashed frozen by submerging the pieces in liquid nitrogen for a few minutes. In order to facilitate pulverization, the small pieces were then broken into even smaller pieces with a disinfected pulverizing tool. These were stored at -80°C until the day of pulverization (**Figure 1**).

**Characterization of Rat Liver Biomatrix Scaffolds**

Freshly isolated rodent livers were obtained from healthy rats weighing 250-300 g. Liver decellularization was achieved as described above. After decellularization, the liver biomatrix scaffolds had a whitish, opaque appearance with visible branching of the vasculature throughout the acellular scaffold. The decellularized liver tissue was slightly larger in size when compared to that of the native liver but retained its liver shape and macroscopic appearance (**Figure 1**).

To estimate the efficiency of the decellularization and examine characteristics that might affect hepatic differentiation, samples of the liver biomatrix scaffolds were subjected to a variety of assays and compared to native livers as controls. The amount of nucleic acids remaining in the biomatrix scaffolds after decellularization was measured and determined to be insignificant when compared to the nucleic acid content found in fresh liver tissue, confirming the efficiency of the decellularization process.

Collagen is a primary component of the extracellular matrix to which many other factors (e.g. glycoproteins and proteoglycans) are attached and is comprised of cross-linked collagens and nascent collagens that are not cross-linked. The collagen content was analyzed and quantified by methods utilizing the fact that hydroxyproline (Hyp) is a unique component of collagens and collagenous proteins. The results were estimated based on the Hyp value of 300 residues/collagen and demonstrates that the decellularization process results in biomatrix scaffolds that retain ~99% of the collagens found in the native liver (**Figure 2**). Additional matrix components found to be present included fibronectins, laminins, and elastin among others (8). Proteoglycans and their glycosaminoglycan (GAG) chains are the primary chemical scaffolds for bound growth factors and cytokines (82). Growth factor analysis determined that most of these growth factor and cytokine components were preserved and were found at levels comparable to those in samples of fresh liver tissue (**Figure 2).** With a few exceptions, there was an equally proportional decrease in FIUs across over forty growth factors indicating uniformity in the decellularization process.

**Pulverization of Biomatrix Scaffolds**

Pulverization at liquid nitrogen temperatures was used as a method to generate powders of biomatrix scaffolds that might be used as an industrially scalable product. Prior to pulverization, the grinding vials, caps, and magnets (Spex Sample Prep) were disinfected in 10% bleach for 30 minutes, 1% bleach for an hour, and sterile water overnight. The following procedure was performed on dry ice (**Figure 1**). Specific quantities of flash frozen biomatrix scaffolds were aliquoted to attain specific concentrations when re-suspending the pulverized biomatrix powder with medium in preparation for cell culture. The disinfected grinding vials were capped on one side with a magnet inside. The measured quantities of frozen biomatrix scaffolds were carefully placed into the grinding vial with the magnet already inside while leaving some space near the top for the magnet to move initially in the pulverization cycle and for the grinding

vial to be capped. The vial was transferred and positioned within a Freezer/Mill (SpexSamplePrep). With safety gloves and apparel in place, liquid nitrogen was poured into the open Freezer/Mill (Spex SamplePrep) until nearly full. The placement of the grinding vial was in the pulverization slot of the top part of the machine and two others were placed in the incubating area right above (**Figure 3**). The top was then slowly lowered into the bottom of the Freezer/Mill to avoid liquid nitrogen overflow. The three samples were allowed to sit for 5 minutes to reach liquid nitrogen temperature before the machine was started. The Freezer/Mill was run for 5 minutes at a grinding rate of 14 impacts/second/side. When completed, the machine was opened and the vial from the pulverization slot was removed and placed at room temperature. One of the vials in the incubation slot was moved to the pulverization slot and replaced with another prefilled grinding vial and the machine was run again after the machine was refilled with liquid nitrogen. This cycle was repeated until all the samples in the grinding vials had been pulverized. Unless the grinding vials are compatible with the vial opener, the pulverized vials were allowed to sit at room temperature for at least 5 minutes for safety reasons before attempting to remove the caps by hand. While the powder was still frozen inside, the grinding vial was disinfected and the cap was removed with a back and forth wobble movement in the hood. The powder was then removed with a cold spatula that had been stored in dry ice, placed into a cold 50 mL conical tube, and stored at -80°C until thawed for cell culture (**Figure 3**).

**Hyaluronan Hydrogel Cultures containing Pulverized Liver Biomatrix Scaffolds**

Since the pulverized liver biomatrix powder is suspended in a solution or medium when thawed, many of the components can be lost during media changes when used in cell culture. To prevent this, hyaluronans, found naturally in all tissues, were utilized as a gelation factor to retain as many of the matrix components as possible. The hyaluronans, even prior to gelation, form a somewhat viscous solution into which cells can be suspended. Biomatrix-hyaluronan mixtures were prepared with final concentrations of 20 mg/mL of hyaluronic acid sodium salt

from Streptococcus equi (Sigma) and from 10 to 150 mg/mL of the pulverized liver biomatrix scaffolds.

To prepare the materials used in cultures of the hHpSCs, 0.02 g of hyaluronan powder was weighed, and the weigh paper was folded to form an enclosed container for each pair of cultures to keep the powder in a sterile environment (**Figure 3**). Also, 1 mL oral syringes (Becton Dickenson) were placed in sealed plastic bags. Finally, the 50 mL conical tube containing the stocks of pulverized biomatrix scaffolds was placed on dry ice, and enough powder was removed for the cultures planned. This powder was placed into a 15 mL conical tube and allowed to thaw into a liquid. The culture materials, including the hyaluronan containers and the oral syringes, were irradiated for 5 minutes in a Gammacell 1000 ELITE Irradiator for a total of 3250 rads, while the thawed pulverized biomatrix scaffolds were irradiated for 10 minutes for a total of 6500 rads to ensure sterility.

During the following steps, the materials were kept sterile under the hood and the solutions were kept well mixed either by shaking or vortexing before each step. For each duplicate of pulverized liver biomatrix scaffolds and hyaluronan (pLBM-HA) culture, 1 mL of Kubota's Medium was aliquoted into a 5 mL Round Bottom Test Tube (BD). To each test tube, specific volumes of thawed pulverized biomatrix were added and then vortexed to attain desired concentrations (**Figure 3**). For each test tube, the weigh paper containing the pre-weighed hyaluronan powder was removed from the plastic bag and slowly unfolded. The powder was carefully added to the 5 mL round bottom tube while minimizing contact of the powder with the sides of the test tube (**Figure 4**). The tubes were capped, and the mixture was immediately shaken vigorously in an up and down motion until the hyaluronan powder was fully dissolved in the biomatrix scaffold/media mixture. Then, with one last whipping motion, the entire mixture was forced to the bottom of the tube. A 1 mL oral syringe was then carefully removed from the plastic bag and used to gather and slowly aspirate the pLBM-HA mixture into the syringe with an average yield of 0.5 mL (**Figure 4**). Equal volumes of the aspirated mixture were added to one

of two wells in a 24-well plate. This was repeated for each mixture of pLBM-HA cultures. After allowing the material to incubate and settle into an even surface in the wells of the 24-well plate for ~20 minutes, the pLBM-HA mixture had an opaque appearance with some visible white streaks throughout the mixture that resembled webbing (**Figure 4**).

Each culture was then seeded with 50-100 hHpSC colonies. The colonies were allowed to equilibrate into this viscous material for 2-3 hours and then 1 mL of Kubota's Medium was very slowly added drop-wise to each well to try to avoid disturbing the pLBM-HA culture (**Figure 4**). After 24 hours, the medium was then slowly aspirated and replaced in the same drop-wise fashion with either Kubota's Medium or with a Hormonally defined Medium for Liver (HDM-L). Media changes were done every other day for 5-7 days. The collected medium was stored at -20°C for further analysis. Additional colonies of hHpSCs were picked on the day the cultures were seeded to serve as controls.

**Characterization of hHpSCs in pLBM-HA cultures**

Two weeks after the liver cell suspensions were plated onto plastic, hHpSC colonies began to appear and had a round appearance with clear borders. However, after isolating and seeding them into the pLBM-HA cultures, these hHpSC colonies formed 3D structures that transitioned into hepatic organoids. After a day of equilibrating in the pLBM-HA culture conditions, the hHpSC colonies lacked a distinct border and had an appearance of aggregates of cell clusters (**Figure 5a,5c,5e**). These cell clusters were visible throughout the colony and were slightly pigmented in appearance; the significance of the pigmentation is assumed related to differentiation but is not yet fully understood. After five days of culture, the hHpSC colonies retained a clear border once again by forming hepatic organoids with a much darker coloration as compared to the original slightly pigmented appearance (**Figure 5b,5d,5f**). In some cases, hHpSC colonies could be seen forming attachments to the bottom of the well (**Figure 5d**). Also, the pulverized biomatrix scaffold material was visible in culture and disappeared around the

colonies after 5 days of culture particularly in samples with higher concentrations of biomatrix scaffold material.

**Functional assays of hepatic metabolism for hHpSCs cultured in pLBM-HA.**

Immunosorbent assays were conducted on media samples collected every other day throughout the 5-7 days in culture to measure concentrations of secretory proteins indicative of hepatic functions and were compared between cultures with varying concentrations of pulverized liver biomatrix scaffolds (**Figure 6**). Measurements for each sample were calculated by normalizing to the respective amount of target initially secreted after 1 day of equilibration and calculating the fold change in order to account for variability in cell number between samples. Sample concentrations are represented to be compared over time (**Figure 6a,6b)** and between concentrations (**Figure 6c,6d)**. Throughout the 7 days in culture, the hHpSCs secreted both AFP and Albumin at increasing concentrations into the medium with concentrations peaking on day 5 and decreasing minimally on day 7 (**Figure 6).** AFP and Albumin secretion rates always increased in each respective sample with the greatest change at the pulverized liver biomatrix concentration of 100 mg/ml (**Figure 6**)**.** Secretion rates for both AFP and Albumin/day of media samples displayed a positive correlation with respect to pulverized liver biomatrix concentration with 0 mg/ml having the smallest change and 100 mg/ml having the greatest change (**Figure 6**).

**Gene expression in hHpSCs cultured in pLBM-HA**

The hHpSC colonies cultured in pLBM-HA were analyzed for mRNA expression of specific genes. Measurements of mRNA expression of hHpSCs isolated from fetal livers (n=3) were normalized to GAPDH expression (**Figure 7-9**). All measurements are expressed as fold changes normalized to the mRNA expression levels of hHpSC colonies isolated the same day but not seeded into the pLBM-HA environment.

After being cultured for 5 days in the pLBM-HA mixture, the cells in the hHpSC colonies developed phenotypic traits of an intermediate transitional stage between that of hepatoblasts (hHBs) and mature hepatocytes (**Figure 7,9**). This can be seen in the increased expression levels of AFP and Albumin along with the increased expression levels of an array of genes commonly found in the expression profile of mature hepatocytes (e.g. glucose-6-phophatase, tyrosine aminotransferase, transferrin). When comparing the freshly isolated hHpSC colonies to the hHpSC colonies cultured in the pLBM-HA mixture for 5 days, the differences were significant in the mRNA expression of genes commonly expressed by hHBs and mature hepatocytes (**Figure 7,9**)**.** Despite the similarities in their mRNA expression profiles, the expression levels of these genes in the hHpSC colonies cultured in pLBM-HA were much lower and achieved around 20% of the levels expressed by mature hepatocytes after 5 days of culture (**Supplemental Figure 1**) and around 10% of the levels after 7 days of culture (**Supplemental Figure 2**). Furthermore, the expression levels of certain genes in the hHpSC colonies cultured in the pLBM-HA mixture for 5 days were surprisingly similar to that of the freshly isolated hHpSC colonies (**Supplemental Figure 3**). This could indicate that some of the cells in the hHpSC colonies cultured in the pLBM-HA mixtures retained some properties of the cells in the hHpSC colonies when they were freshly isolated.

In addition to the differences between hHpSC colonies cultured in the pLBM-HA mixture and the freshly isolated hHpSC colonies, expression levels also varied between hHpSC colonies cultured in various concentrations of pulverized liver biomatrix when comparing the mRNA expression profiles of genes commonly expressed by hHBs and mature hepatocytes. After 5 days of culture in the pLBM-HA mixture, the hHpSC colonies cultured at the various concentrations of pulverized liver biomatrix scaffolds displayed a positive correlation in mRNA expression with 0 mg/ml having the lowest expression levels and 100 mg/ml having the highest expression levels with a few exceptions (**Figure 7,9**). Despite this trend in increased expression as the concentration of pulverized biomatrix increases, many of the differences between the

expression levels could not be characterized as significant (**Figure 7**). However, on day 7, hHpSC colonies cultured at the concentration of 100 mg/ml of pulverized liver biomatrix had an expression profile that was significantly different from the expression profile of the hHpSC colonies cultured at the concentration of 0 mg/ml of pulverized liver biomatrix scaffolds with the hHpSC colonies at the concentration of 100 mg/ml having much higher mRNA expression levels of genes commonly expressed by hHBs and mature hepatocytes (**Figure 8**).

**Discussion**

We have developed a strategy by which to establish functional human hepatic organoids derived from hepatic stem cells by culturing them with serum-free HDM-L, designed for mature liver cells, and in hyaluronan hydrogels into which are mixed pulverized liver biomatrix scaffolds. The design is permissive for industrial scalability.

The need for complex forms of extracellular matrix has been made apparent by decades of studies, especially ones within recent years (96, 122-127, 129, 147, 197). The old methods of plating cells onto simple collagens or even in collagen sandwiches enabled cells to have many more adult functions than in cells cultured on plastic but the effects proved transient and only partially effective (20, 21, 26-28). Better results to date have been made possible with the use of matrix extracts prepared by decellularization of tissues with methods ranging from freezing and enzymatic protocols (174) to delipidation followed by distilled water washes (7, 132).

However, the potency of matrix scaffolds has been minimized by the methods by which the scaffolds have been prepared, methods that cause major losses in matrix components. With the protocols of others, the loss of matrix components occurs at every step, even the first step (delipidation). Most decellularization methods use detergents to delipidate the cells, and the delipidation strategies usually make use of harsh solutions such as Triton X-100, sodium dodecyl sulfate (SDS), and CHAPS, (7, 130, 132). SDS binds tightly to the matrix making it toxic, and requires long washes to minimize that toxicity (140). In addition, these detergents

disrupt the native architecture of the matrix and enhance its solubility (28). A gentler alternative was used in our experiments and involved bile salts. particularly sodium deoxycholate (SDC) used in conjunction with the enzyme Phospholipase A2 (PLA2). This method quickly (within 20 minutes) delipidates the tissue. Specifically, PLA2 is activated by SDC and degrades the phosphoglyceride on both the cytoplasmic and mitochondrial membranes into a surfactant called lysolecithin, which causes rapid cell necrosis (8).

Secondary to delipidation, the decellurization protocols by others use freezing or even some matrix-degrading enzymes (174) and then all make use of washes that are with low ionic strength buffers and even distilled water. The combination of these steps, especially after the delipidation steps, results in the dissolution of most of the matrix components except for the cross-linked collagens and their associated factors (198).

All efforts yield scaffolds with some biological activity, certainly much more than the use of purified, single matrix components (199, 200). However, all methods with the exception of the one reported here cause such a loss of matrix components that compensatory efforts are required to restore cell attachment or to overcome loss of patency with the matrix remnants of the vascular channels. In addition, the cells must be cultured for long periods of time (often weeks) to allow functionality of the cells to be restored (7, 131-134). Though these compensatory efforts help, they do not restore the histologically accurate location of the matrix components. The more successful compensatory methods have been the transplantation of scaffolds seeded with cells in order to let restoration occur *in vivo* (129, 130, 197)

Our protocol contrasts sharply with those of others in that it retains far more of the matrix chemistry and maintenance of histologically accurate positioning of the matrix components (8, 201). The experimental design that allowed this is derived from a focus on the collagens, which are the central scaffolds of the matrix. By retaining as much and as many of the collagens as possible, including cross-linked, non-crosslinked and nascent forms, we theorized we would

retain more of the extracellular matrix. We made use of the methods of Edward Miller (145, 146, 202) who used buffers at salt solubility constants known to keep the collagens insoluble.

We determined the collagen types in liver (e.g. types I, III, IV, V, VI) and then utilized buffers with a salt concentration requisite to keep these collagens insoluble (8, 147). This enabled preservation of essentially all of the collagens (~98-99%) including both nascent and cross-linked ones. This also preserved the matrix components and the other factors bound to those collagens. These include the proteoglycans, whose glycosaminoglycan chains constitute the chemical scaffolds for cytokines and growth factors (8). The resulting biomatrix scaffolds consist of a complex of collagens, collagen-bound extracellular matrix components, cytokines, and growth factors that act as a supporting framework and provide a composite set of signals for cell migration, proliferation, and differentiation (130, 203). Frozen sections of liver biomatrix scaffolds have been shown to promote the differentiation of hHpSCs to mature parenchymal cells and to maintain this differentiated phenotype for more than 8 weeks (8). The biophysical and biochemical properties of these biomatrix scaffolds are tissue-specific and retain localization of matrix components in histologically accurate fashion.

Biomatrix scaffolds retain patency with respect to the vascular channels (8, 201). Indeed, ultrasound imaging of the biomatrix scaffolds indicated a matrix architecture far more complex than scaffolds that are primarily or solely cross-linked collagens. The biomatrix scaffolds have branching vascular and microvascular channels down to ~150 microns – levels close to those of capillaries. There are no other protocols that retain microvascular channels to this extent (201).

The intact biomatrix scaffolds were shown also to permit hepatic organoid formation, with retention of acinar-specific localization of those functions assayed, even when recellularized with a hepatoma cell line, Hep3B (201). Efforts are ongoing to use biomatrix scaffolds for recellularization with normal fetal liver cell suspensions (Hanson et al. Manuscipt in preparation).

Initial efforts to exploit the potency of the biomatrix scaffolds for industrial scale culture systems made use of pulverized scaffolds that were dispersed onto culture dishes (8). However, the plating of the pulverized matrix onto plastic resulted in a loss of some of the biological activity due to what is assumed to be a loss of factors that became soluble in the culture media because the matrix was pulverized. To overcome this deficit, we elected to mix the powdered biomatrix scaffolds with hyaluronans to preserve the biologically active factors, and then to embed the hHpSC colonies into the mix. To maximize the ability to readily retrieve the cells, the hyaluronans used were not cross-linked into a stable hydrogel. Consequently, a nominal amount of hyaluronan is lost with each medium change. Initially, the culture mixture is thick and viscous but gradually acquires the consistency of a slightly viscous liquid. This allows for the hHpSC colonies to form into organoids when initially cultured in the pLBM-HA system and to be carefully removed without further manipulation after 5 days in culture to be utilized in additional testing.

Hyaluronans are ideal as a base material to be mixed with the powdered biomatrix scaffolds. They are conserved across species, are a primary component of all stem cell niches, and do not cause any inflammatory or immunologic responses (204). They form hydroscopic, non-rigid structures with perfect elasticity; are fully equilibrated with all components in the medium, but have no sulfate groups and very few sites for binding of signaling molecules. Thus, the signaling components will be derived from the powdered scaffold material combined with the hyaluronans. The efforts of Glenn Prestwich et al. (U. Utah) have resulted in chemical strategies to generate modular units of hyaluronans that can be assembled into cost effective biomaterials useful for tissue engineering strategies (204-207). Hyaluronans are an FDA approved product that is readily available and are already used in clinical applications such as the repair of wounds and the regeneration of organs (43, 208). Combining all of these factors with the ease with which this molecule can be modified makes hyaluronan an ideal biomaterial in the

fabrication of a culture system that can promote the differentiation of hepatic stem cells to mature liver cells.

The pulverization of the liver biomatrix scaffolds is essential for scalability. The process eliminates the gross, macroscopic and microscopic native structure of the scaffold but preserves the matrix components in a powder form. As valuable as that native structure is, it is a barrier to industrial scalability. By pulverizing the scaffold, it is feasible to provide the matrix components in a digitized form, and when in combination with the hyaluronans, a form can be presented in 3D. A critical step in the method was to optimize the ratio of hyaluronans to biomatrix scaffold material to elicit the differentiation effects desired. Secreted protein analysis suggests that the metabolic activities of the hHpSC colonies seeded in the pLBM-HA cultures are dependent on liver biomatrix concentration. Increases in the secretion rates of factors that indicate hepatic functionality (e.g. Albumin) correlated to increases in pulverized liver biomatrix concentration with the concentration of 100 mg/ml having the greatest increase. The pulverized liver biomatrix could be seen to influence the hHpSCs at concentrations as low as 10 mg/ml. However, concentrations above 100 mg/ml seemed to have a detrimental effect on the secretion of these factors suggesting that this concentration is the upper limit for healthy hHpSC cultures. When hHpSCs were cultured using undiluted pulverized liver biomatrix alone, most cells did not survive (data not shown). It is possible that there may be a salt residue left in the biomatrix after decellularization that is negatively affecting the hHpSCs and that the pulverization process is only magnifying that impact. When lower concentration levels were tested and the secretion rates of cultures with pulverized liver biomatrix were compared to cultures with only hyaluronan, it is clear that the differentiation potential of the hHpSC colonies is positively affected by pulverized liver biomatrix and that certain concentrations can have a promotive effect on the hepatic differentiation of the hHpSCs.

Analysis of gene expression provides evidence that the survival and growth of these hHpSCs in these cultures of pulverized biomatrix and hyaluronan mixtures are concentration

dependent; the pulverized biomatrix concentration can be adjusted to levels that promote healthy cell culture and differentiation. Common stem cell markers such as CXCR4 and EpCAM, along with early hepatocytic genes including CK19 and CK7, were evaluated. EpCAM is typically found in cell-cell binding interactions while CXCR4 is a transmembrane cell surface receptor. Both are found periportally in the adult liver and are stabilized in cells bound to hyaluronans (65, 209). CK19 and CK7 are intermediate filament proteins partly responsible for structural integrity in the cytoplasm (73). These markers were found to be at levels that were either comparable or lower than the levels found in the hHpSC controls, suggesting that some of the cells had maintained some properties of a stem cell phenotype while some had differentiated into phenotypes that lack the expression of these genes (i.e. mature hepatocytes).

The hHB marker, AFP, and the expression of albumin, found in hHBs and in mature hepatocytes, were also evaluated. AFP is a secreted protein that binds various factors found in serum and is replaced by albumin in more mature hepatocytic cell phenotypes (77). Gene expression of both of these markers had a positive correlation with the concentration of pulverized biomatrix and the difference between the cultures with pulverized biomatrix and without pulverized biomatrix was even more pronounced after 7 days despite an overall decrease in gene expression levels. These results provide evidence that these hHpSCs have differentiated into cell phenotypes that are similar or even more mature than hHBs and committed hepatocytic progenitors.

Mature hepatocytic markers that were assayed were zone 1 genes, such as glucose-6-phosphatase (G6PC), and zone 2 genes such as tyrosine amino-transferase (TAT) and transferrin. G6PC is the rate-limiting enzyme in hepatic glycogenolysis and gluconeogenesis, while TAT is an enzyme that breaks down the tyrosine found in many foods. Both activities are found in mature hepatocytes particularly in the midacinar zone (210, 211). Transferrin plays a major role in iron uptake, required by all polymerases, and in metabolism in mature hepatocytes (212). These mature hepatocytic genes were also expressed in a concentration dependent

manner and also had a positive correlation with respect to an increase in pulverized matrix concentration. From these results, it is reasonable to conclude that many of the hHpSCs have differentiated into cell phenotypes similar to that of mature parenchymal cells.

In this study, we outline a method that utilizes the pulverized product of a decellularization procedure that preserves more of the native matrix components than other existing protocols and mixes them with hyaluronan to enable use of the mix for industrial scale stabilized cultures of hepatic organoids. We show that the composition of the microenvironment surrounding human hHpSCs in culture can drive differentiation. More specifically, these experiments examine the correlation between modifying the biological properties of a microenvironment and their growth and differentiation by subjecting hHpSCs to various concentrations of matrix components that comprise the pulverized product of a decellularized liver biomatrix scaffold. The pulverized matrix and hyaluronan used in our culture system are cross species compatible (213, 214) and biodegradable (204, 215) and thus have the potential to be cost effective and a safe option for *in vivo* cell-based therapies. The pLBM-HA mixture can act as the initial support structure for the transplanted cells by either facilitating or maintaining their differentiation in hopes that these cells will eventually be able to secrete their own extracellular matrix to gradually replace the originally supplemented microenvironment.

Our method also provides an *ex vivo* model for the study of stem cell functions in a 3D culture microenvironment that is more representative of the environment found in the native liver and allows for the accelerated growth and differentiation of these stem cells to phenotypes similar to those of mature hepatocytes. Since this pulverization product is industrially scalable, this method overcomes any size constraints of the source of the decellularized tissue and can conceivably be used to mass-produce culture systems which have implications in numerous industrial applications.

**Figures and Tables**

**Figure 20**: Schematics of the Decellularization of Liver and Preparation of Grinding Vials

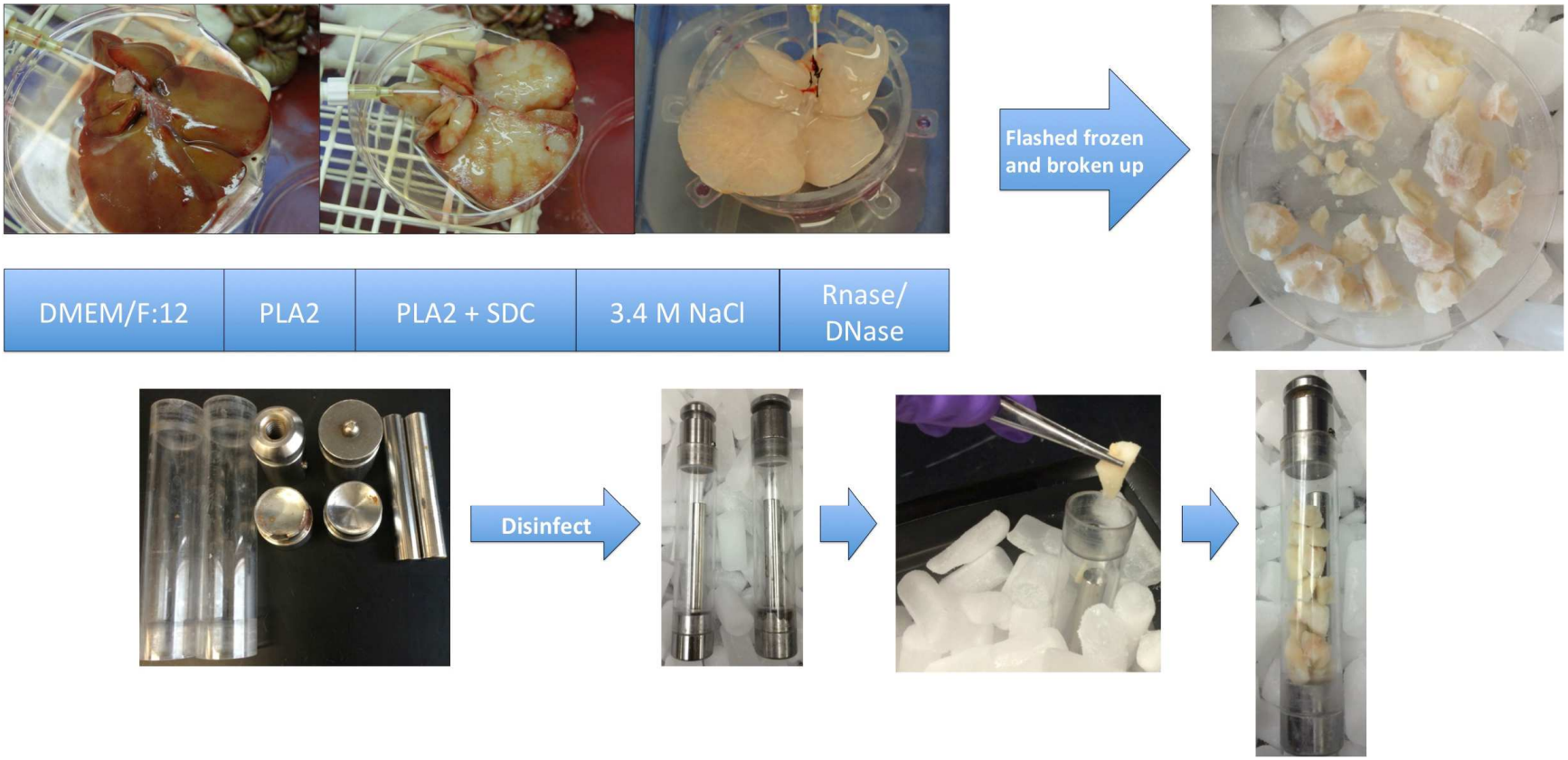

**Figure 21**: Collagen Analysis and Growth Factor Array of Decellularized Tissue compared to Fresh Liver Tissue. All data reported as mean ± 1 standard deviation

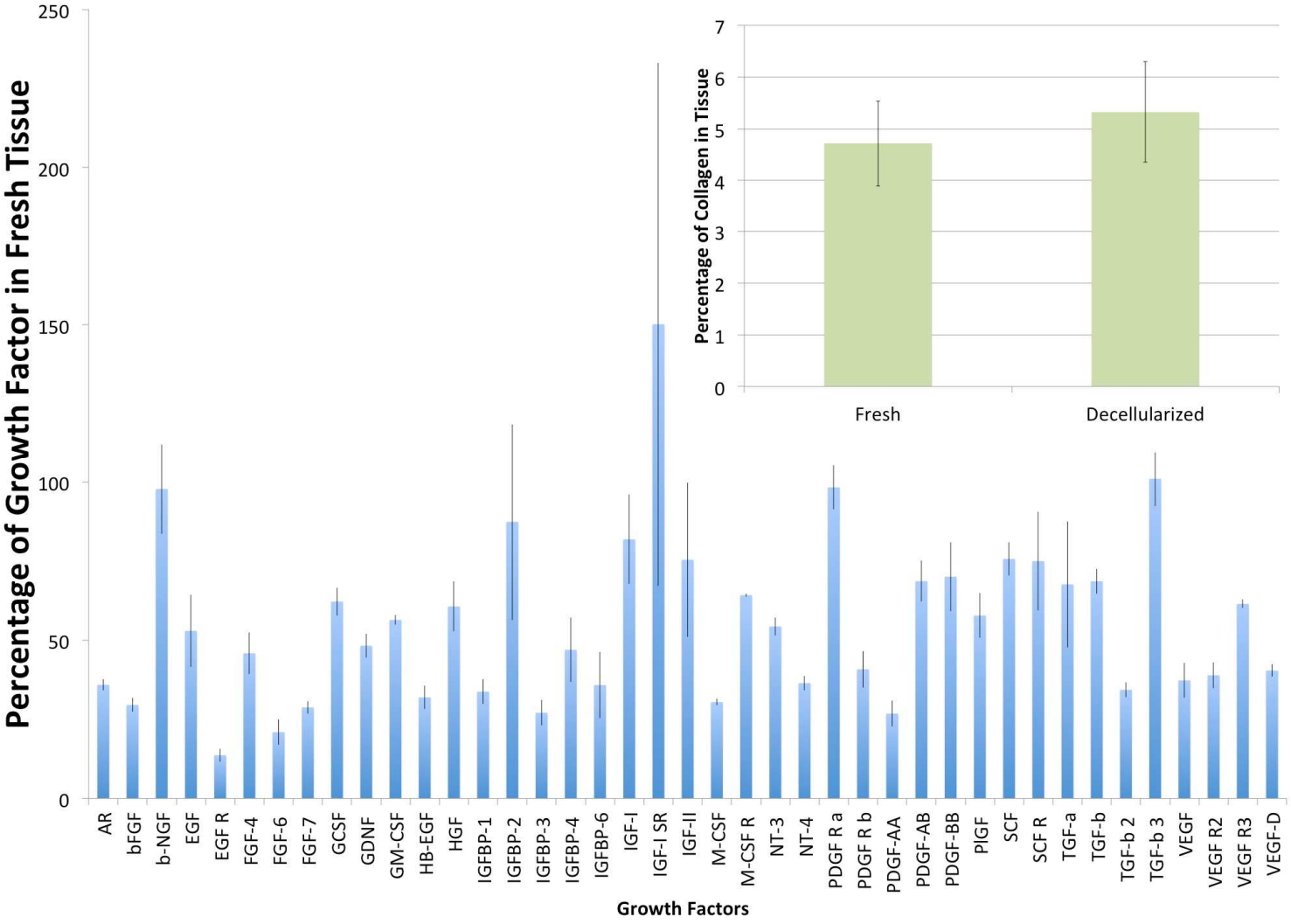

**Figure 22**: Schematics of the Pulverization Process and Preparation of LBM-HA Culture Materials

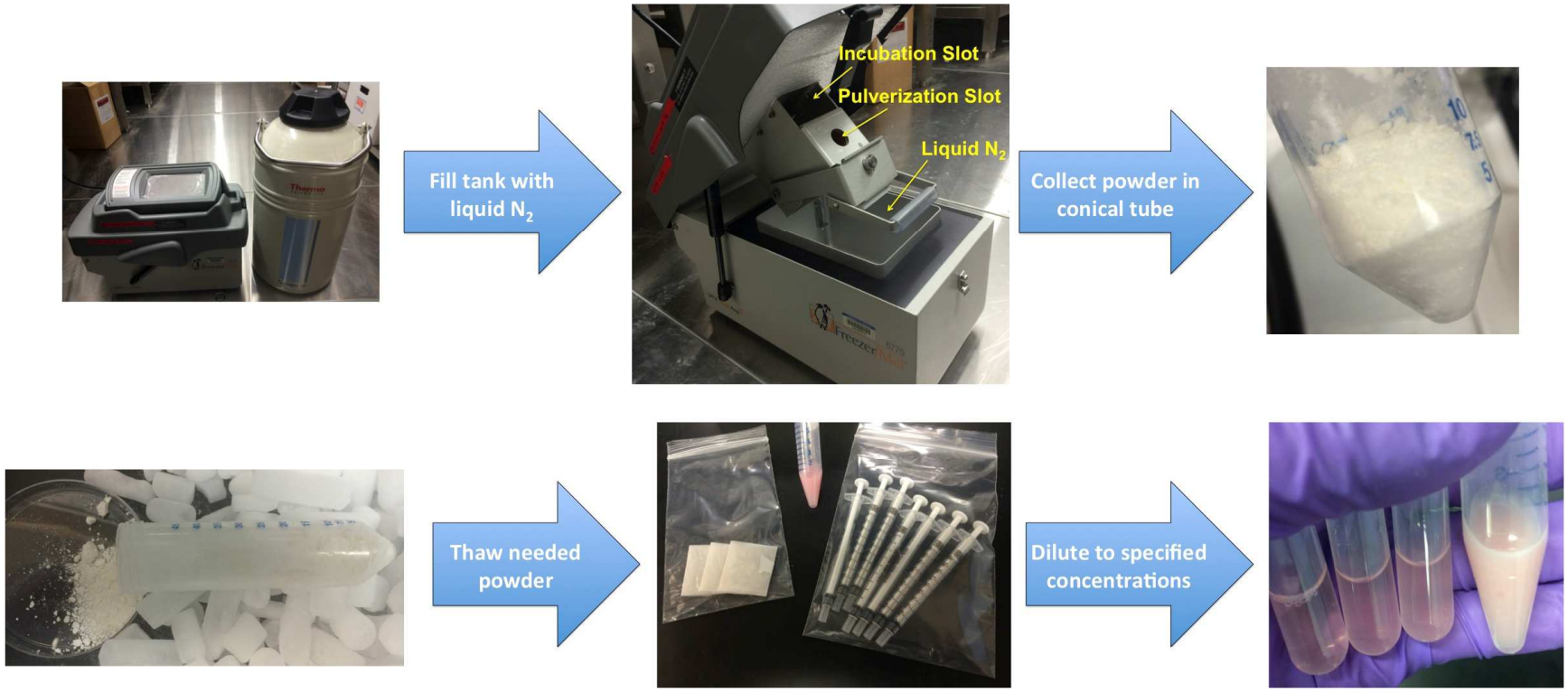

**Figure 23**: Schematics of the Preparation of Pulverized Liver Biomatrix and Hyaluronan Cultures

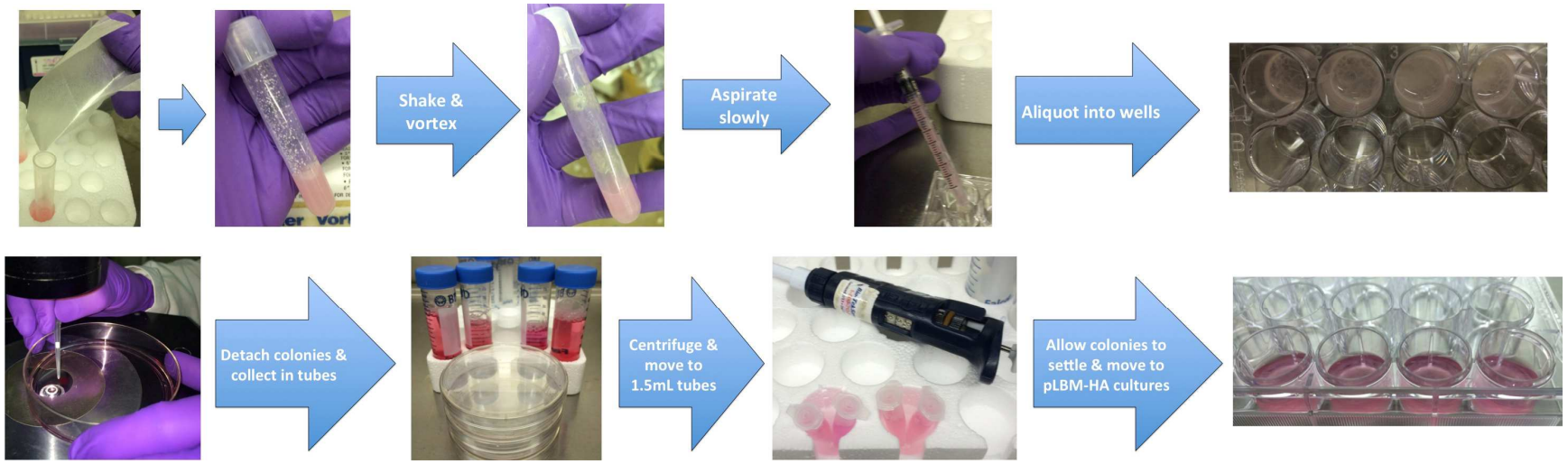

**Figure 24**: Phase contrast imaging of hHpSC colonies in pLBM-HA cultures. Day 1 (A) and Day 5 (B) of culture in 0 mg/ml of pulverized liver biomatrix and 20 mg/ml of hyaluronan. Day 1 (C) and Day 5 (D) of culture in 50 mg/ml of pulverized liver biomatrix and 20 mg/ml of hyaluronan. Day 1 (E) and Day 5 (F) of culture in 100 mg/ml of pulverized liver biomatrix and 20 mg/ml of hyaluronan. Some colonies could be seen to have formed attachments to the culture surface after 5 days (blue arrows).

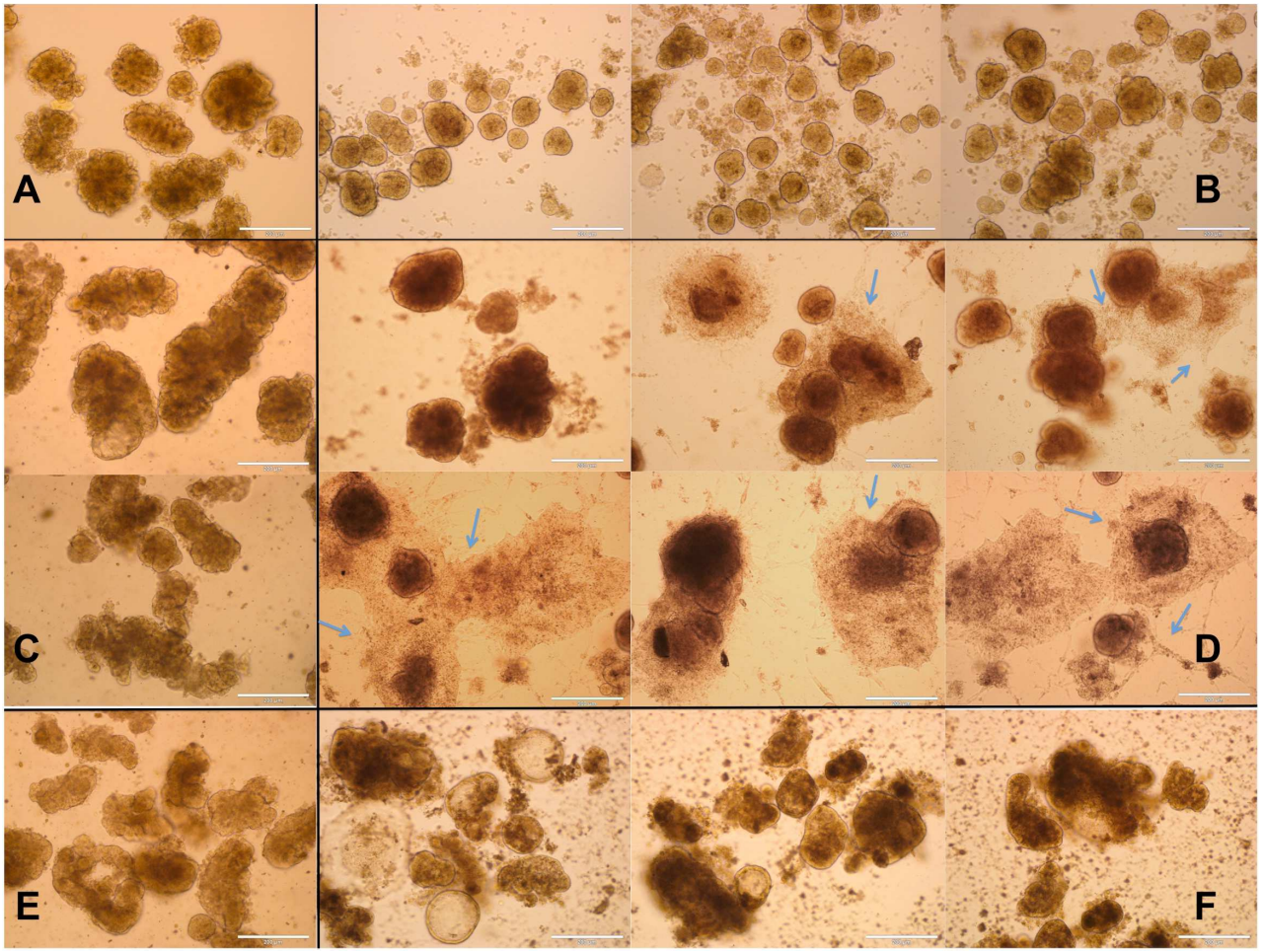

**Figure 25**: Functional assays of hepatic functions over time to compare hHpSCs when cultured at various concentrations of pulverized biomatrix hyaluronan mixed with hyaluronans. AFP and Albumin secretion are reported as fold change normalized to initial target levels 24h after seeding. (A) Change in AFP secretion measured over time. (B) Change in Albumin secretion measured over time. Significance levels for secretion rates of hepatic factors (p-value: * < 0.05, ** < 0.01, *** < 0.001) are reported with respect to secretion rates 24h after seeding for each pulverized biomatrix concentration (two-tailed Student's *t*-test). All data reported as mean ± 1 standard error.

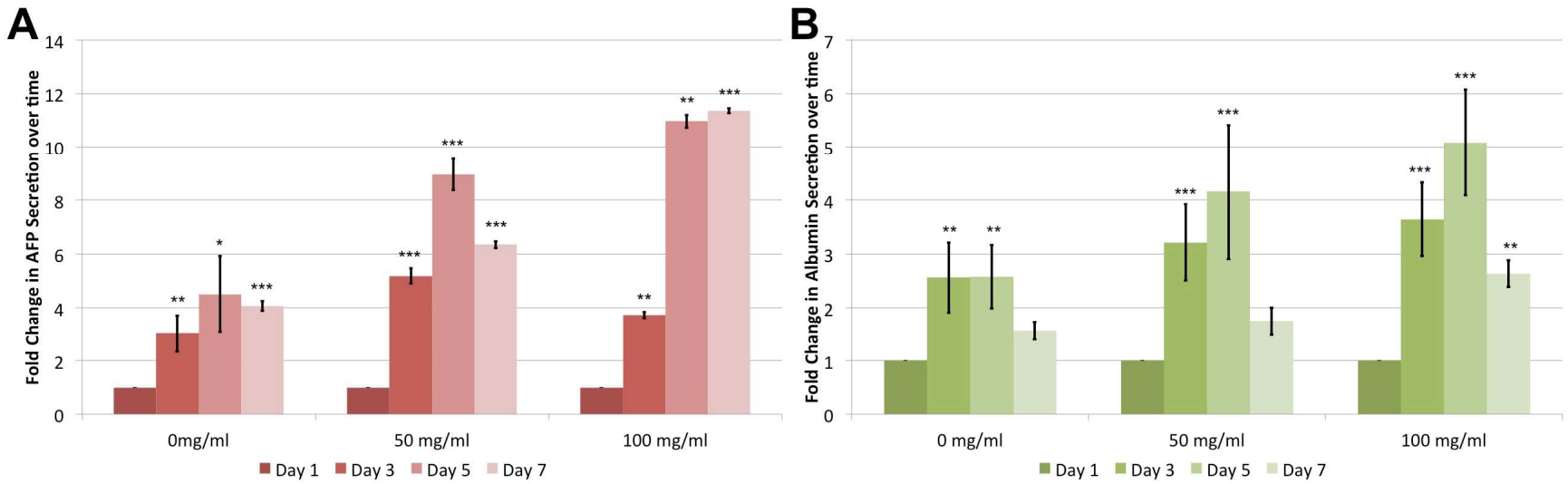

**Figure 26**: Gene Expression levels for differentiation markers in hHpSCs cultured in Human Differentiation Medium for Liver with hyaluronan and various concentrations of pulverized biomatrix after 5 days by qRT-PCR. Target mRNA expression levels are normalized to GAPDH expression and fold changes are normalized to initial target mRNA expression levels in hHpSCs . Significance levels for secretion rates of hepatic factors (p-value: * < 0.05, ** < 0.01, *** < 0.001) are reported with respect to expression levels of hHpSCs isolated the same day the cultures were started (two-tailed Student's *t*-test). All data reported as mean ± 1 standard deviation.

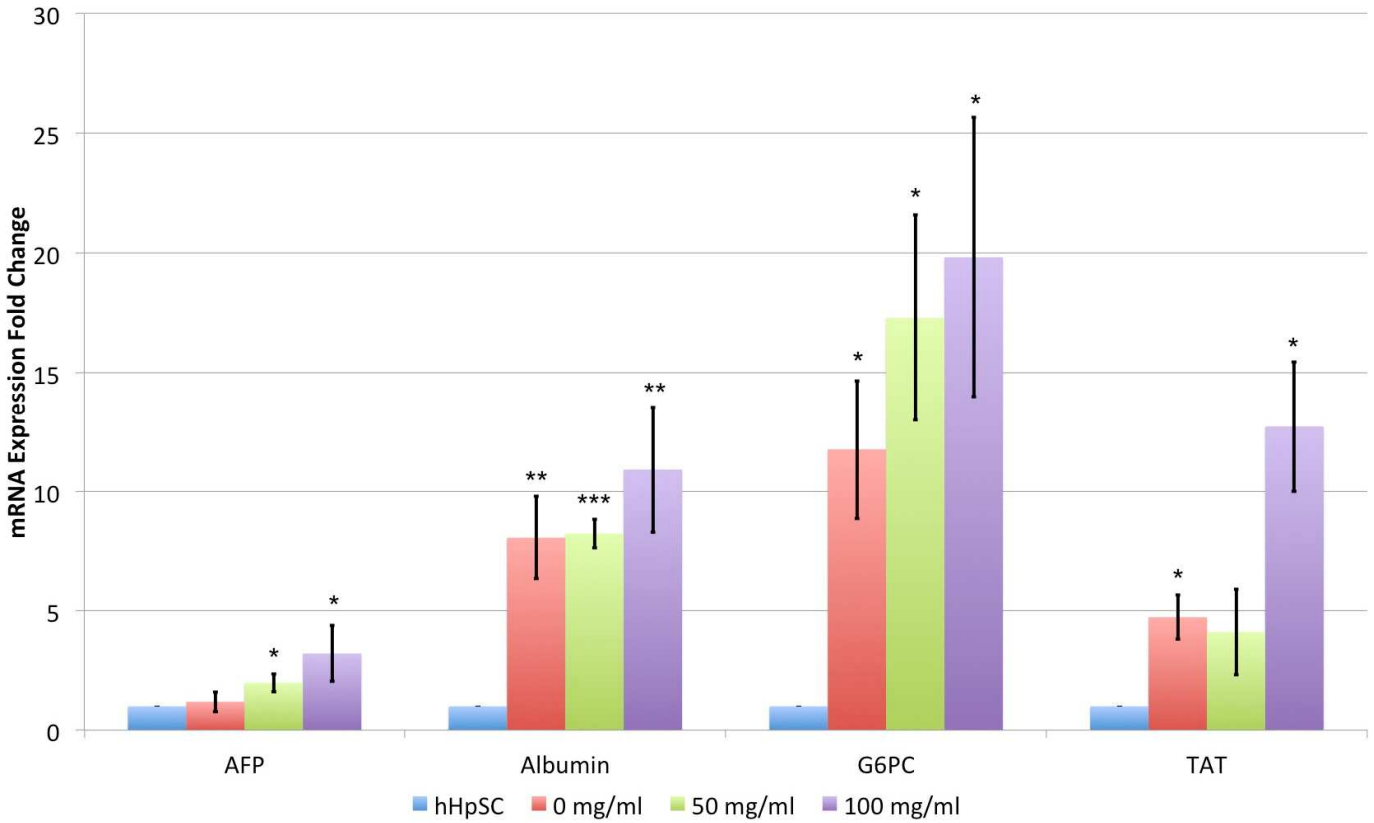

**Figure 27**: Gene Expression levels for differentiation markers in hHpSCs cultured in Human Differentiation Medium for Liver with hyaluronan and various concentrations of pulverized biomatrix after 7 days by qRT-PCR. Target mRNA expression levels are normalized to GAPDH expression and fold changes are normalized to initial target mRNA expression levels in hHpSCs. Significance levels for secretion rates of hepatic factors (p-value: * < 0.05, ** < 0.01, *** < 0.001) are reported with respect to expression levels of hHpSCs isolated the same day the cultures were started (two-tailed Student's *t*-test). Target mRNA expression levels of samples at the concentration of 100 mg/ml are also compared to the samples at 0 mg/ml for significance (blue). All data reported as mean ± 1 standard deviation.

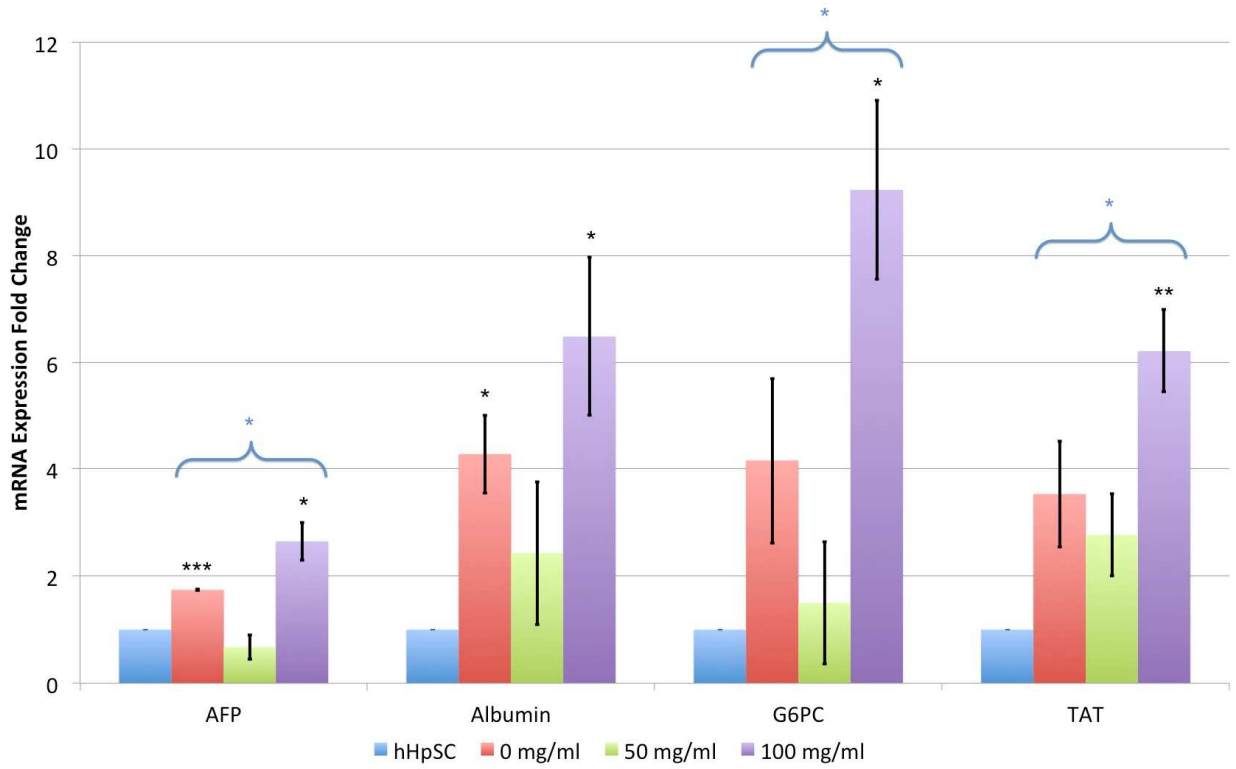

**Figure 28**: Gene Expression levels for the mature hepatocyte marker transferrin in hHpSCs cultured in Human Differentiation Medium for Liver with hyaluronan and various concentrations of pulverized biomatrix after 5 and 7 days by qRT-PCR. Target mRNA expression levels are normalized to GAPDH expression and fold changes are normalized to initial target mRNA expression levels in hHpSCs. Significance levels for secretion rates of hepatic factors (p-value: * < 0.05, ** < 0.01, *** < 0.001) are reported with respect to expression levels of hHpSCs isolated the same day the cultures were started (two-tailed Student's *t*-test). All data reported as mean ± 1 standard deviation.

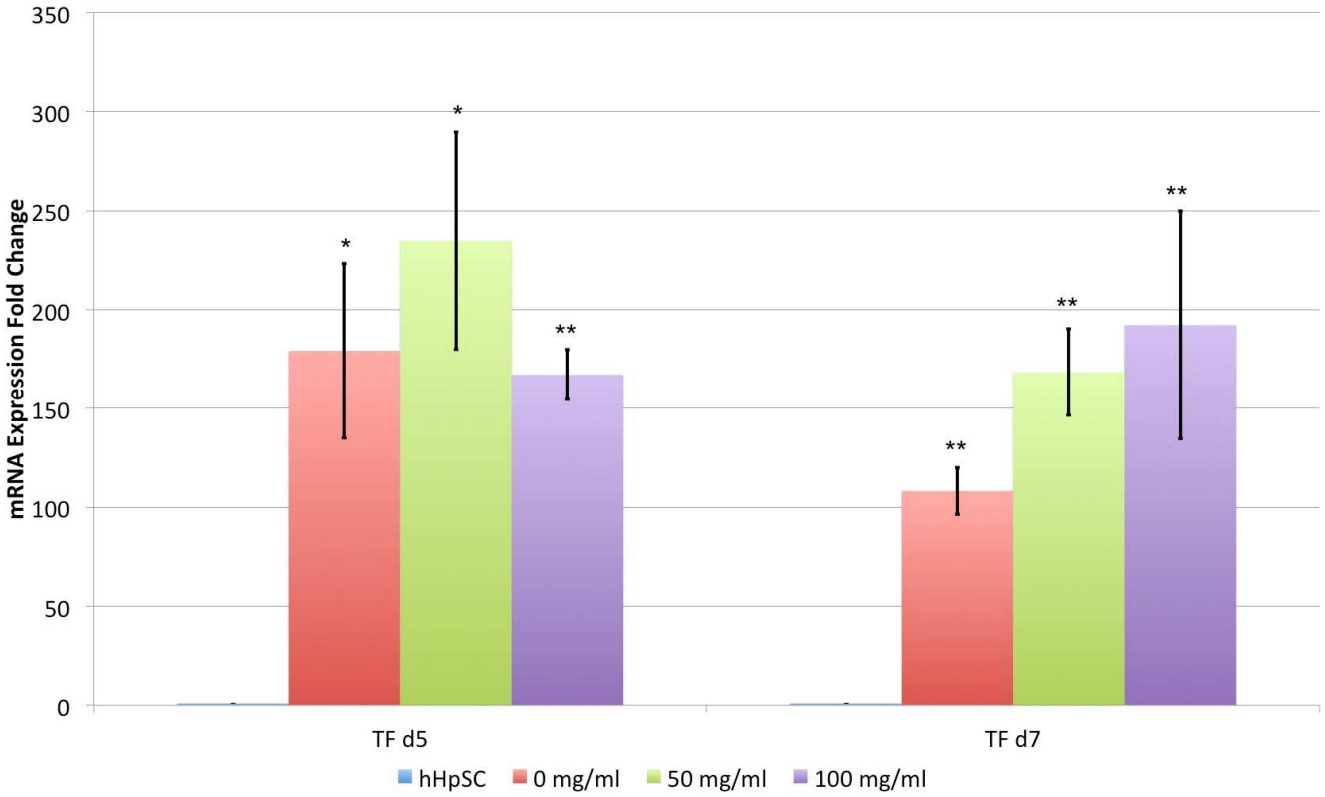

**Supplemental Figures and Tables**

**Table 4:** Primer sequences used in gene expression assays for hHpSC differentiation

| Gene (NCBI ID) | Description | Primer Sequence (5' → 3') | NCBI Ref. Seq. | Positive Control |
|---|---|---|---|---|
| EPCAM | Epithelial Cell Adhesion Molecule | Forward: GACTTTTGCCGCAGCTCAGGAAG<br>Reverse: GCCAGCTTTGAGCAAATGACAGTATTTTG | NM_002354.1 | hHpSC |
| CXCR4 | Chemokine receptor 4 | Forward: TACACCGAGGAAATGGGCTCA<br>Reverse: AGATGATGGAGTAGATGGTGGG | NM_003467.2 | |
| KRT7 | Cytokeratin 7 | Forward: TGCTGCCTACATGAGCAAGGT<br>Reverse: TCTGTCAACTCCGTCTCATTGAG | NM_005556.3 | Hep3B |
| KRT19 | Cytokeratin 19 | Forward: CCGCGACTACAGCCACTACT<br>Reverse: GTCGATCTGCAGGACAATCC | NM_002276.4 | |
| AFP | α-fetoprotein (hepatic-specific variant) | Forward: CCATGAAGTGGGTGGAATCAA<br>Reverse: TCTGCAGTACATTGGTAAGAATCCA | NM_001134 | |
| ALB | Albumin | Forward: TGCTGATGAGTCAGCTGAAAA<br>Reverse: TCAGCCATTTCACCATAGGTT | NM_000477.4 | HepG2 |
| TF | Transferrin | Forward: CCTCCTACCTTGATTGCATCAG<br>Reverse: TTTTGACCCATAGAACTCTGCC | NM_001063.3 | |
| TAT | Tyrosine aminotransferase | Forward: TTTGGGACCCTGTACCATTGT<br>Reverse: GCATTGGACTTGAGGAAGCTC | NM_000353.2 | |
| G6PC | Glucose-6-phosphatase | Forward: TCAGGGAAAGATAAAGCCGACC<br>Reverse: AGGTAGATTCGTGACAGACAGAC | NM_000151.3 | |
| GAPDH | Glycerine aldehyde-3-phosphate dehydrogenase | Forward: AAGGTGAAGGTCGGAGTCAA<br>Reverse: AATGAAGGGGTCATTGATGG | NM_002046.3 | Endogenous housekeeping |

**Figure 29:** Comparison of differentiation marker gene expression levels between mature hepatocytes and hHpSCs cultured in Human Differentiation Medium for Liver with hyaluronan and various concentrations of pulverized biomatrix after 5 days by qRT-PCR. Target mRNA expression levels are normalized to GAPDH expression and fold changes are normalized to initial target mRNA expression levels in hHpSCs. All data reported as mean ± 1 standard deviation.

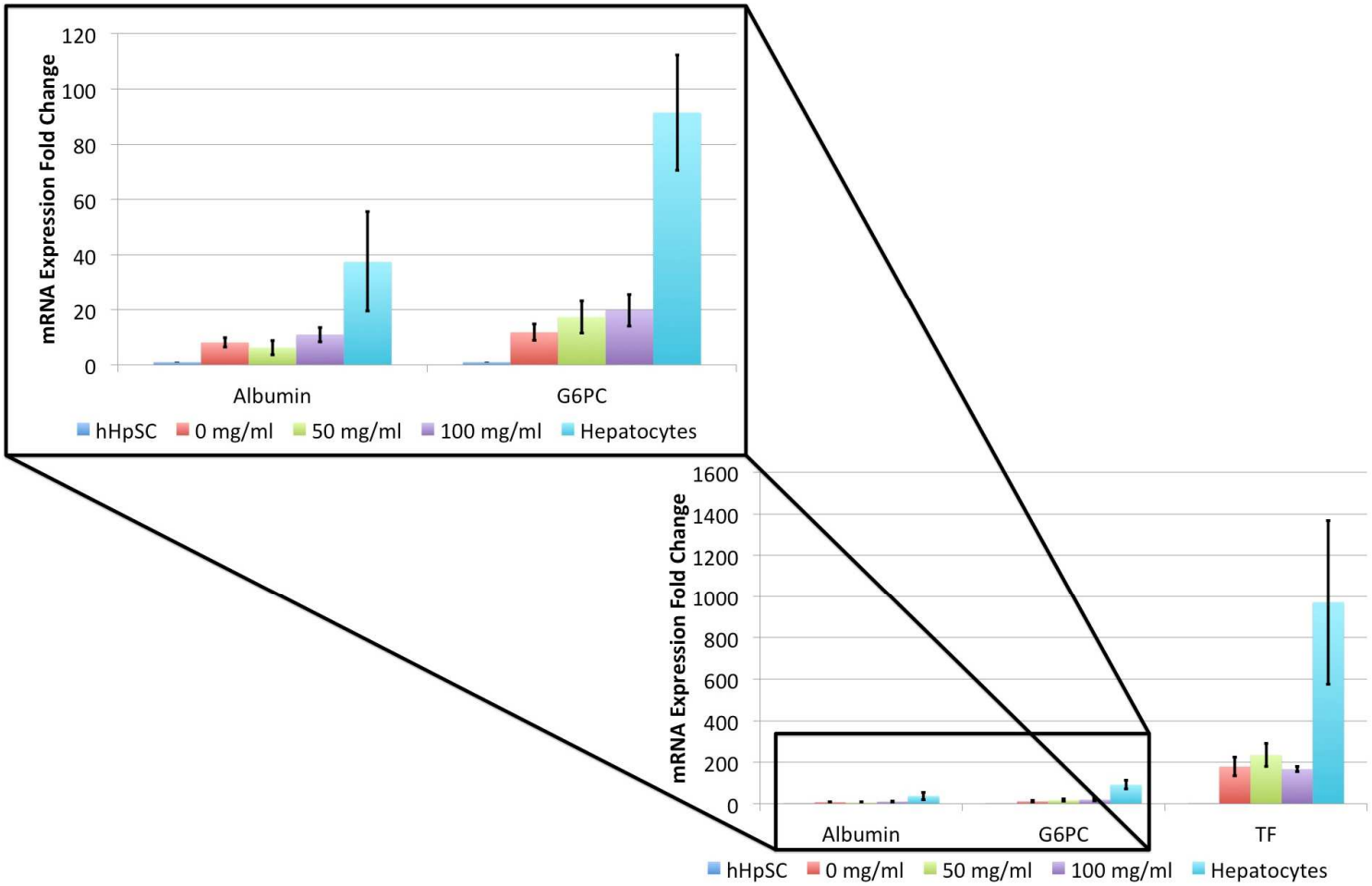

**Figure 30:** Comparison of differentiation marker gene expression levels between mature hepatocytes and hHpSCs cultured in Human Differentiation Medium for Liver with hyaluronan and various concentrations of pulverized biomatrix after 7 days by qRT-PCR. Target mRNA expression levels are normalized to GAPDH expression and fold changes are normalized to initial target mRNA expression levels in hHpSCs. All data reported as mean ± 1 standard deviation.

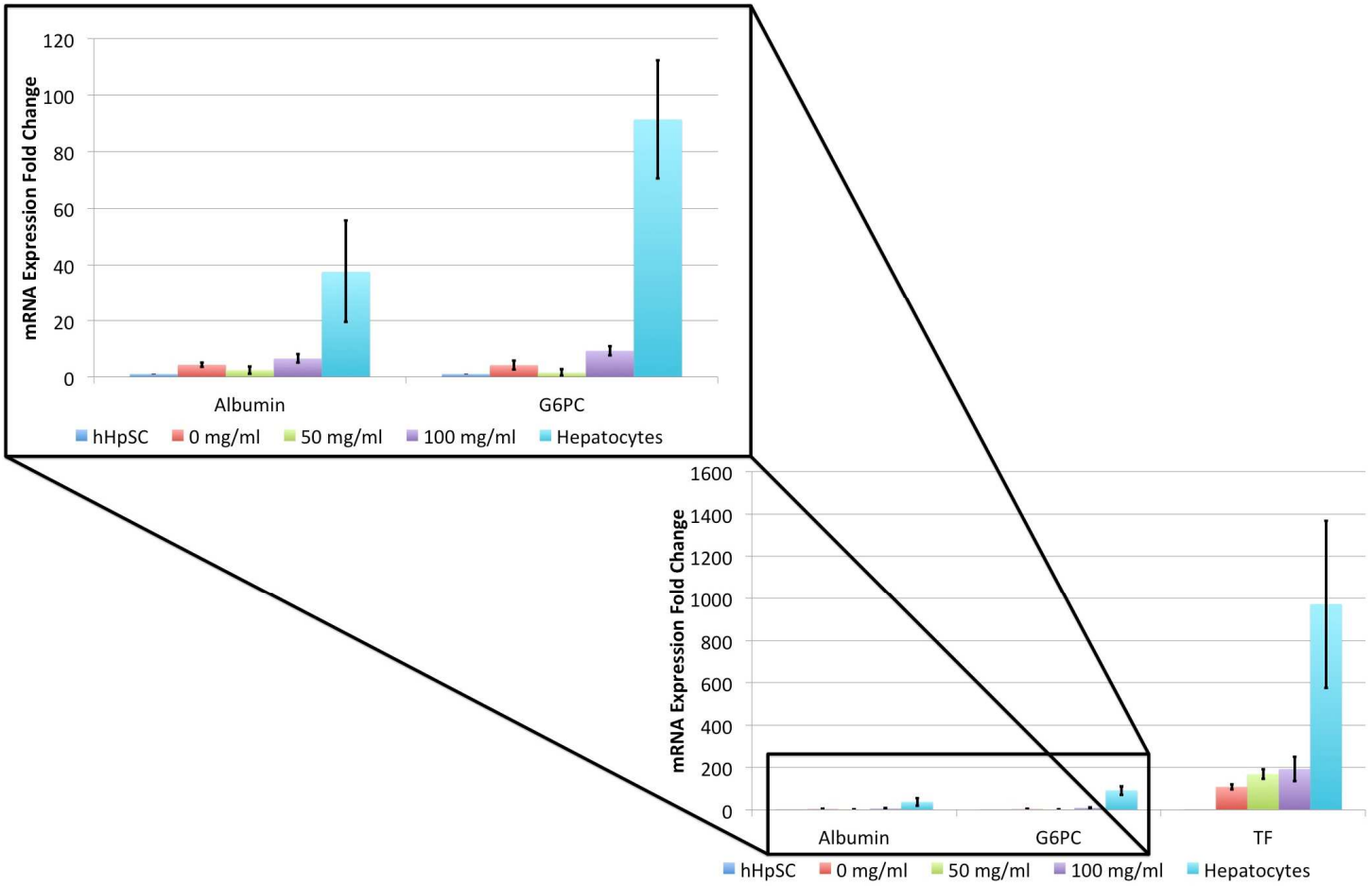

**Figure 31**: Gene Expression levels for stem cell markers in hHpSCs cultured in Human Differentiation Medium for Liver with hyaluronan and various concentrations of pulverized biomatrix after 5 days by qRT-PCR. Target mRNA expression levels are normalized to GAPDH expression and fold changes are normalized to initial target mRNA expression levels in hHpSCs. All data reported as mean ± 1 standard deviation.

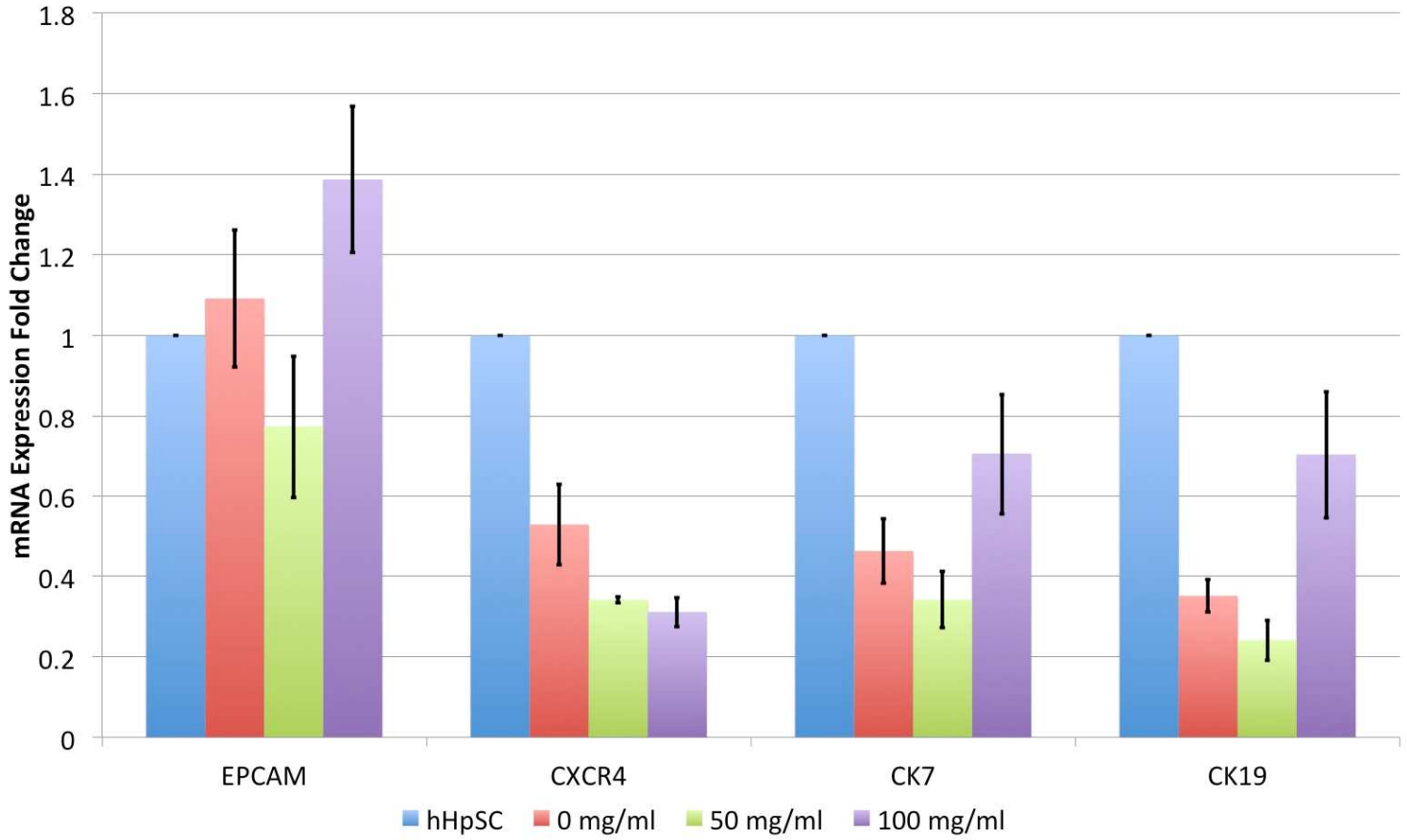

**Figure 32**: Functional assays of hepatic functions over time to compare hHpSCs cultured in Kubota's Medium to hHpSCs cultured in Human Differentiation Medium for Liver. Cultures consisted of hyaluronan and various concentrations of pulverized biomatrix. AFP and Albumin secretion are reported as fold change normalized to initial target levels 24h after seeding. (A) Change in AFP secretion measured over time. (B) Change in Albumin secretion measured over time. All data reported as mean ± standard error.

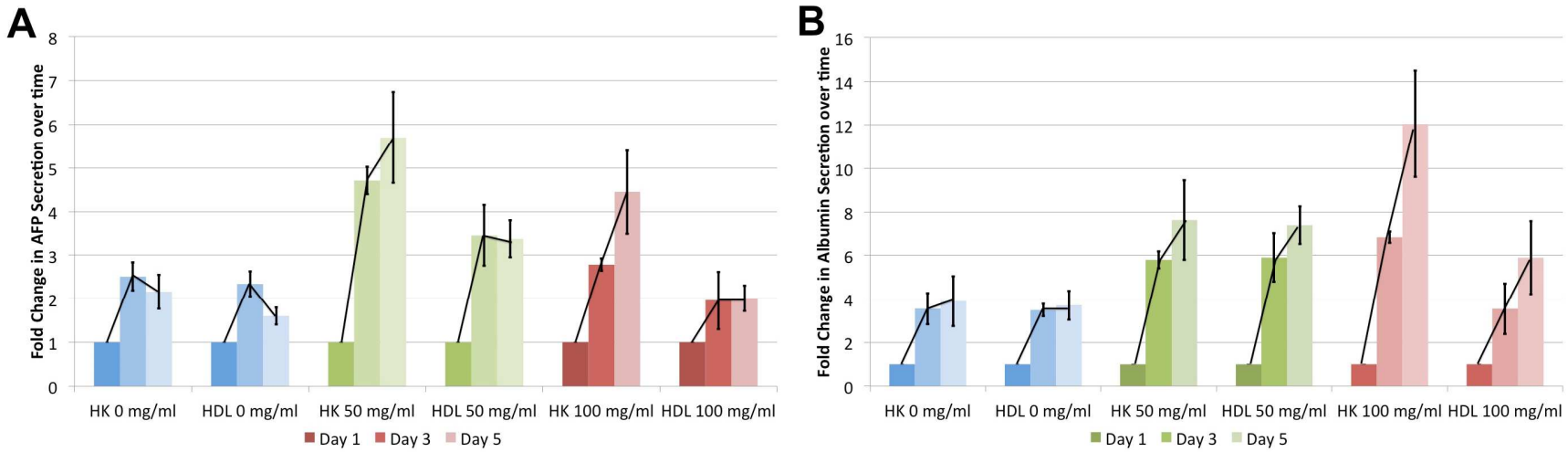

**Figure 33**: Gene Expression levels for differentiation markers to compare hHpSCs cultured in Kubota's Medium to hHpSCs cultured in Human Differentiation Medium for Liver with hyaluronan and various concentrations of pulverized biomatrix after 5 days by qRT-PCR. Target mRNA expression levels are normalized to GAPDH expression and fold changes are normalized to initial target mRNA expression levels in hHpSCs. All data reported as mean ± 1 standard deviation.

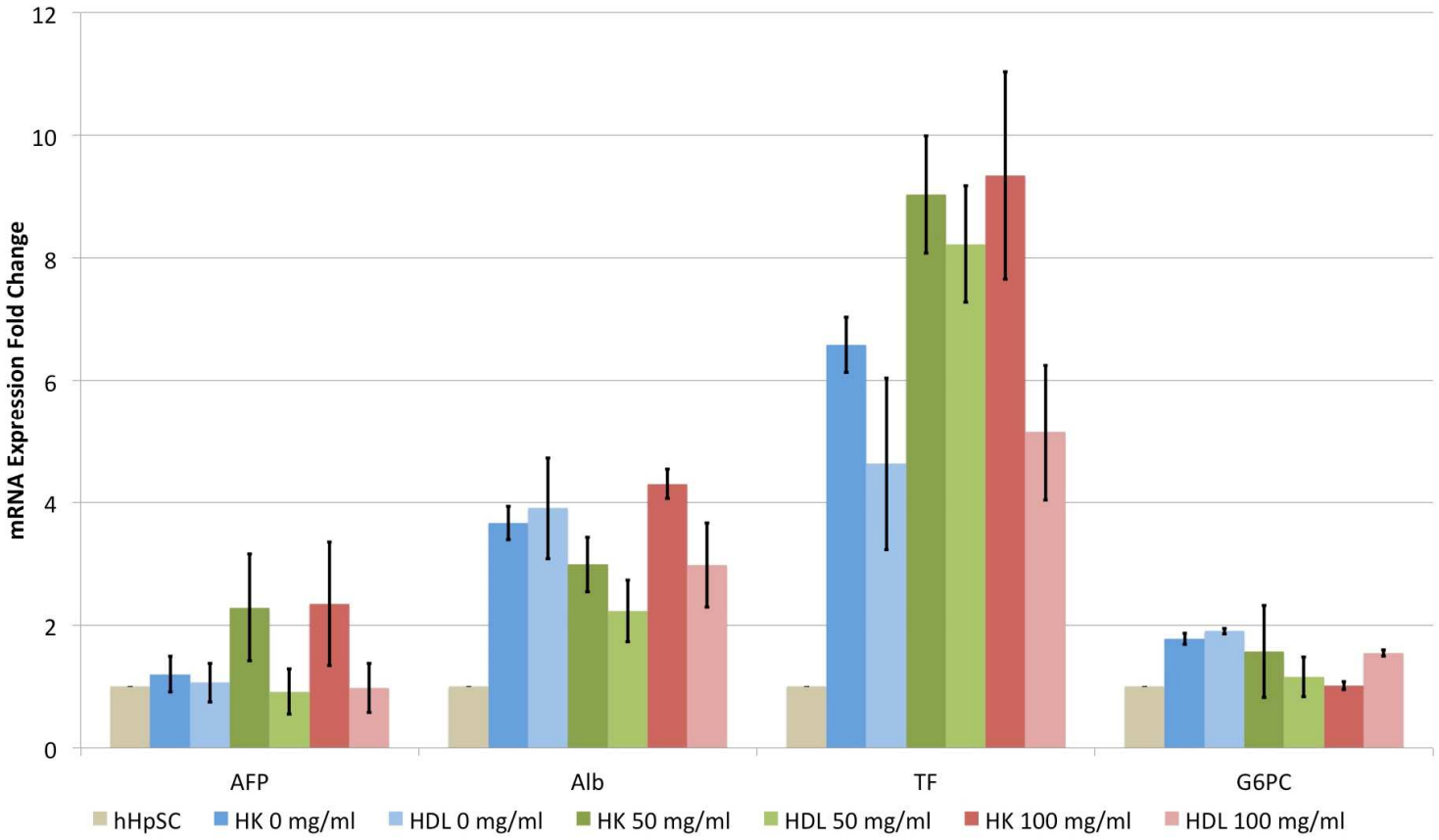

# CHAPTER VI

# Conclusions

## Rationale Behind *ex vivo* Model Development

Liver regenerative medicine research has become a multidisciplinary effort with contributions from diverse fields. A common focus of these studies has been on either regenerating or fully replacing the tissue of the liver with the end goal of restoring some degree of functionality. There has also been a focus on using these technologies as a model system for liver disease research and studies on drug response and toxicity. Many industry standard protocols that are currently being used in the study of various drug and chemical hepato-toxicities utilize hepatocytes cultured either on plastic or in suspension. Even though these primary human hepatocytes most accurately model liver disease and the hepatotoxicity of drugs, many problems are associated with these models including the limited availability of these cells, variability between donors, and inability of current culture systems to maintain hepatic phenotypes or even sustain viable cultures.

It is evident that there is a need for a sustainable source of mature hepatocytes and for improved *in vitro* three-dimensional (3D) culture systems that integrate the external cues needed for healthy hepatic cultures. Some of these cues include the gradients of the various extracellular matrix (ECM) components, gradients in the soluble signals in the plasma, and the mechanical properties found in the liver. Systems that give recognition to these variables have already been found to be integral to the differentiation of stem cells to functional hepatocytes.

*In vitro* models can be more easily manipulated and controlled while allowing scalability. They can provide the materials for high-throughput testing of various combinations of experimental parameters. The integration of increasingly complex combinations of cell types, culture techniques that mimic the native structural and mechanical properties of the liver, and extracellular matrix scaffolds with the native matrix components preserved has allowed for the recapitulation of the native liver environment to varying degrees. Application of these culture systems to industrial applications are especially attractive due to their ability to provide a representative environment that incorporates various native properties of the liver that can be scalable – such a method would enable cost-effective drug and toxicology studies.

### *Ex Vivo* Maintenance Concerns including 2D vs 3D and Culture Media

The interactions between cells and their surrounding environment are integral to their viability and functionality. Recent developments in cell culture have transitioned from monolayer (2D) to 3D cultures. Studies in the past that have utilized 2D cultures had cells with severely muted tissue-specific functions (usually less than 1% of the levels of functions *in vivo*) and with regulation of genes found to be entirely posttranscriptional mainly due to properties that affect the half-life, translation efficiency, and protein stability (13). Transcriptional regulation of tissue-specific genes has been shown dependent on the presence of specific soluble signals (growth factors, cytokines, hormones), certain extracellular matrix components (especially the proteoglycans), and the ability of the cells to change shape in order for the chromatin to undergo requisite topological changes to bring specific regulatory elements into registration (29, 82, 83).

Three-dimensional systems have become the focus of studies on hepatic functions (or rather the tissue-specific functions of all differentiated cells) as these cultures promote the self-assembly of tissues and achieve cell differentiation at levels previously not seen in traditional monolayer culture systems. Recent studies have shown that there are complex and dynamic

interactions between the configuration of the ECM and the various intracellular activities that regulate hepatocyte morphology and hepatic function.

Classical cell culture since the 1940s has comprised use of glass or plastic substrata cultured with basal media supplemented with some type of serum. Eventually it was realized that serum is not a logical biological fluid to use in cultures as no cell in the body is in contact with serum except in a wound – conditions that drive cells towards a fibrotic or cirrhotic response (i.e. scar tissue formation). Due to the pioneering work of Gordon Sato in the 1970s and early 1980s, there was a transition to utilizing serum-free, hormonally defined media (HDM) with the constituents defined with respect to the cell type, the maturational lineage stage of the cell, and the physiological functions to be achieved (216). The use of HDM enabled the posttranscriptional regulation of tissue-specific functions in cells to be stabilized. However, the HDM did not lead to restoration of transcriptional controls of tissue-specific genes (13). It was learned subsequently that matrix components, particularly proteoglycans, in combination with the HDM, were required to restore mRNA synthesis of these genes (83).

**Importance of Extracellular Matrix and Maturational Gradients**

Recent studies have also shown the importance in the composition of the ECM in the culture of hepatic cell types. The ECM has been described as the scaffolding of all organs with insoluble chemical signals and cues that allow for the organization of tissues and the cells within those tissues. The same groups of molecules can be found in different tissue types, and it is their respective ratios, concentrations, and their array of interactions with the cells that affect their differentiation and consequently their functions.

Culture methods have been developed making use of dishes coated with attachment proteins or collagens, of embedding cells into hydrogels (e.g. collagen-based gels, Matrigel, alginate, and even PEG-based gels). Although far more functional than cells on culture plastic, these cells miss the dynamic interactions between multiple cell types that provided the

necessary cell-cell interactions needed for proper hepatocyte functions. Because of the diversity of functions that can be found in the multitude of cells that comprise a tissue, the composition and structure of the ECM varies based on the function the cells in the area serve.

The structure of the ECM of various tissue types is organized into both microstructural and macrostructural units that each provide a unique set of signals to the cells within. Specifically in the liver, there is a microstructural organization of the various extracellular components that provide the zonation of signals and cues to form a maturational gradient beginning with the most immature cells, such as the stem cells located around the portal triad, to the fully mature cells around the central vein within each acinus. Such a gradient exists in all tissues and organs. The matrix chemistry in the stem cell niches transitions to matrix chemistries distinct for each mature cell type in the tissue or organ. That chemistry derives from factors from the epithelial cells, the mesenchymal cells, and other cell types (e.g. neuronal cells), and constitutes the paracrine signals among these various cell types in the community forming the tissue or organ. The epithelial cells, and in parallel, their partner mesenchymal cells progress through the maturational lineage stages coordinated with one another via the paracrine signaling.

Recent studies that utilize purified ECM substrata to culture cells overlook the fact that the ECM is incredibly complex with many factors and components yet to be identified. This dynamic mixture of matrix components and factors cannot be replaced simply by individual matrix components or a mixture of these purified components.

**Rationale Behind Decellularization Processes and Strategy Comparison**

All of these findings have driven the development of decellularized organs to establish matrix extracts for use with *in vitro* models. These matrix extracts provide a more comprehensive representation of the complexity of the native ECM. The rationale behind all of the protocols is to eliminate nucleic acids, cytoskeletal proteins, and various other cellular

components but to leave behind as much of the original matrix as possible. All other protocols make use of freeze-thawing (which damages vascular channels), while some use enzymes (which damages many different matrix components). Others have delipidation steps often with harsh detergents, such as sodium dodecyl sulfate (SDS), that bind permanently to the matrix and then use low ionic strength buffers (some even use distilled water) that washes away all but the cross-linked collagens and anything that is not bound tightly to these cross-linked collagens.

By contrast, our protocol focuses on the collagen chemistry as established by collagen chemists in the 1970s and makes use of a strategy of extracting with buffers that preserve all of the known collagens of the tissue including both the cross-linked and non-cross-linked and even the nascent (newly synthesized) collagens. Thus, the protocol used collagen chemistry as a "hook" to retain all of the collagens and anything bound to those collagens. The net result is that the scaffolds generated by our strategies are far more complex and contain most (if not all) of the native attachment proteins, proteoglycans, and other components. Also retained are physiological levels of all known growth factors, hormones and cytokines that are matrix bound. The extract has been shown to be potent in the maintenance of cells *ex vivo*.

**Non-invasive Ultrasound Techniques for Evaluation of Matrix Substrata**

Recent developments in ultrasound techniques have enabled a more thorough way to characterize these biomatrix scaffolds by non-invasive methods. Ultrasound technologies are currently used in a variety of therapeutic and imaging applications. A new application that has recently been realized is the utilization of this technology non-invasively to visualize the structure and to characterize the material properties of these scaffolds. This technology will provide quantitative tools to monitor the functionality of the scaffolds in real-time. Feedback will be available immediately for the optimization of various parameters during scaffold fabrication studies and will obviate the use of destructive methods in scaffold analysis. Specifically in our studies, the use of microbubbles as a contrast agent in conjunction with two distinct contrast-

enhanced ultrasound methods helped us analyze the structure of the scaffolds. We were also able to visualize and quantify the vascular channels at levels close to the capillary levels while mapping perfusion rates throughout the scaffold after decellularization. Knowledge of the patency and flow rates of various areas within the scaffold allow for the selection of patent scaffolds and the optimization of recellularization efforts. Our technique has the potential to be a cost-effective method to characterize these scaffolds at a higher depth and resolution than other technologies such as optical imaging. Although the matrix scaffolds are the logical 3D substrata for cells, they are not readily scalable for industrial scale experimental protocols and applications.

**Organoid Cultures**

Organoid Cultures typically incorporate multiple cell types that have the potential to aggregate into small functional units making use of the cell types normally organized together within the 3D microenvironment of the tissue or organ. These are now increasingly popular, since they can be established rapidly and easily, and the cells remain viable and functional for weeks to months (especially when cultured in serum-free HDM). They show the importance of the variables noted above including the need for a) serum-free conditions; b) specific mixes of purified hormones, nutrients, and cytokines; c) three dimensionality; d) mixes of the key cell types to establish epithelial-mesenchymal relationships (which have long been known as important).

Disrupting the native cell-cell interactions results in a loss of differentiated functions and minimizes their ability to metabolize drugs or to behave in physiologically specific ways. The newest variable is that these relationships are lineage dependent with specific lineage stages of epithelial cells partnered with particular stages of mesenchymal cells with the paracrine signaling being distinct at each lineage stage.

The recurring themes are that the co-culture of hepatocytes or hepatic-specific iPSCs with non-parenchymal cell types will always yield hepatocytes with higher levels of functionality than when hepatocytes are cultured alone. These organoid culture methods yield hepatocytes at higher functional levels dependent on how the organoids are assembled and with the differences in the level of functionality increasing as time progresses through the experiment.

Even though the assay techniques utilized to evaluate the functionality of the hepatocytes in these studies were incredibly diverse, a commonly used assay that roughly allows comparison is the secretion of albumin. However, even for albumin secretion, many of the units of measurement cannot be reconciled and thus limit comparability except in a few cases. The most significant result could be seen when comparing our method with one used by Huch et al. (6). This was the only group to compare their albumin secretion to that of mature hepatocytes. The LGR5+ liver stem cells in their study were able to achieve ~5% of the albumin secretion of mature hepatocytes, while our hHpSCs isolated from fetal livers were able to achieve ~20%. This increase can most likely be attributed to the potency of our matrix extract that we added to the organoid cultures. Presented to our hHpSCs in a pulverized form, this biomatrix scaffold powder still maintained the original factors from the decellularized scaffold and conceivably stabilized the culture and accelerated the differentiation of these stem cells to functional cell types similar to mature hepatocytes.

**Current Status of *in vitro* Model Development**

The development of a reproducible and sustainable *in vitro* culture of fully differentiated hepatocytes with complete functionality for extended periods of time has been the goal of many studies. Demand for an *in vitro* model system that can be used to accurately understand the relationship between the exposure to a certain drug or compound and the respective cellular and metabolic responses is only increasing as the need for novel and improved therapies becomes greater. Much progress has been made in the understanding of cell-cell interactions,

the importance of the composition and configuration of the ECM, the relationship between gradients of these matrix molecules that form zonal microenvironments and the maturational lineages of the various mesenchymal and epithelial cell types within the liver. This level of understanding is completely necessary in the development of hepatic culture systems that are able to mimic the drug toxicities found *in vivo* by accurately reproducing the attempts of these cells to metabolize and adapt to these substances.

**Current Major Challenges in the Development of *in vitro* Models**

Many challenges currently exist towards achieving this goal. Further studies need to be performed to better understand various aspects of hepatocyte activity including the pathways and systems that are associated in the uptake, metabolism, and excretion of these toxins. Also, the interactions between cells specifically pertaining to how they adapt to the exposure of toxins needs to be better understood. Finally, very few *in vitro* systems have been developed that fully recapitulate the complex 3D architecture of the liver specifically relating to the relationship between the hepatic sinusoids and the bile ducts. Much development is still needed to develop a system that fully mimics the architecture found in the native liver.

**Future Directions of Our Studies**

Further studies will need to be performed to more thoroughly assay the level of functionality achieved with our method. Questions that need to be addressed include whether addition of select purified matrix components (e.g. type IV collagen, laminin) to the hydrogels, along with the biomatrix powder, will confer even greater functions. Also needed is empirically to test the scalability of the system. Studies need to be performed to determine how large the volumes of the hydrogels can be and still retain the ability of nutrient and soluble signal access. The future of this approach to attaining better model systems and improving cell-based therapies is incredibly promising.

**Future Applications of *in vitro* Models**

Developments in any of these areas noted above will help in progressing towards the goal of creating an *in vitro* system that can be used in both therapeutic and industrial applications. The use of these systems in therapeutic applications will require the incorporation of multiple human cell types into these systems making the customization and personalization of these treatments to each patient possible. Specifically in the industry, the use of these systems in preclinical studies can make immediate and significant impacts by providing an *in vitro* model of the liver that can be carefully controlled and scaled. These models can be used to accurately model the metabolism of drugs and their toxicities to identify new treatments. These systems can also be used to better understand the paracrine signaling between cells in various maturational lineage stages and this knowledge would allow better control over the functionality of the cells. Additionally, these systems can be used to eliminate compounds early on in the drug development process to reduce time and costs and better prevent patients from being exposed to improperly tested and dangerous compounds in clinical trials. Finally, they can be used in research to avoid many concerns involved with *in vivo* testing in regards to scientific and ethical dilemmas.

## REFERENCES


1. Hepatology, J.H.M.G.a. Cholangiocarcinoma: Anatomy.

2. Sheppard, T. Collagen.

3. Sorokin, L. The impact of the extracellular matrix on inflammation. Nature Reviews Immunology **10**, 712, 2010.

4. Yamada, M., Utoh, R., Ohashi, K., Tatsumi, K., Yamato, M., Okano, T., and Seki, M. Controlled formation of heterotypic hepatic micro-organoids in anisotropic hydrogel microfibers for long-term preservation of liver-specific functions. Biomaterials **33**, 8304, 2012.

5. Takebe, T., Sekine, K., Enomura, M., Koike, H., Kimura, M., Ogaeri, T., Zhang, R.-R., Ueno, Y., Zheng, Y.-W., and Koike, N. Vascularized and functional human liver from an iPSC-derived organ bud transplant. Nature **499**, 481, 2013.

6. Huch, M., Dorrell, C., Boj, S.F., van Es, J.H., Li, V.S., van de Wetering, M., Sato, T., Hamer, K., Sasaki, N., Finegold, M.J., Haft, A., Vries, R.G., Grompe, M., and Clevers, H. *In vitro* expansion of single Lgr5+ liver stem cells induced by Wnt-driven regeneration. Nature **494**, 247, 2013.

7. Baptista, P.M., Siddiqui, M.M., Lozier, G., Rodriguez, S.R., Atala, A., and Soker, S. The use of whole organ decellularization for the generation of a vascularized liver organoid. Hepatology **53**, 604, 2011.

8. Wang, Y., Cui, C., Miguez, P., Yamauchi, M., Costello, J., Wauthier, E., Gerber, D., and Reid, L.M. Lineage restriction of hepatic stem cells to mature fates is made efficient by tissue-specific biomatrix scaffolds. Hepatology **53**, 293, 2011.

9. Colognato, H., and Yurchenco, P.D. Form and function: the laminin family of heterotrimers. Developmental Dynamics **218**, 213, 2000.

10. AllWorthLettingGo. The Modular Structure of Fibronectin with its Binding Domains. 2008.

11. Wauthier, E., McClelland, R., Turner, W., Schmelzer, E., Kubota, H., Zhang, L., Ludlow, J., Bruce, A., Yao, H., Furth, M.E., LeCluyse, E., Moss, N., Turner, R., Merrick, P., Barbier, C., Lozoya, O., Ruiz, J., and Reid, L.M. Hepatic stem cells and hepatoblasts: identification, isolation and *ex vivo* maintenance Methods for Cell Biology (Methods for Stem Cells) **86**, 137, 2008.

12. Lin, R.Z., and Chang, H.Y. Recent advances in three‐dimensional multicellular spheroid culture for biomedical research. Biotechnology Journal **3**, 1172, 2008.

13. Jefferson, D.M., Clayton, D.F., Darnell, J.E., Jr., and Reid, L.M. Post-transcriptional modulation of gene expression in cultured rat hepatocytes. Mol Cell Biol **4**, 1929, 1984.

14. Guguen-Guillouzo, C., Clément, B., Baffet, G., Beaumont, C., Morel-Chany, E., Glaise, D., and Guillouzo, A. Maintenance and reversibility of active albumin secretion by adult rat hepatocytes co-cultured with another liver epithelial cell type. Experimental cell research **143**, 47, 1983.

15. Clement, B., Guguen‐Guillouzo, C., Campion, J.P., Glaise, D., Bourel, M., and Guillouzo, A. Long‐Term Co‐Cultures of Adult Human Hepatocytes with Rat Liver Epithelial Cells: Modulation of Albumin Secretion and Accumulation of Extracellular Material. Hepatology **4**, 373, 1984.

16. Guillouzo, A., Beaune, P., Gascoin, M.-N., Begue, J.-M., Campion, J.-P., Guengerich, F.P., and Guguen-Guillouzo, C. Maintenance of cytochrome P-450 in cultured adult human hepatocytes. Biochemical pharmacology **34**, 2991, 1985.

17. Guguen-Guillouzo, C. Role of homotypic and heterotypic cell interactions in expression of specific functions by cultured hepatocytes. Isolated and cultured hepatocytes: Les Editions INSERM & John Libbey Eurotext Paris; 1986. pp. 259.

18. Goulet, F., Normand, C., and Morin, O. Cellular interactions promote tissue‐specific function, biomatrix deposition and junctional communication of primary cultured hepatocytes. Hepatology **8**, 1010, 1988.

19. Khetani, S.R., and Bhatia, S.N. Microscale culture of human liver cells for drug development. Nature biotechnology **26**, 120, 2008.

20. Turner, W.S., Schmelzer, E., McClelland, R., Wauthier, E., Chen, W., and Reid, L.M. Human hepatoblast phenotype maintained by hyaluronan hydrogels. Journal of Biomedical Materials **82**, 156, 2007.

21. McClelland, R., Wauthier, E., Zhang, L., Barbier, C., Melhem, A., Schmelzer, E., and Reid, L.M. *Ex vivo* conditions for self-replication of human hepatic stem cells Tissue Engineering **14**, 1, 2008.

22. Everitt, E.A., Malik, A.B., and Hendey, B. Fibronectin enhances the migration rate of human neutrophils *in vitro*. Journal of leukocyte biology **60**, 199, 1996.

23. Shirahashi, H., Wu, J., Yamamoto, N., Catana, A., Wege, H., Wager, B., Okita, K., and Zern, M.A. Differentiation of human and mouse embryonic stem cells along a hepatocyte lineage. Cell transplantation **13**, 197, 2004.

24. Berthiaume, F., Moghe, P.V., Toner, M., and Yarmush, M.L. Effect of extracellular matrix topology on cell structure, function, and physiological responsiveness: hepatocytes cultured in a sandwich configuration. FASEB Journal **10**, 1471, 1996.

25. Demetriou, A.A., Whiting, J.F., Feldman, D., Levenson, S.M., Chowdhury, N.R., Moscioni, A.D., and Kram, M. Replacement of liver function in rats by transplantation of microcarrier-attached hepatocytes. Science **233**, 1190, 1986.

26. Mooney, D., Hansen, L., Vacanti, J., Langer, R., Farmer, S., and Ingber, D. Switching from differentiation to growth in hepatocytes: control by extracellular matrix. JOURNAL OF CELLULAR PHYSIOLOGY **151**, 497, 1992.

27. Michalopoulos, G.K., Bowen, W.C., Zajac, V.F., Beer-Stolz, D., Watkins, S., Kostrubsky, V., and Strom, S.C. Morphogenetic events in mixed cultures of rat hepatocytes and nonparenchymal cells maintained in biological matrices in the presence of hepatocyte growth factor and epidermal growth factor [see comments]. Hepatology **29**, 90, 1999.

28. Moghe, P.V., Berthiaume, F., Ezzell, R.M., Toner, M., Tompkins, R.G., and Yarmush, M.L. Culture matrix configuration and composition in the maintenance of hepatocyte polarity and function. BIOMATERIALS **17**, 373, 1996.

29. Muschel, R., Khoury, G., and Reid, L.M. Regulation of insulin mRNA abundance and adenylation: dependence on hormones and matrix substrata. Molecular & Cellular Biology **6**, 337, 1986.

30. Doerr, R., Zvibel, I., Chiuten, D., D'Olimpio, J., and Reid, L.M. Clonal growth of tumors on tissue-specific biomatrices and correlation with organ site specificity of metastases. Cancer Res **49**, 384, 1989.

31. Allen, J., and Bhatia, S. Engineering Liver Therapies for the Future. Tissue Eng **8**, 725, 2002.

32. Reilly, G.C., and Engler, A.J. Intrinsic extracellular matrix properties regulate stem cell differentiation. Journal of biomechanics **43**, 55, 2010.

33. Kilian, K.A., Bugarija, B., Lahn, B.T., and Mrksich, M. Geometric cues for directing the differentiation of mesenchymal stem cells. Proceedings of the National Academy of Sciences **107**, 4872, 2010.

34. Zhu, C., Coombe, D.R., Zheng, M.H., Yeoh, G.C., and Li, L. Liver progenitor cell interactions with the extracellular matrix. Journal of tissue engineering and regenerative medicine **7**, 757, 2013.

35. Pampaloni, F., Reynaud, E.G., and Stelzer, E.H. The third dimension bridges the gap between cell culture and live tissue. Nature reviews Molecular cell biology **8**, 839, 2007.

36. Berthiaume, F., Maguire, T.J., and Yarmush, M.L. Tissue engineering and regenerative medicine: history, progress, and challenges. Annual review of chemical and biomolecular engineering **2**, 403, 2011.

37. Atala, A., Kasper, F.K., and Mikos, A.G. Engineering complex tissues. Science translational medicine **4**, 160rv12, 2012.

38. Putnam, A.J., and Mooney, D.J. Tissue engineering using synthetic extracellular matrices. Nature medicine **2**, 824, 1996.

39. Underhill, G.H., Chen, A.A., Albrecht, D.R., and Bhatia, S.N. Assessment of hepatocellular function within PEG hydrogels. Biomaterials **28**, 256, 2007.

40. Kern, A., Bader, A., Pichlmayr, R., and Sewing, K.F. Drug metabolism in hepatocyte sandwich cultures of rats and humans. Biochem Pharmacol **54**, 761, 1997.

41. Kienhuis, A.S., Wortelboer, H.M., Hoflack, J.-C., Moonen, E.J., Kleinjans, J.C., van Ommen, B., van Delft, J.H., and Stierum, R.H. Comparison of coumarin-induced toxicity between sandwich-cultured primary rat hepatocytes and rats *in vivo*: a toxicogenomics approach. Drug metabolism and disposition **34**, 2083, 2006.

42. Yamasaki, C., Tateno, C., Aratani, A., Ohnishi, C., Katayama, S., Kohashi, T., Hino, H., Marusawa, H., Asahara, T., and Yoshizato, K. Growth and differentiation of colony-forming human hepatocytes *in vitro*. Journal of hepatology **44**, 749, 2006.

43. Shepard, S., Becker, H., and Hartman, J. Using Hyaluronic Acid to Create a Fetal-like Environment *in vitro*. Annals of Plastic Surgery **36**, 65, 1996.

44. Khalil, M., Shariat-Panahi, A., Tootle, R., Ryder, T., McCloskey, P., Roberts, E., Hodgson, H., and Selden, C. Human hepatocyte cell lines proliferating as cohesive spheroid colonies in alginate markedly upregulate both synthetic and detoxificatory liver function. Journal of hepatology **34**, 68, 2001.

45. Hwang, C.M., Sant, S., Masaeli, M., Kachouie, N.N., Zamanian, B., Lee, S.-H., and Khademhosseini, A. Fabrication of three-dimensional porous cell-laden hydrogel for tissue engineering. Biofabrication **2**, 035003, 2010.

46. Lancaster, M.A., and Knoblich, J.A. Organogenesis in a dish: Modeling development and disease using organoid technologies. Review. Science **345**, 283, 2014.

47. Wang, X., and Ye, K. Three-dimensional differentiation of embryonic stem cells into islet-like insulin-producing clusters. Tissue Engineering, Part A **15**2009.

48. Riccalton-Banks, L., Liew, C., Bhandari, R., Fry, J., and Shakesheff, K. Long-term culture of functional liver tissue: three-dimensional coculture of primary hepatocytes and stellate cells. Tissue Eng **9**, 401, 2003.

49. Thomas, R.J., Bhandari, R., Barrett, D.A., Bennett, A.J., Fry, J.R., Powe, D., Thomson, B.J., and Shakesheff, K.M. The effect of three-dimensional co-culture of hepatocytes and hepatic stellate cells on key hepatocyte functions *in vitro*. Cells Tissues Organs, 67, 2005.

50. Mabuchi, A., Mullaney, I., Sheard, P.W., Hessian, P.A., Mallard, B.L., Tawadrous, M.N., Zimmermann, A., Senoo, H., and Wheatley, A.M. Role of hepatic stellate cell/hepatocyte interaction and activation of hepatic stellate cells in the early phase of liver regeneration in the rat. Journal of hepatology **40**, 910, 2004.

51. Thomas, R., Bennett, A., Thomson, B., and Shakesheff, K. Hepatic stellate cells on poly (DL-lactic acid) surfaces control the formation of 3D hepatocyte co-culture aggregates *in vitro*. European cells & materials **11**, 16, 2005.

52. Arenson, D.M., Friedman, S.L., and Bissell, D.M. Formation of extracellular matrix in normal rat liver: lipocytes as a major source of proteoglycan. Gastroenterology **95**, 441, 1988.

53. Friedman, S.L., Roll, F.J., Boyles, J., and Bissell, D.M. Hepatic lipocytes: the principal collagen-producing cells of normal rat liver. Proceedings of the National Academy of Sciences **82**, 8681, 1985.

54. Michalopoulos, G.K. Liver regeneration. Journal of cellular physiology **213**, 286, 2007.

55. Patel, S.J., Milwid, J.M., King, K.R., Bohr, S., Iracheta-Vellve, A., Li, M., Vitalo, A., Parekkadan, B., Jindal, R., and Yarmush, M.L. Gap junction inhibition prevents drug-induced liver toxicity and fulminant hepatic failure. Nature biotechnology **30**, 179, 2012.

56. Jindal, R., Nahmias, Y., Tilles, A.W., Berthiaume, F., and Yarmush, M.L. Amino acid-mediated heterotypic interaction governs performance of a hepatic tissue model. The FASEB Journal **23**, 2288, 2009.

57. Bhatia, S., Balis, U., Yarmush, M., and Toner, M. Effect of cell–cell interactions in preservation of cellular phenotype: cocultivation of hepatocytes and nonparenchymal cells. The FASEB Journal **13**, 1883, 1999.

58. Michalopoulos, G.K., Bowen, W.C., Mulè, K., and Stolz, D.B. Histological organization in hepatocyte organoid cultures. The American journal of pathology **159**, 1877, 2001.

59. Nahmias, Y., Schwartz, R.E., Hu, W.-S., Verfaillie, C.M., and Odde, D.J. Endothelium-mediated hepatocyte recruitment in the establishment of liver-like tissue *in vitro*. Tissue engineering **12**, 1627, 2006.

60. Khetani, S.R., Szulgit, G., Del Rio, J.A., Barlow, C., and Bhatia, S.N. Exploring interactions between rat hepatocytes and nonparenchymal cells using gene expression profiling. Hepatology **40**, 545, 2004.

61. Navarro-Alvarez, N., Soto-Gutierrez, A., Chen, Y., Caballero-Corbalan, J., Hassan, W., Kobayashi, S., Kondo, Y., Iwamuro, M., Yamamoto, K., and Kondo, E. Intramuscular transplantation of engineered hepatic tissue constructs corrects acute and chronic liver failure in mice. Journal of hepatology **52**, 211, 2010.

62. Soto-Gutierrez, A., Navarro-Alvarez, N., Yagi, H., Nahmias, Y., Yarmush, M.L., and Kobayashi, N. Engineering of an hepatic organoid to develop liver assist devices. Cell transplantation **19**, 815, 2010.

63. Lu, Y., Zhang, G., Shen, C., Uygun, K., Yarmush, M.L., and Meng, Q. A novel 3D liver organoid system for elucidation of hepatic glucose metabolism. Biotechnology and bioengineering **109**, 595, 2012.

64. Au, S.H., Chamberlain, M.D., Mahesh, S., Sefton, M.V., and Wheeler, A.R. Hepatic organoids for microfluidic drug screening. Lab on a Chip **14**, 3290, 2014.

65. ***Schmelzer, E.**, ***Zhang, L.**, Bruce, A., E., W., Ludlow, J., Yao, H., Moss, N., Melhem, A., McClelland, R.l., Turner, W., Kulik, M.l., Sherwood, S., Tallheden, T., Cheng, N., ****Furth, M.E.**, ****Reid, L.M.**, authors, c.-e.f., and authors, c.-e.s. Human hepatic stem cells from fetal and postnatal donors. Journal of Experimental Medicine **204**, 1973, 2007.

66. Kuwahara, R., Kofman, A.V., Landis, C.S., Swenson, E.S., Barendswaard, E., and Theise, N.D. The hepatic stem cell niche: identification by label retaining cell assay. Hepatology **47**, 1994, 2008.

67. Saxena, R., and Theise, N. Canals of Hering: recent insights and current knowledge. Seminars in Liver Disease **24**, 43, 2004.

68. Zhang, L., Theise, N., Chua, M., and Reid, L.M. The stem cell niche of human livers: symmetry between development and regeneration. Hepatology **48**, 1598, 2008.

69. Schmelzer, E., Wauthier, E., and Reid, L.M. Phenotypes of pluripotent human hepatic progenitors. Stem Cell **24**, 1852, 2006.

70. Sicklick, J.K., Li, Y.X., Melhem, A., Schmelzer, E., Zdanowicz, M., Huang, J., Caballero, M., Fair, J.H., Ludlow, J.W., McClelland, R.E., ***Reid, L.M.**, ***Diehl, A.M.**, and authors, c.-e.s. Hedgehog signaling maintains resident hepatic progenitors throughout life American Journal of PhysiologyGastrointestinal Liver Physiology **290**, G859, 2006.

71. Tanaka, M., Okabe, M., Suzuki, K., Kamiya, Y., Tsukahara, Y., Saito, S., and Miyajima, A. Mouse hepatoblasts at distinct developmental stages are characterized by expression of EpCAM and DLK1: drastic change of EpCAM expression during liver development. . Mechanisms of Development **126**, 665, 2009.

72. Sigal, S.H., Brill, S., Fiorino, A.S., and Reid, L.M. The liver as a stem cell and lineage system. American Journal of Physiology **263**, G139, 1992.

73. Haruna, Y., Saito, K., Spaulding, S., Nalesnik, M.A., and Gerber, M.A. Identification of bipotential progenitor cells in human liver development. Hepatology **23**, 476, 1996.

74. Zhang, L., Theise, N., Chua, M., and Reid, L.M. Human hepatic stem cells and hepatoblasts: Symmetry between Liver Development and Liver Regeneration. Hepatology **48**, 1598, 2008.

75. Kubota, H., Yao, H., and Reid, L.M. Identification and characterization of vitamin A-storing cells in fetal liver. Stem Cell **25**, 2339, 2007.

76. Wang, Y., Yao, H., Barbier, C., Wauthier, E., Cui, C., Moss, N., Yamauchi, M., Sricholpech, M., Costello, M.J., Gerber, D., Loboa, E.G., and Reid, L.M. Lineage-Dependent Epithelial-Mesenchymal Paracrine Signals Dictate Growth versus Differentiation of Human Hepatic Stem Cells to Adult Fates. Hepatology **52**, 1443, 2010.

77. Kubota, H., Storms, R.W., and Reid, L.M. Variant forms of alpha-fetoprotein transcripts expressed in human hematopoietic progenitors. Implications for their developmental potential towards endoderm. Journal of Biological Chemistry **277**, 27629, 2002.

78. Tan, J., Hytiroglou, P., Wieczorek, R., Park, Y.N., Thung, S.N., Arias, B., and Theise, N.D. Immunohistochemical evidence for hepatic progenitor cells in liver diseases. Liver **22**, 365, 2002.

79. Sobaniec-Lotowska, M.E., Lotowska, J.M., and Lebensztejn, D.M. Ultrastructure of oval cells in children with chronic hepatitis B, with special emphasis on the stage of liver fibrosis: The first pediatric study. World Journal of Gastroenterology **13**, 2918, 2007.

80. Alpini, G. Molecular and functional heterogeneity of cholangiocytes from rat liver after bile duct ligation. American Journal of Physiology **272**, G289, 1997.

81. Mitaka, T., Mizuguchi, T., Sato, F., Mochizuki, C., and Mochizuki, Y. Growth and maturation of small hepatocytes. [Review] [44 refs]. Journal of Gastroenterology & Hepatology **13**, S70, 1998.

82. Fujita, M., Spray, D.C., Choi, H., Saez, J.C., Watanabe, T., Rosenberg, L.C., Hertzberg, E.L., and Reid, L.M. Glycosaminoglycans and proteoglycans induce gap junction expression and restore transcription of tissue-specific mRNAs in primary liver cultures. Hepatology **7**, 1S, 1987.

83. Spray, D.C., Fujita, M., Saez, J.C., Choi, H., Watanabe, T., Hertzberg, E., Rosenberg, L.C., and Reid, L.M. Proteoglycans and glycosaminoglycans induce gap junction synthesis and function in primary liver cultures. J Cell Biol **105**, 541, 1987.

84. Paul, D.L. Molecular cloning of cDNA for rat liver gap junction protein. J Cell Biol **103**, 123, 1986.

85. Geerts, A., Schuppan, D., Lazeroms, S., De Zanger, R., and Wisse, E. Collagen type I and III occur together in hybrid fibrils in the space of Disse of normal rat liver. Hepatology **12**, 233, 1990.

86. Geerts, A., Geuze, H.J., Slot, J.W., Voss, B., Schuppan, D., Schellinck, P., and Wisse, E. Immunogold localization of procollagen III, fibronectin and heparan sulfate proteoglycan on ultrathin frozen sections of the normal rat liver. Histochemistry **84**, 355, 1986.

87. Gressner, A.M., and Vasel, A. Proteochondroitin sulfate is the main proteoglycan synthesized in fetal hepatocytes. Proc Soc Exp Biol Med **180**, 334, 1985.

88. Lindros, K.O. Zonation of cytochrome P450 expression, drug metabolism and toxicity in liver. General Pharmacology: The Vascular System **28**, 191, 1997.

89. Lindros, K., Oinonen, T., J., I., Nagy, P., and Thorgeirsson, S.S. Zonal distribution of transcripts of four hepatic transcription factors in the mature rat liver Cell BIology and Toxicology, 257, 1997.

90. Gumucio, J.J. Hepatocyte heterogeneity and liver function. Madrid: Springer International; 1989.

91. Gupta, S. Hepatic polyploidy and liver growth control Seminars in Cancer Biology **10**, 161, 2000.

92. Sigal, S.H., Rajvanshi, P., Gorla, G.R., Sokhi, R.P., Saxena, R., Gebhard, D.R., Jr., Reid, L.M., Gupta, S., and authors), C.-s. Partial hepatectomy-induced polyploidy attenuates hepatocyte replication and activates cell aging events. American Journal of Physiology - Gastrointestinal and Liver Physiology **276**, G1260, 1999.

93. Jungermann, K. Zonal liver cell heterogeneity. [Review] [6 refs]. Enzyme **46**, 5, 1992.

94. Brown, B.N., Barnes, C.A., Kasick, R.T., Michel, R., Gilbert, T.W., Beer-Stolz, D., Castner, D.G., Ratner, B.D., and Badylak, S.F. Surface characterization of extracellular matrix scaffolds. Biomaterials **31**, 428, 2010.

95. Brill, S., Zvibel, I., Halpern, Z., and Oren, R. The role of fetal and adult hepatocyte extracellular matrix in the regulation of tissue-specific gene expression in fetal and adult hepatocytes. Eur J Cell Biol **81**, 43, 2002.

96. Rojkind, M., Giambrone, M.-A., and Biempica, L. Collagen types in normal and cirrhotic liver. Gastroenterology **76**, 710, 1979.

97. Martinez-Hernandez, A., and Amenta, P.S. The hepatic extracellular matrix. I. Components and distribution in normal liver [editorial]. Virchows Archiv - A, Pathological Anatomy & Histopathology **423**, 1, 1993.

98. Carlsson, R., Engvall, E., Freeman, A., and Ruoslahti, E. Laminin and Fibronectin Cell Adhesion: Enhanced Adhesion of Cells from Regenerating Liver to Laminin. Proceedings of the National Academy of Sciences of the United States of America **78**, 2403, 1981.

99. Daley, W.P., Peters, S.B., and Larsen, M. Extracellular matrix dynamics in development and regenerative medicine. Journal of Cell Science **21**, 255, 2008.

100. Colognato, H., and Yurchenco, P.D. Form and function: the laminin family of heterotrimers. Dev Dyn **218**, 213, 2000.

101. Kruegel, J., and Miosge, N. Basement membrane components are key players in specialized extracellular matrices. Cellular and Molecular Life Sciences **67**, 2879, 2010.

102. Sottile, J., and Hocking, D.C. Fibronectin polymerization regulates the composition and stability of extracellular matrix fibrils and cell-matrix adhesions. Molecular biology of the cell **13**, 3546, 2002.

103. Hocking, D.C., Sottile, J., and Langenbach, K.J. Stimulation of integrin-mediated cell contractility by fibronectin polymerization. Journal of Biological Chemistry **275**, 10673, 2000.

104. Sottile, J., Hocking, D.C., and Swiatek, P.J. Fibronectin matrix assembly enhances adhesion-dependent cell growth. Journal of cell science **111**, 2933, 1998.

105. Hahn, E., Wick, G., Pencev, D., and Timpl, R. Distribution of basement membrane proteins in normal and fibrotic human liver: collagen type IV, laminin, and fibronectin. Gut **21**, 63, 1980.

106. Cheng, N., Yao, H.-l., and Reid, L.M. Hepatic Stem Cells: Lineage Biology and Pluripotency. Principles of Regenerative Medicine, 344, 2008.

107. RESCAN, P.-Y., RISSEL, M., and GUILLOUZO, A. Distribution and cellular origin of collagen VI during development and in cirrhosis. Gastroenterology **102**, 980, 1992.

108. Bissell, D., and Choun, M. The role of extracellular matrix in normal liver. Scandinavian Journal of Gastroenterology **23**, 1, 1988.

109. MacSween, R.N.M., and Scothorne, R.J. Developmental anatomy and normal structure. In: MacSween R.N.M., Anthony P.P., Scheuer P.J., Burt A.D., Portmann B.C., eds. Pathology of the Liver. Edinburgh: Churchill Livingstone; 1994. pp. 1.

110. Gallai, M., Sebestyén, A., Nagy, P., Kovalszky, I., Ónody, T., and Thorgeirsson, S.S. Proteoglycan gene expression in rat liver after partial hepatectomy. Biochemical and biophysical research communications **228**, 690, 1996.

111. Polin, R.A., Fox, W.W., and Abman, S.H. Fetal and Neonatal Physiology: Expert Consult (2-Volume Set): Elsevier Health Sciences; 2011.

112. Rappaport, A., Borowy, Z., Lougheed, W., and Lotto, W. Subdivision of hexagonal liver lobules into a structural and functional unit. Role in hepatic physiology and pathology. The Anatomical Record **119**, 11, 1954.

113. McClelland, R., Wauthier, E., Uronis, J., and Reid, L. Gradients in the liver's extracellular matrix chemistry from periportal to pericentral zones: influence on human hepatic progenitors. Tissue Engineering Part A **14**, 59, 2008.

114. Martinez-Hernandez, A., Delgado, F.M., and Amenta, P.S. The extracellular matrix in hepatic regeneration. Localization of collagen types I, III, IV, laminin, and fibronectin. Lab Invest **64**, 157, 1991.

115. Reid, L.M., Fiorino, A.S., Sigal, S.H., Brill, S., and Holst, P.A. Extracellular matrix gradients in the space of Disse: relevance to liver biology. Hepatology **15**, 1198, 1992.

116. Ji, R., Zhang, N., You, N., Li, Q., Liu, W., Jiang, N., Liu, J., Zhang, H., Wang, D., and Tao, K. The differentiation of MSCs into functional hepatocyte-like cells in a liver biomatrix scaffold and their transplantation into liver-fibrotic mice. Biomaterials **33**, 8995, 2012.

117. Sellaro, T.L., Ranade, A., Faulk, D.M., McCabe, G.P., Dorko, K., Badylak, S.F., and Strom, S.C. Maintenance of human hepatocyte function *in vitro* by liver-derived extracellular matrix gels. Tissue Engineering Part A **16**, 1075, 2009.

118. Sellaro, T.L., Ravindra, A.K., Stolz, D.B., and Badylak, S.F. Maintenance of hepatic sinusoidal endothelial cell phenotype *in vitro* using organ-specific extracellular matrix scaffolds. Tissue engineering **13**, 2301, 2007.

119. Song, J.J., Guyette, J.P., Gilpin, S.E., Gonzalez, G., Vacanti, J.P., and Ott, H.C. Regeneration and experimental orthotopic transplantation of a bioengineered kidney. Nature medicine **19**, 646, 2013.

120. Shamis, Y., Hasson, E., Soroker, A., Bassat, E., Shimoni, Y., Ziv, T., Sionov, R.V., and Mitrani, E. Organ-specific scaffolds for *in vitro* expansion, differentiation, and organization of primary lung cells. Tissue Engineering Part C: Methods **17**, 861, 2011.

121. Woods, E., Walsh, C., Sidner, R., Zieger, M., Lakey, J., Ricordi, C., and Critser, J. Improved *in vitro* function of islets using small intestinal submucosa. presented at the" Transplantation proceedings, Year.

122. Mammoto, T., Jiang, E., Jiang, A., and Mammoto, A. ECM structure and tissue stiffness control postnatal lung development through the LRP5-Tie2 signaling system. Am J Respir Mol Biol **49**, 1009, 2013.

123. Bi, H., and Jin, Y. Current progress of skin tissue engineering: Seed cells, bioscaffolds, and construction strategies. Burns and Trauma **1**, 63, 2013.

124. Corona, B.T., Wu, X., Ward, C.L., McDaniel, J.S., Rathbone, C.R., and Walters, T.J. The promotion of a functional fibrosis in skeletal muscle with volumetric muscle loss injury following the transplantation of muscle-ECM. Biomaterials **34**, 3324, 2013.

125. Sebinger, D.D.R., Ofenbauer, A., Gruber, P., Malik, S., and Werner, C. ECM modulated early kidney development in embryonic organ culture. Biomaterials **34**, 6670, 2013.

126. Sreejit, P., and Verma, R.S. Natural ECM as biomaterial for scaffold based cardiac regeneration using adult bone marrow derived stem cells. Stem Cell Reviews and Reports **9**, 158, 2013.

127. Uygun, B.E., Soto-Gutierrez, A., Yagi, H., Izamis, M.-L., Guzzardi, M.A., Shulman, C., Milwid, J., Kobayashi, N., Tilles, A., and Berthiaume, F. Organ reengineering through development of a transplantable recellularized liver graft using decellularized liver matrix. Nature medicine **16**, 814, 2010.

128. Badylak, S.F., Taylor, D., and Uygun, K. Whole-organ tissue engineering: decellularization and recellularization of three-dimensional matrix scaffolds Annual Review Biomedical Engineering **13**, 27, 2011.

129. Baptista, P.M., Vyas, D., Moran, E., Wang, Z., and Soker, S. Human liver bioengineering using a whole liver decellularized bioscaffold. Organ Regeneration: Springer; 2013. pp. 289.

130. Lang, R., Stern, M.M., Smith, L., Liu, Y., Bharadwaj, S., Liu, G., Baptista, P.M., Bergman, C.R., Soker, S., Yoo, J.J., Atala, A., and Zhang, Y. Three-dimensional culture of hepatocytes on porcine liver tissue-derived extracellular matrix Biomaterials **32**, 7042, 2011.

131. Orlando, G., Baptista, P., Birchall, M., De Coppi, P., Farney, A., Guimaraes‐Souza, N.K., Opara, E., Rogers, J., Seliktar, D., and Shapira‐Schweitzer, K. Regenerative medicine as applied to solid organ transplantation: current status and future challenges. Transplant International **24**, 223, 2011.

132. Soto-Gutierrez, A., Zhang, L., Medberry, C., Fukumitsu, K., Faulk, D., Jiang, H., Reing, J., Gramignoli, R., Komori, J., Ross, M., Nagaya, M., Lagasse, E., Stolz, D., Strom, S.C., Fox, I.J., and Badylak, S.F. A whole-organ regenerative medicine approach for liver replacement. Tissue Eng Part C Methods **17**, 677, 2011.

133. Zhou, P., Lessa, N., Estrada, D.C., Severson, E.B., Lingala, S., Zern, M.A., Nolta, J.A., and Wu, J. Decellularized liver matrix as a carrier for the transplantation of human fetal and primary hepatocytes in mice. Liver Transplantation **17**, 418, 2011.

134. Gilbert, T.W., Sellaro, T.L., and Badylak, S.F. Decellularization of tissues and organs. Biomaterials **27**, 3675, 2006.

135. Orlando, G., Wood, K.J., Stratta, R.J., Yoo, J.J., Atala, A., and Soker, S. Regenerative medicine and organ transplantation: past, present, and future. Transplantation **91**, 1310, 2011.

136. De Filippo, R.E., Yoo, J.J., and Atala, A. Urethral replacement using cell seeded tubularized collagen matrices. The Journal of urology **168**, 1789, 2002.

137. Falke, G., Yoo, J.J., Kwon, T.G., Moreland, R., and Atala, A. Formation of corporal tissue architecture *in vivo* using human cavernosal muscle and endothelial cells seeded on collagen matrices. Tissue engineering **9**, 871, 2003.

138. Freytes, D.O., Badylak, S.F., Webster, T.J., Geddes, L.A., and Rundell, A.E. Biaxial strength of multilaminated extracellular matrix scaffolds. Biomaterials **25**, 2353, 2004.

139. Grauss, R.W., Hazekamp, M.G., Oppenhuizen, F., van Munsteren, C.J., Gittenberger-de Groot, A.C., and DeRuiter, M.C. Histological evaluation of decellularised porcine aortic valves: matrix changes due to different decellularisation methods. European journal of cardio-thoracic surgery **27**, 566, 2005.

140. Woods, T., and Gratzer, P.F. Effectiveness of three extraction techniques in the development of a decellularized bone–anterior cruciate ligament–bone graft. Biomaterials **26**, 7339, 2005.

141. Hudson, T.W., Liu, S.Y., and Schmidt, C.E. Engineering an improved acellular nerve graft via optimized chemical processing. Tissue engineering **10**, 1346, 2004.

142. Hudson, T.W., Zawko, S., Deister, C., Lundy, S., Hu, C.Y., Lee, K., and Schmidt, C.E. Optimized acellular nerve graft is immunologically tolerated and supports regeneration. Tissue engineering **10**, 1641, 2004.

143. Dahl, S.L., Koh, J., Prabhakar, V., and Niklason, L.E. Decellularized native and engineered arterial scaffolds for transplantation. Cell transplantation **12**, 659, 2003.

144. Ott, H.C., Matthiesen, T.S., Goh, S.K., Black, L.D., Kren, S.M., Netoff, T.I., and Taylor, D.A. Perfusion-decellularize matrix using nature's platform to engineer a bioartificial heart. Nature Medicine **14**, 213, 2008.

145. Miller, E.J. The collagens of the extracellular matrix. Society of General Physiology Ser **32**, 71, 1977.

146. Miller, E.J., and Rhodes, R.K. Preparation and characterization of the different types of collagen Methods in Enzymology **82**, 33, 1982.

147. Rojkind, M., Gatmaitan, Z., Mackensen, S., Giambrone, M.A., Ponce, P., and Reid, L.M. Connective tissue biomatrix: its isolation and utilization for long-term cultures of normal rat hepatocytes. Journal of Cell Biology **87**, 255, 1980.

148. Enat, R., Jefferson, D.M., Ruiz-Opazo, N., Gatmaitan, Z., Leinwand, L.A., and Reid, L.M. Hepatocyte proliferation *in vitro*: its dependence on the use of serum- free hormonally defined medium and substrata of extracellular matrix. Proc Natl Acad Sci U S A **81**, 1411, 1984.

149. Puppi, J., Strom, S.J., Hughes, R.D., Bansal, S., Castell, J.V., Dagher, I., Ellis, E.C.S., Ericzon, B., Fox, I.J., Gómez-Lechón, J., Guha, C., Gupta, S., Mitry, J.R., Ohashi, K., Ott, M., Reid, L.M., Roy-Chowdhury, J., Sokal, E., Weber, A., and Dhawan, A. Improving the Techniques for Human Hepatocyte Transplantation: Report from a Consensus Meeting in London/ Cell Transplantation **21**, 1, 2012.

150. Smith, J.M., Biggins, S.W., Haselby, D.G., Kim, W.R., Wedd, J., Lamb, K., Thompson, B., Segev, D.L., Gustafson, S., Kandaswamy, R., Stock, P.G., Matas, A.J., Samana, C.J., Sleeman, E.F., Stewart, D., Harper, A., Edwards, E., Snyder, J.J., Kasiske, B.L., and Israni, A.K. Kidney, Pancreas and Liver Allocation and Distribution in the United States. . American Journal of Transplantation **12**, 3191, 2012.

151. Gerlach, J.C., Zeilinger, K., and Patzer, J.F. Bioartificial liver systems: why, what, whither? (Review) Regenerative Medicine **3**, 575, 2008.

152. Catapano, G., Patzer, J.F., and Gerlach, J.C. Transport advances in disposable bioreactors for liver tissue engineering Biochemical Engineering Biotechnologies **115**, 117, 2010.

153. Macdonald, J., Griffin, J., Kubota, H., Griffith, L., Fair, J., and Reid, L.M. Bioartificial Livers. In: Kuhtreiber W.M., Lanza R.P., Chick W.L., eds. Cell Encapsulation Technology and Therapeutics. Boston: Birkhauser; 1999. pp. 252.

154. Smith, L.E., Smallwood, R., and MacNeil, S. A comparison of imaging methodologies for 3D tissue engineering Microscopic Research Techniques **73**, 1123, 2010.

155. Xu, H., Othman, S.F., and Magin, R.L. Monitoring tissue engineering using magnetic resonance imaging Journal of Biosciences and Bioengineering **106**, 515, 2008.

156. Young, S., Kretlow, J.D., Nguyen, C., Bashoura, A.G., Baggett, L.S., Jansen, J.A., Wong, M., and Mikos, A.G. Microcomputed tomography characterization of neovascularization in bone tissue engineering applications. . Tissue Engineering, Part B Rev **14**, 295, 2008.

157. Liang, X., Graf, B.W., and Boppart, S.A. Imaging engineered tissues using structural and functional optical coherence tomography Journal of Biophotonics **2**, 643, 2009.

158. McGuigan, A.P., and Sefton, M.V. Vascularized organoid engineered by modular assembly enables blood perfusion Proceedings of the National Academy of Sciences USA **103**, 11461, 2006.

159. Foster, F.S., Zhang, M.Y., Y.Q., Z., Liu, G., J., M., Cherin, E., Harasiewicz, K.A., Starkoski, B.G., Zan, L., Knapik, D.A., and Adamson., S.L. A new ultrasound instrument for *in vivo* microimaging of mice. Ultrasound MedicalBiology **28**, 1165, 2002.

160. Behler, R.H., Nichols, T.C., Zhu, H., Merricks, E.P., and Gallippi, C.M. ARFI imaging for noninvasive material characterization of atherosclerosis Part II: Toward *in vivo* characterization. ULtrasound Medical Biology **35**, 278, 2009.

161. Gessner, R.C., S.R., A., and Dayton. , P.A. Mapping microvasculature with acoustic angiography yields quantifiable differences between healthy and tumor-bearing tissue volumes in a rodent model Radiology **264**, 733, 2012.

162. Feingold S, G.R., Guracar I.M., and P.A. Dayton. Quantitative volumetric perfusion mapping of the microvasculature using contrast ultrasound. Invest Radiology. Investigations in Radiology **45**, 669, 2010.

163. Gessner, R., Lukacs, M., Lee, M., Cherin, E., Foster, F.S., and Dayton, P.A. High-resolution, high-contrast ultrasound imaging using a prototype dual-frequency transducer: *in vitro* and *in vivo* studies. IEEE Trans Ultrasonic Ferroelectricity Frequency Control **57**, 1772, 2010.

164. Streeter, J.E., Herrera-Loeza, S.G., Neel, N.F., Yeh, J.J., and Dayton. , P.A. A comparative evaluation of ultrasound perfusion imaging, molecular imaging, and volume measurements in evaluating the response to therapy. Technology Cancer Research Treatments **12**, 311, 2013.

165. Knowles, B.B., Howe, C.C., and Aden, D.P. Human hepatocellular carcinoma cell lines secrete the major plasma proteins and hepatitis B surface antigen. Science **209**, 497, 1980.

166. Darlington GJ, Kelly, J.H., and Buffone, G.J. Growth and hepatospecific gene expression of human hepatoma cells in a defined medium. *In Vitro* Cell and Developmental Biology **23**, 349, 1987.

167. Lindnerm, J.R., Song, J., Jayaweera, A.R., Sklenar, J., and Kaul, S. Microvascular rheology of definity microbubbles after intra-arterial and intravenous administration Journal of the American Society of Echocardiography **15**, 396, 2002.

168. Wei, K., Jayaweera, A.R., Firoozan, S., Linka, A., Skyba, D.M., and Kaul., S. Quantification of myocardial blood flow with ultrasound-induced destruction of microbubbles administered as a constant venous infusion Circulation **97**, 473, 1998.

169. Kruse, D.E., and Ferrara, K.W. A new imaging strategy using wideband transient response of ultrasound contrast agents IEEE Trans Ultrason Ferroelectr Freq Control **52**, 1320, 2005.

170. Kogan, P., Johnson, K.A., Feingold, S., Garrett, N., Guracar, I., Arendshorst, W.J., and Dayton, P.A. Validation of dynamic contrast-enhanced ultrasound in rodent kidneys as an absolute quantitative method for measuring blood perfusion. Ultrasound Medical Biology **37**, 900, 2011.

171. Gupta, S., Rajvanshi, P., Sokhi, R., Slehria, S., Yam, A., Kerr, A., and Novikoff, P.M. Entry and integration of transplanted hepatocytes in rat liver plates occur by disruption of hepatic sinusoidal endothelium. Hepatology **29**, 509, 1999.

172. Malhi, H., Irani, A., Volenberg, I., Schilsky, M.L., and Gupta, S. Early cell transplantation in LEC rats modeling Wilson's Disease eliminates hepatic copper with reversal of liver Disease. Gastroenterology **122**, 438, 2002.

173. Badylak, S., Arnoczky, S., Plouhar, P., Haut, R., Mendenhall, V., Clarke, R., and Horvath, C. Naturally occurring extracellular matrix as a scaffold for musculoskeletal repair. CLINICAL ORTHOPAEDICS AND RELATED RESEARCH, S333, 1999.

174. Badylak, S.F. The extracellular matrix as a scaffold for tissue reconstruction. Semin Cell Dev Biol **13**, 377, 2002.

175. Taylor, D.A., Atkins, B.Z., Hungspreugs, P., Jones, T.R., Reedy, M.C., Hutcheson, K.A., Glower, D.D., and Kraus, W.E. Regenerating functional myocardium: improved performance after skeletal myoblast transplantation. Nature Medicine **4**, 929, 1998.

176. Baptista, P.M., Orlando, G., Mirmalek-Sani, S., Siddiqui, M., Atala, A., and Soker, S. Whole organ decellularization-a tool for bioscaffold fabrication and organ bioengineering. 31st Annual international Conference of the IEEE EMBS, 6526, 2009.

177. Kubota, H., and Reid, L.M. Clonogenic hepatoblasts, common precursors for hepatocytic and biliary lineages, are lacking classical major histocompatibility complex class I antigens. Proc Natl Acad Sci (USA) **97**, 12132, 2000.

178. ***Cardinale, V.**, ***Wang, Y.**, Carpino, G., Cui, C., Inverardi, L., Dominguez-Bendala, J., Ricordi, C., Mendel, G., Furth, M.E., ****Gaudio, E.**, ****Alvaro, D.**, ****Reid, L.**, ***first-authors.**, and ****senior-authors**. Multipotent stem cells in the extrahepatic biliary tree give rise to hepatocytes, bile ducts and pancreatic islets. Hepatology **54**, 2159, 2011.

179. *Carpino, G., *Cardinale, V., Onori, P., Franchitto, A., Bartolomeo Berloco, P., Rossi, M., Wang, Y., Semeraro, R., Anceschi, M., Brunelli, R., **Alvaro, D., **Reid, L.M., **Gaudio, G., *first-authors;, and **senior-authors. Biliary tree stem/progenitor cells in glands of extrahepatic and intraheptic bile ducts: an anatomical *in situ* study yielding evidence of maturational lineages. Journal of Anatomy **220**, 186, 2012.

180. Wang, Y., *Lanzoni, G., *Carpino, G., Cui, C., Dominguez-Bendala, J., Wauthier, E., Cardinale, V., Oikawa, T., Pilegg, A., Gerber, D., Furth, M.E., **Alvaro, D., **Gaudio, E., **Inverardi, L., **Reid, L.M., and **senior-authors, s.-a. Biliary Tree Stem Cells, Precursors to Pancreatic Committed Progenitors: Evidence for Life-long Pancreatic Organogenesis. . Stem Cells **31**, 1966, 2013.

181. Berzat, A., and Hall, A.C. Cellular responses to extracellular guidance cues. EMBO Journal **29**, 2734, 2010.

182. Lin, P., Chan, W.C., Badylak, S.F., and Bhatia, S.N. Assessing porcine liver-derived biomatrix for hepatic tissue engineering. Tissue Eng **10**, 1046, 2004.

183. Barakat, O., Abbasi, S., Rodriguez, G., Rios, J., Wood, R.P., Ozaki, C., Holley, L.S., and Gauthier, P.K. Use of decellularized porcine liver for engineering humanized liver organ. . Journal of Surgical Research **173**, e11, 2012.

184. Badylak, S.F. Xenogeneic extracellular matrix as a scaffold for tissue reconstruction. Transplant Immunology **12**, 367, 2004.

185. Ren, H., Shi, X., Tao, L., Xiao, J., Han, B., Zhang, Y., Yuan, X., and Ding, Y. Evaluation of two decellularization methods in the development of a whole-organ decellularized rat liver scaffold. Liver International **33**, 448, 2013.

186. Cheng, Y., Wang, Y., Kang, Y.Z., Hu, P.Y., Gao, Y., and Pan, M.X. *In vitro* culture of tumour-derived hepatocytes in decellularised whole-liver biological scaffolds. Digestion **87**, 189, 2013.

187. Kaya, M., Gregory, T.S.t., and Dayton, P.A. Changes in lipid-encapsulated microbubble population during continuous infusion and methods to maintain consistency. . Ultrasound Medical Biology **35**, 1748, 2009.

188. Martins, P.N., and Neuhaus, P. Surgical anatomy of the liver, hepatic vasculature and bile ducts in the rat. Liver International **27**, 384, 2007.

189. Bale, S.S., Vernetti, L., Senutovitch, N., Jindal, R., Hegde, M., Gough, A., McCarty, W.J., Bakan, A., Bhushan, A., Shun, T.Y., Golberg, I., DeBiasio, R., Usta, O.B., Taylor, D.L., and Yarmush, M.L. *In vitro* platforms for evaluating liver toxicity.Review Experimental BIology in Medicine (Maywood) **239**, 1180, 2014.

190. Macdonald, J.M., Xu, A., Kubota, H., Lecluyse, E., Hamilton, G., Liu, H., Rong, Y., Moss, N., Lodestro, C., Luntz, T., Wolfe, S.P., and Reid, L.M. Liver cell culture and lineage biology. In: Atala A., Lanza R.P., eds. Methods of Tissue Engineering. London: Academic Press; 2002. pp. 151.

191. Ye, J., Shirakigawa, N., and Ijima, H. Hybrid organoids consisting of extracellular matrix gel particles and hepatocytes for transplantation. Journal of Bioscience and Bioengineering 2015.

192. Bhatia, S.N., Underhill, G.H., Zaret, K.S., and Fox, I.J. Cell and tissue engineering for liver disease. Science Translational Medicine **6**, 245sr2, 2014.

193. Gilbert, T.W., Freund, J.M., and Badylak, S. Quantification of DNA in biologic scaffold materials. . Journal of Surgical Research **152**, 135, 2009.

194. Yamauchi, M., and Shiiba, M. Lysine hydroxylation and cross-linking of collagen. Methods Molecular Biology **446**, 95, 2008.

195. Pfaffl, M.W. A new mathematical model for relative quantification in real-time RT-PCR. Nucleic acids research **29**, e45, 2001.

196. Larionov, A., Krause, A., and Miller, W. A standard curve based method for relative real time PCR data processing. BMC bioinformatics **6**, 62, 2005.

197. Badylak, S.F., Taylor, D., and Uygun, K. Whole-organ tissue engineering: decellularization and recellularization of three-dimensional matrix scaffolds. Annual review of biomedical engineering **13**, 27, 2011.

198. Huber, J.E., Spievack, A., Simmons-Byrd, A., Ringel, R.L., and Badylak, S. Extracellular matrix as a scaffold for laryngeal reconstruction. Annals of Otol Rhinol Laryngology **112**, 428, 2003.

199. Elliott, N.T., and Yuan, F. A review of three‐dimensional *in vitro* tissue models for drug discovery and transport studies. Journal of pharmaceutical sciences **100**, 59, 2011.

200. Ota, H., and Miki, N. Microtechnology-based three-dimensional spheroid formation. Frontiers in bioscience (Elite edition) **5**, 37, 2012.

201. Gessner, R.C., Hanson, A., Feingold, S., Cashion, A., Corcimaru, A., Wu, B., Mullins, C., Aylward, S.R., Reid, L.M., Dayton, P.A., and authors*), S. New Ultrasound Perfusion Imaging Techniques Enable Functional Assessment of Biomatrix Scaffolds for Human Organoid Formation. . Biomaterials **34**, 9341, 2013.

202. Miller, E.J. A review of biochemical studies on the genetically distinct collagens of the skeletal system. Clinical Orthopedics Related Research **92**, 260, 1973.

203. Skardal, A., Smith, L., Bharadwaj, S., Atala, A., Soker, S., and Zhang, Y. Tissue specific synthetic ECM hydrogels for 3-D *in vitro* maintenance of hepatocyte function. Biomaterials **33**, 4565, 2012.

204. Shu, X.Z., Liu, Y., Luo, Y., Roberts, M.C., and Prestwich, G.D. Disulfide cross-linked hyaluronan hydrogels. Biomacromolecules **3**, 1304, 2002.

205. Shu, X.Z., Ahmad, S., Liu, Y., and Prestwich, G.D. Synthesis and evaluation of injectable, in situ crosslinkable synthetic extracellular matrices for tissue engineering. Journal of Biomedical Materials Research Part A **79**, 902, 2006.

206. Shu, X.Z., Liu, Y., Palumbo, F.S., Luo, Y., and Prestwich, G.D. In situ crosslinkable hyaluronan hydrogels for tissue engineering. Biomaterials **25**, 1339, 2004.

207. Shu, X.Z., and Prestwich, G.D. Therapeutic biomaterials from chemically modified hyaluronan. Chemistry and biology of hyaluronan, 475, 2004.

208. Vrochides, D., Papanikolaou, V., Pertoft, H., Antoniades, A.A., and Heldin, P. Biosynthesis and degradation of hyaluronan by nonparenchymal liver cells during liver regeneration. Hepatology **23**, 1650, 1996.

209. Lapidot, T., and Petit, I. Current understanding of stem cell mobilization: the roles of chemokines, proteolytic enzymes, adhesion molecules, cytokines, and stromal cells. Experimental hematology **30**, 973, 2002.

210. Pajvani, U.B., Shawber, C.J., Samuel, V.T., Birkenfeld, A.L., Shulman, G.I., Kitajewski, J., and Accili, D. Inhibition of Notch signaling ameliorates insulin resistance in a FoxO1-dependent manner. Nature medicine **17**, 961, 2011.

211. Costa, R.H., Holterman, A., Rausa, F.M., and Adami, G. Gene regulation and *in vivo* function of liver transcription factors. The liver: biology and pathobiology, 4th ed Lippincott Williams & Wilkins, Philadelphia, Pa, 59, 2001.

212. Thorstensen, K., and Romslo, I. The role of transferrin in the mechanism of cellular iron uptake. Biochemical journal **271**, 1, 1990.

213. Struecker, B., Raschzok, N., and Sauer, I.M. Liver support strategies: cutting-edge technologies. Nature Reviews Gastroenterology & Hepatology **11**, 166, 2014.

214. Mirmalek-Sani, S.-H., Sullivan, D.C., Zimmerman, C., Shupe, T.D., and Petersen, B.E. Immunogenicity of decellularized porcine liver for bioengineered hepatic tissue. The American journal of pathology **183**, 558, 2013.

215. Prestwich, G.D. Simplifying the extracellular matrix for 3‐D cell culture and tissue engineering: A pragmatic approach. Journal of cellular biochemistry **101**, 1370, 2007.

216. Sato, G.H. Hormonally defined media and long-term marrow culture: general principles. Kroc Foundation Series **18**, 133, 1984.